CHARACTERIZATION AND OPTIMIZATION OF DIRECT DRIVE FRICTION WELDING PARAMETERS IN SMALL STAINLESS STEEL TUBE WELDS

by

Alex Jackson Adams

A thesis submitted in partial fulfillment
of the requirements for the degree

of

Master of Science

in

Mechanical Engineering

MONTANA STATE UNIVERSITY
Bozeman, Montana

July 2013

APPROVAL

of a thesis submitted by

Alex Jackson Adams

This thesis has been read by each member of the thesis committee and has been found to be satisfactory regarding content, English usage, format, citation, bibliographic style, and consistency and is ready for submission to The Graduate School.

Dr. David A. Miller

Approved for the Department of Mechanical and Industrial Engineering

Dr. Christopher H.M. Jenkins

Approved for The Graduate School

Dr. Ronald W. Larsen

STATEMENT OF PERMISSION TO USE

In presenting this thesis in partial fulfillment of the requirements for a master's degree at Montana State University, I agree that the Library shall make it available to borrowers under rules of the Library.

If I have indicated my intention to copyright this thesis by including a copyright notice page, copying is allowable only for scholarly purposes, consistent with "fair use" as prescribed in the U.S. Copyright Law. Requests for permission for extended quotation from or reproduction of this thesis in whole or in parts may be granted only by the copyright holder.

Alex Jackson Adams

July 2013

ACKNOWLEDGEMENTS

First of all, thank you Mom and Dad for supporting me every step of the way in my pursuit of education. I definitely would not have made it this far without you. My work at Montana State University has been very enjoyable on many different levels. I would like to thank my professors at both the undergraduate and graduate level. I have had a very positive learning experience. It is also worth thanking all the friends I have made and kept throughout my time in Bozeman. Having fun with my friends kept me sane while working on this project. Academically and recreationally, Montana State University has been everything I've hoped for in an education.

Dr. David Miller, thank you so much for taking me in on this project. Working with you has been a very enjoyable experience, and it has opened the door to some opportunities I never would have thought about. Thanks also goes out to Kevin Amende and Dr. Christopher Jenkins for participating on my advising committee. Also, thank you Dr. Roberta Amendola for helping me with the etching process. I would also like to thank the staff in the Mechanical and Industrial Engineering office. From placing dozens of orders to scanning and copying documents, you made my work here a lot easier.

TABLE OF CONTENTS

TABLE OF CONTENTS CONTINUED

TABLE OF CONTENTS CONTINUED

LIST OF TABLES

LIST OF TABLES CONTINUED

LIST OF FIGURES

LIST OF FIGURES CONTINUED

Figure Page

LIST OF FIGURES CONTINUED

Figure Page

LIST OF FIGURES CONTINUED

Figure Page

LIST OF FIGURES CONTINUED

ABSTRACT

Rotational friction welding is a common joining process used to join cylindrical metal components. Typically, one piece is rotated and a secondary piece is held rigid. The two samples are then forced together in a controlled manner, and the resulting friction generates enough heat to weld the two pieces. This process was characterized and optimized for 304 Stainless Steel tubes with a .317 cm (.125 in) outer diameter and .14 cm (.055 in) inner diameter. The goal was to characterize and optimize parameters around a weld with no leak, strong ultimate tensile strength, and proper through-hole integrity. Also, solid bars were welded to some tubes to analyze a capped system. Key parameters to the process that were monitored and/or controlled include rotational speed, applied force, temperature, duration, and material upset. Often times the applied force is divided into two steps. A lower force is applied during heating (friction force), and a larger force is applied once rotation stops (forging force). The material upset, maximum temperature, and forging fore were the primary controlling variables in this study. Other parameters were held constant. A testing setup was built to analyze these factors. Modifications were made to a three axis mill to perform friction welding in a controlled environment. Then, tests were run to understand the effects each parameter had on weld quality. Welds with an upset greater than .1 cm held a pressure at a much higher success rate than welds with lower upsets. In general, the forging force was shown to have a large positive impact on ultimate tensile force. The integrity of the through-hole was compromised in many of the tube to tube tests. Several welds were post-drilled to recreate the through-hole. Tests with this done held a pressure 66.67% of the time. It was found that successful welding can be accomplished with this process, and different adjustments to testing procedures can maximize different qualities in the weld.

INTRODUCTION

General Information

Problem Statement

The problem originates from a pressurized testing device used at Los Alamos National Laboratory, New Mexico. A small tube connects two containers in this test device. The tube is made of 304 stainless steel. It has an outer diameter of .317 cm (1/8 in) and an inner diameter of .14 cm (.055 in). For testing purposes, this tube needs to be cut and resealed frequently. It is of interest to the National Laboratory to explore different methods for re-sealing the stainless steel tube. The tube needs to be quickly resealed in an energy efficient manner. Furthermore, the tubing is required to maintain a leak-free environment. It will be operational with an internal pressurized gas.

Friction welding is one method that the lab would like to investigate. The lab has given a primary problem as well as a secondary problem. The primary problem is to develop a controlled method of friction welding two 304 stainless steel tubes together. The dimensions of the tubes would be those given previously. This problem has many inherent difficulties. The resulting welded samples need to maintain pressure, maintain straightness, support necessary loads, and maintain the integrity of the hole through the tube. These challenges will be explored throughout this study. If some of these goals evade solution, the secondary problem will be addressed.

The secondary problem is to friction weld a solid cylindrical section to the end of an open tube. The goal here would be to essentially weld a cap on the end of a tube. This cap would need to withstand the same pressures and loads that the tube-to-tube weld

would experience. The difference would be that the problem of maintaining integrity of the hole would no longer be a concern. The goal here would be to create a completely sealed fixture. A solution to this problem would still be of use to the National Laboratory.

Purpose of Study

The overall purpose of this study is to describe and analyze the method of friction welding .317 cm (1/8 in) outer diameter, .14 cm (.055 in) inner diameter, 304 stainless steel tubes. In doing this, there are many smaller goals that need to be reached. Understanding the importance of the controlling parameters will be vital. These parameters include rotational speed, material upset, applied pressure, duration, and temperature (ASM International, 1985; Vill, 1962). Each parameter will be explored in detail. As mentioned previously, achieving a sealed system with a solid cylinder friction welded to a tube is also of significance.

Importance of Study

The success of this study will be very beneficial to the National Laboratory. The lab will have a method to quickly perform the tasks required in the testing device. This will facilitate a quicker completion of their tests and experiments. Success in this study will then benefit the recipients of National Laboratory work.

Also, this study will help the welding and engineering communities. Manufacturing companies will be able to look to this report for information about welding small stainless steel tubes. Further research in this area will also have this study as a solid platform to start from. Currently, there are quite a few reports and procedures detailing friction welding for larger diameter bars and pipes. Most available literature

discusses materials greater than 2.54 cm in diameter, and the smallest diameter found in literature was 10 mm (Sahin, 2005). This is part of the reason the National Lab needs this study completed. Information on friction welding tubes of the size in this study is not easily accessible, if it even exists at all. It will be very helpful for people in the future who wish to study friction welding on this scale.

Scope of Study

Only one size of tubing was examined. Variations in geometry were left for future work. The samples were all be prepared in the same manner. The use of lubricants, different surface coatings, or any other non-specified sample preparation method was not be covered. Also, solid cylinders friction welded to solid cylinders was not covered. The rotational speed, material upset, applied pressure, temperature, and duration were all be investigated.

The experiments were performed only using one machine: a three axis mill. The experiments were performed in open shop air; this process was not done in a vacuum or a fume hood. There was also no purging gas used. Only axial force was measured. The rotational speed was controlled by the mill. The applied pressure was controlled by an automated system. This force was measured with a load cell and recorded with LabVIEW. Upset was measured by an LVDT, and time was measured through LabVIEW. The temperature was monitored by an optical infrared sensor.

Rationale of Study

Friction welding is a common practice used in many manufacturing processes. Due to the rotational aspect, it is primarily used for round parts. Even though there wasn’t

literature available on small tubes, the large amount of friction welding information was a positive start. This process has led to many benefits in various areas; it was logical that everything could be scaled down. For this task, it was well worth investigating friction welding. If implementation into a lab environment is successful, the National Laboratory will have great benefits.

Friction Welding Overview

Welding processes can generally be lumped into two broad categories: fusion and pressure welding (Vill, 1962). Fusion welding is when the samples to be joined are melted, and liquid metal mixes and bonds together. Sometimes additional filling metal is added to the process, but that is not always necessary. Pressure welding is when the metals do not reach the liquid state. This process is typically performed when metals are highly plastic. To get to this plastic state, heat is often used, but there are other methods available. In general, friction welding falls into the pressure welding category. Metals are placed in contact to generate friction, the friction generates heat, the metals become very plastic, and pressure is applied to bond the samples together. Temperatures throughout the process remain below the melting point of the materials (Alves, 2012).

The friction welding considered here involved two contacting parts creating friction with each other. This should not be confused with friction stir welding. There are two primary styles of friction welding. Both linear and rotational friction welding methods are used in industry. Linear friction welding uses vibration to generate heat. One piece of metal is held stationary while the other is vibrated very rapidly. The contacting pieces generate heat, and pressure is applied to weld them together (Shtrikman, 2010).

This method can be used for many geometries; it can easily accommodate square edges and pieces. The linear method will not be pursued further in this study, but the reader should be aware of its use.

Rotary friction welding, often called friction spin welding, is the other style of friction welding. Although linear friction welding has its place in certain applications, rotary friction welding is more common (Shtrikman, 2010). The basic concept is straightforward. The rotation of one rod against another generates heat from friction. An applied pressure welds the two pieces together. The rotation can be generated in several different ways. Figure 1 shows the three primary orientations of rotary friction welding (Vill, 1962).

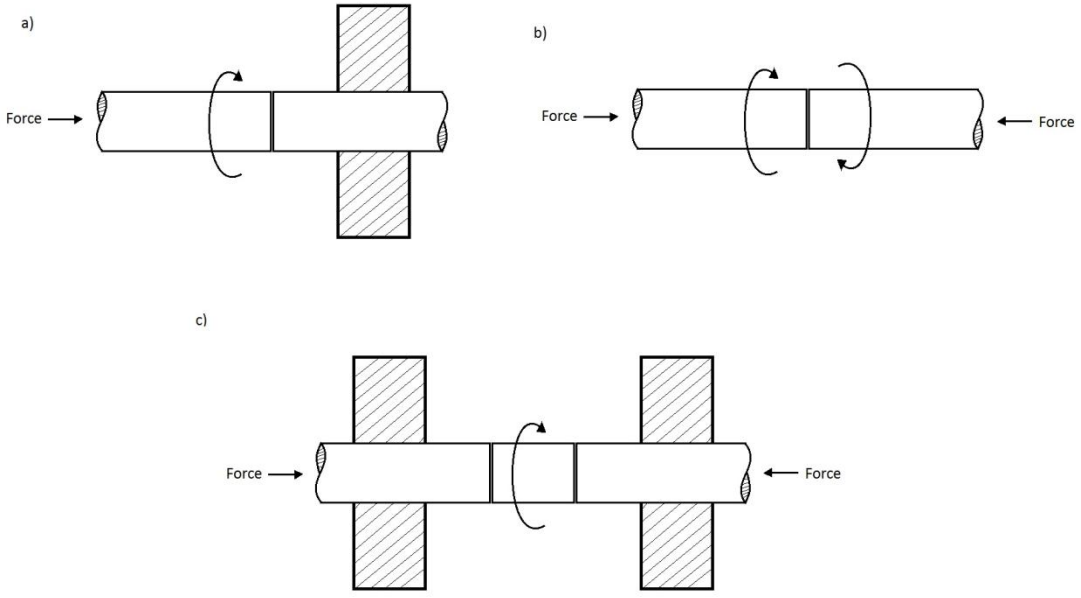

Figure 1: Different rotational orientations.

It is most common to orient the system in the form of Figure 1a. In this case, one end is held rigid while the other piece is rotated to a predetermined rotational speed. The force can be either applied from the rotating piece, the stationary piece, or both. This design is the simplest to set up and implement in normal conditions. When high rotational speeds are required, Figure 1b is a preferred orientation. The individual rotational speed of each piece can be reduced, and the relative rotational speed between pieces can be maintained at a high value. If the samples to be welded are very long or difficult to move, the set up in Figure 1c would be ideal. This method involves inserting a new piece in between two longer pieces; it is sometimes used to join long pipe sections (Lancaster, 1993). There are two weld locations with this procedure. The configuration of Figure 1a was the method that was used in this study.

There are still more variables to consider when determining a rotary friction welding method. After the heat has been generated, the entire process needs to stop rotating at some point. Two different ways to do this distinguish the direct drive and inertia drive methods (Vill, 1962). The direct drive method, also known as continuous drive, is when a rotation is held at a fixed speed, and then it is stopped instantly with a brake. The inertia drive system gets the rotating part to a certain speed before contact of the two samples to be welded. Then, once contact begins, the rotational driving power is stopped. The piece will still rotate for a short time, but the friction will eventually bring everything to a stop. The direct drive method was used in this study. For the duration of the study, when the term “friction welding” is used, it will refer to direct drive rotational friction welding (unless otherwise specified).

BACKGROUND

History

It is difficult to determine exactly when friction welding was first attempted. Some literature suggests that the process began as early as 1891 (Murthy, 2011). Other sources claim that the first recording of friction welding was by a Russian named Klopstock (Houldcroft, 1977). He was attempting the method, but he didn't make any breakthrough progress. In either case, it wasn't until the 1950's that the process began to become more established. A Russian by the name of Chudikov is recognized as doing the first true friction welding. He developed the first practical method to this procedure, and he received a Russian patent for his design in 1956 (Murthy, 2011). Chudikov used a direct drive system to manually weld low carbon steel rods with diameter of 30 mm. His methods are essentially still used today, although they have become much more sophisticated.

In the 1960's several American companies began to commercially implement this process (Houldcroft, 1977). The original designs were just done on machine shop lathes. Over the years, specific machines for friction welding have been built. Today, fully automated machines are available to the consumer. They are expensive of course, but they can save money over time (Vill, 1962).

Governing Parameters

To successfully complete the goals of the study, the majority of the project will be concerning the optimization and understanding of the governing parameters. As

mentioned previously, these include the rotational speed, applied pressure, material upset, temperature, and duration. Each of these will now be explored to show how they are known affect the outcome of the weld.

Rotational Speed

The rotational speed is perhaps the most tangible factor, but it is also the least sensitive. That is to say, it is still important, but if the other parameters are carefully controlled, a successful weld can be produced for a wide variety of operating speeds (Vill, 1962). With this in mind, there is still an optimum operating speed for every scenario. There exists a unique relationship between rotational speed and duration, all other factors being equal.

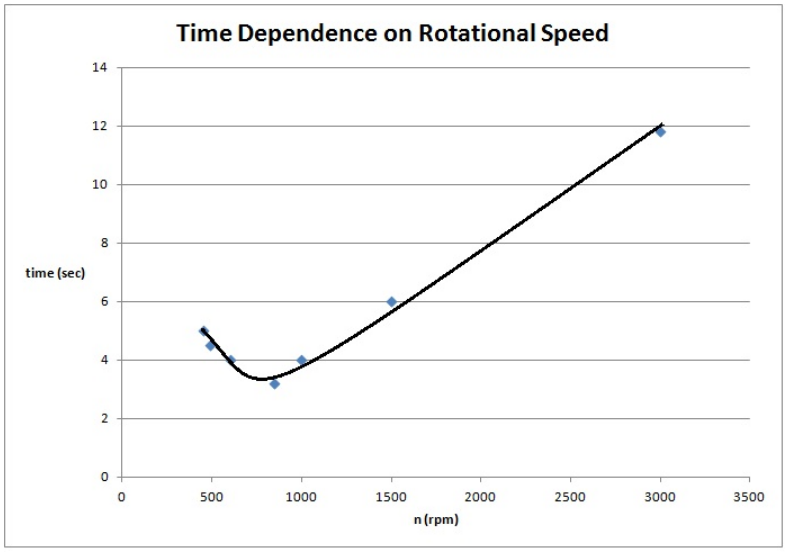

Figure 2: Observed relationship between rotational speed and total weld time (Vill, 1962).

In the above figure, the relationship between rotational speed and weld time can be observed. At low speeds, increasing the rotational speed decreases the time to perform

the weld. Around 800 rpm, this trend reverses, and increasing the rotational speed actually increases the duration. This trend has several implications.

First, there is in fact an optimum rotational speed for every system. In the above figure, the optimal speed is about 800 rpm. At this optimum speed, the weld will be completed in the shortest amount of time. This speed will also be the most efficient as far as power is concerned. Secondly, it can be seen that lower speeds will be more efficient in general. The lower amount of time also reduces the heat lost in the system. Once the operating speed is larger than the optimal speed, increasing the speed increases the time. For experiments focusing on reducing time, this relationship would be important to incorporate into the design process. Minimizing time was not focused on in this study though, so a constant rotational speed was used in testing.

Material Upset

The upset is the amount of plastic movement in the system. It is the measure of how much material has been displaced. This parameter is often a controlling parameter of the friction welding process (Vill, 1962). A desired upset can be set, and a friction welding machine will apply a pressure until the upset has been achieved. The time will then be a byproduct of the upset condition. Determining a value to use for upset is not very straightforward. It is typically derived from experimental results. The following table is an example of some guidelines. The values in the table were all determined experimentally.

Table 1: Welding Procedures for Friction Welding

Base Material	Diameter of the Friction Surface, mm	Relative Rotation Speed, rpm	Unit Pressure kg/mm^2		Upset, mm	Machine Time* to Make the Weld, sec.
			During heating	During upsetting		
Steel St. 3 to St. 3	20	1500	5	5	5	5
Steel St. 3 to St. 3	40	1000	10	10	12	20
Steel St. 5 to St. 5	16	1500	5	5	5	4.5
Steel 20 to steel 20	10	3000	4	4	3	3
Steel R18 to steel 45	13	1500	13	13	6	6
Brass L62 to L62	16	3000	3.3	3.3	6-7	3
Brass LMTs-58-2 to steel 20	30	1500	2.5	2.5	6-8	8

**The entire time of one weld depends on the degree of automation (mechanization) of the equipment.*

Using the correct upset value is a very important factor when doing friction welding. Too little of an upset will not allow enough plastic deformation for the samples to bond properly. A large upset value will result in a long time of welding. A large upset would also produce a large collar, and a lot of material will be wasted. For the small tubes in this study, a large upset value would surely result in material filling the holes in the tubes.

To determine the appropriate upset value, strength testing is usually used. The goal is to achieve a maximum amount of strength while removing a minimal amount of material. If the upset is chosen correctly, the weld will have comparable strength to that of the base metal (Vill, 1962). Lastly, if upset is a controlling parameter then the resulting dimensions will be easily controllable.

Applied Pressure

The applied pressure is a very important parameter. There are typically two methods of applying this pressure. The most obvious is to apply the pressure as a constant value for the duration of the process (Lancaster, 1993). The other method is to use a small pressure during the rotational portion of the procedure and use a larger pressure once the rotation has stopped (ASM International, 1985).

The constant pressure process is easier to control. A singular pressure setting can be selected and maintained for the duration. This method also results in a shorter duration than the stepped pressure method. Despite these two advantages of the constant pressure process, the stepped pressure process has proven to be preferred. The initial heating of the metals does not require large pressure. A small pressure value will result in an adequately heated region. Then, once the rotation has stopped, the applied pressure determines the strength of the weld.

For the stepped pressure method, the pressure can be greatly increased to achieve maximum strength of the weld. Using this stepped procedure results in a savings in power required. Also, with more control on the final pressure, stronger welds can be achieved. There are two disadvantages of the stepped pressure method. The lower initial pressure does result in a slightly longer time of weld. A result from this is that the heat affected zone will be wider. These two disadvantages are small when considering the additional strength and the power savings. A diagram of the stepped nature of the pressure can be seen below.

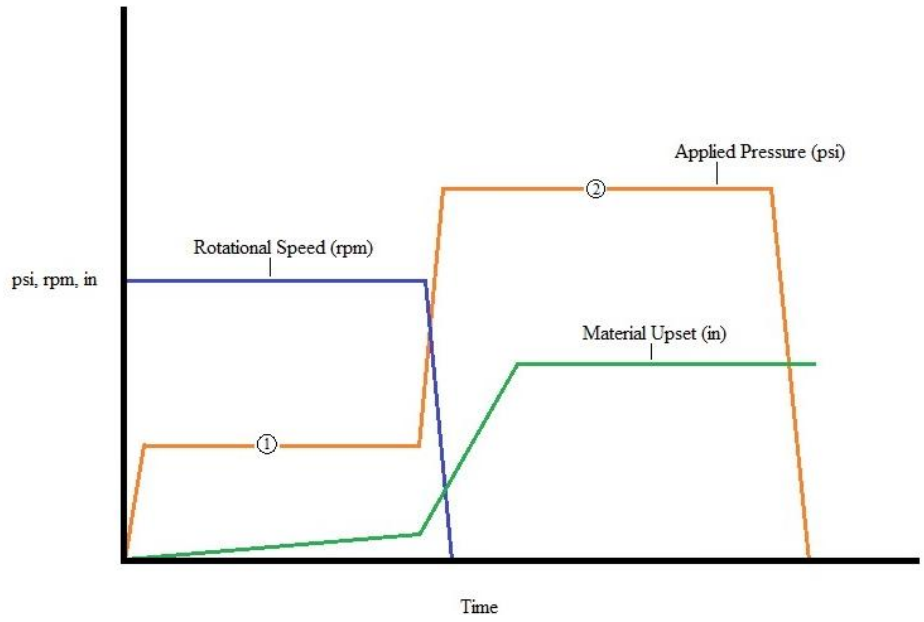

Figure 3: Friction welding characteristics with a stepped pressure value.

Similar to the upset, the applied pressures are determined experimentally. Table 1 shows some recommended pressures for the given materials. Typically, the applied pressures range between 2.5kg/mm^2 to 25 kg/mm ^{2} (Vill, 1962). It is important to use pressures within the capabilities of the material. Too much pressure could cause the material to buckle or deform away from the weld. Too little pressure could cause the samples to not even weld to each other.

Duration

The duration of the weld is similar to the upset in that it can be a controlling parameter or a dependent parameter. Typically either the upset or the time is used to control the system, and the other will be dependent on the process. If time is used as a controlling parameter, there are several things to consider. The initial conditions of each sample are extremely important when the process is controlled by duration. If samples

have even slightly different surface finishes, then the resulting welds will be different. It takes a certain amount of time in the initial heating phase to overcome surface flaws and begin pressing the samples together. The different initial conditions will alter this time, and the upset values of the final weld will be different.

To overcome a variance in initial conditions, a higher rotational speed can be used. This will more quickly remove the surface differences, and the process will reach uniformity quicker. This increase in rotational speed is a possible solution to overcome the initial conditions, but it is often complicated to optimize. A higher rotational speed might also negatively alter other parameters of the weld. It is very desirable to have uniformity in the initial conditions of the samples. Even with careful control, there still exists the potential of small variances from sample to sample. For this reason, the upset is typically used as a controlling parameter (Vill, 1962). The duration of the weld is then dependent on the upset.

Temperature

Temperatures is a very important concern in any welding process, but it is often left unmeasured in friction welding studies (Paventhan, 2012; Sahin, 2005, 2007, 2009; Satyanarayana, 2004). This is perhaps due to the inherent difficulty with temperature measurement. The rotational pieces necessitate optical measurement. In this study, an infrared thermometer was used to directly measure temperature throughout the process. Temperature is very important to friction welding. If the samples do not reach a certain temperature, they will not be plastic enough to bond together, and no weld will occur.

Characteristics of a Successful Weld

There are several characteristics that a good friction weld should have. As in many other forms of welding, a poor weld can still hold the samples together initially. However, once a load is applied, the poor weld is often the first place of failure. The weld should be completely through the thickness of the materials. The cross section of the weld should be consistent through the thickness. Also, the heat affected zone should be minimized. Figure 4 shows several examples of welds.

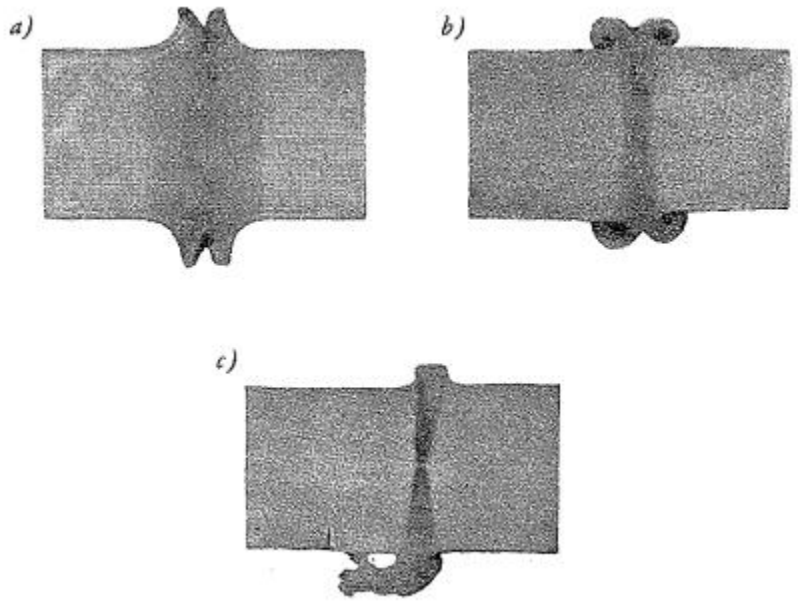

Figure 4: Macrographs of friction welded specimens. Material—St. 3 steel; diameter—20mm. Operating conditions: P=5kg/mm^2; upset—5mm. Rotation speed; a—n=3000 rpm; b---n=800rpm; c—n=430 rpm (Vill, 1962)

The fastest sample, Figure 4a, has the largest HAZ. The slowest sample, Figure 4c, has an inconsistent cross section. Both of the welds in Figure 4a and Figure 4c would

hold under zero load conditions, but they are not very good welds. The weld in figure 4b has a small heat affected zone, and the cross section is consistent throughout.

The quality of each weld is also dependent on the final microstructure at the weld. A good weld will have high strength and high plasticity characteristics. This is a result of a clean weld. The friction welding process creates a welded zone with little to zero voids, flaws, oxides, foreign particles, or other defects. The nature of the process also crushes the grains at the weld surface. This results in very small grain size in the welded zone. Some pictures of this phenomenon can be seen in the following figures.

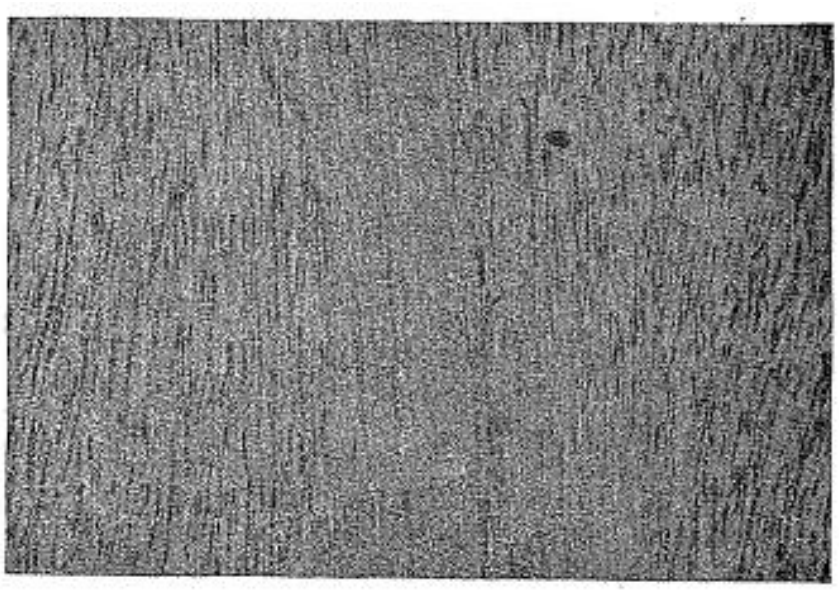

Figure 5:Microstructure of metal in the joint (x70). Material—L62 brass, diameter 10 mm. Operating conditions: n = 3000 rpm; P = 2.0 kg/mm2; tweld = 4 sec; upset—7 mm. (Vill, 1962)

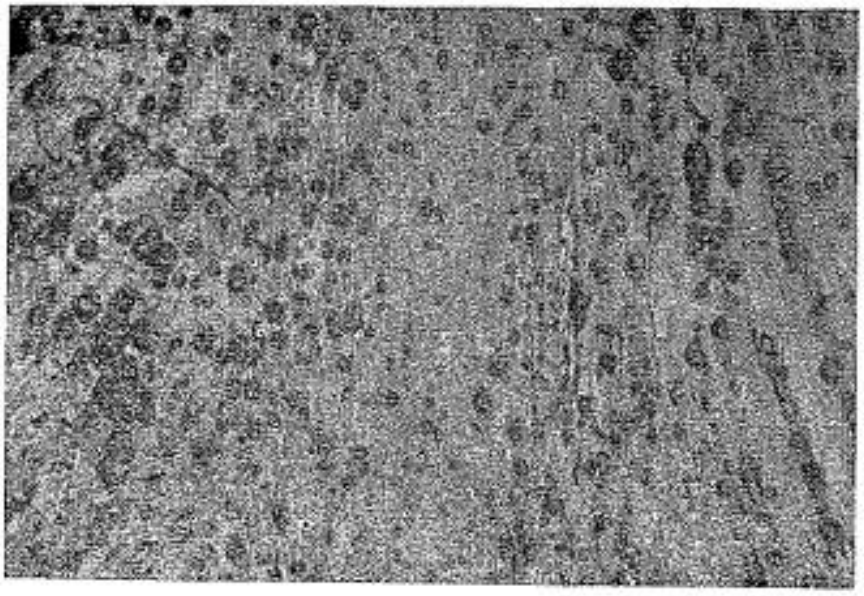

Figure 6: Microstructure of metal in the joint (x70). Material—alloy B-95, diameter 10mm. Operating conditions: n = 3000 rpm; P = 10 kg/mm2; tweld = 1 sec; upset—7mm. (Vill, 1962)

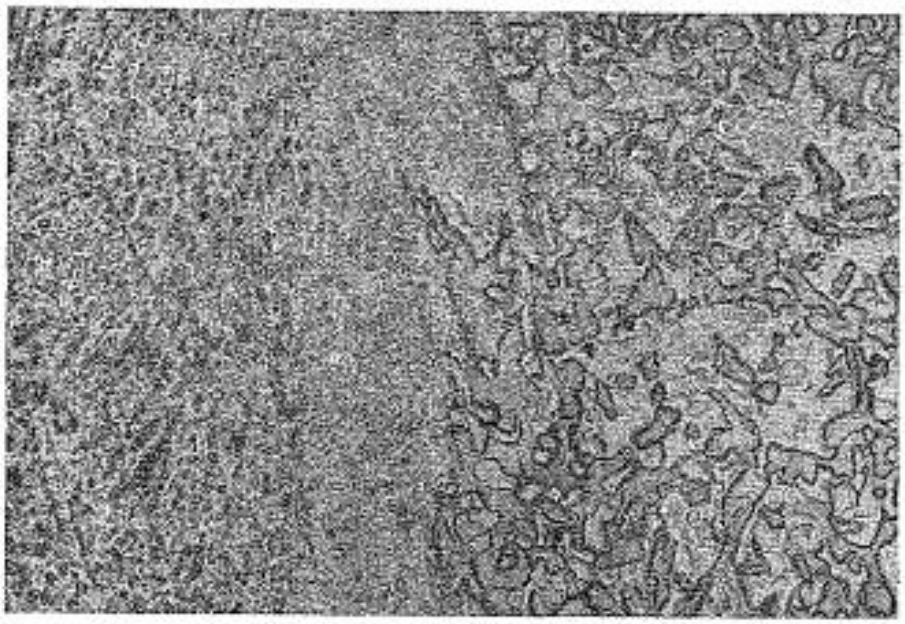

Figure 7: Microstructure of metal in the joint (x70). Material—R9 and 45 steel. Diameter—13 mm. Operating conditions: n = 1500 rpm; P = 10kg/mm2; tweld = 5 sec; upset—5mm. (Vill, 1962)

Notice how the weld area of each sample consists of finely aligned grains. Also, the grains have generally formed new boundaries parallel to the weld surface. This is a primary characteristic of a successful friction weld. Another figure demonstrating the rotational aspects of the weld can be seen in Figure 8.

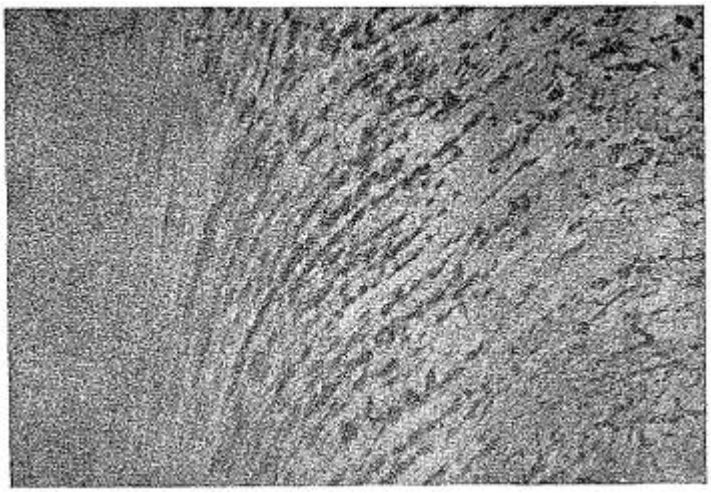

Figure 8: Microstructure of metal in the joint (x70). Sample from steel St. 3, with a 20 mm diameter. Operating conditions: n = 1000 rpm; P = 5 kg/mm2; upset—5 mm; tweld = 6 sec. (Vill, 1962)

In Figure 8, the weld interface was likely on the left edge of the picture. The left edge has very small grains. Angled grain boundaries appear in the middle of the figure; these resulted from the rotation. The material begins to transition back to the larger grain base metal at the far right of the figure. In the weld interface, it was suggested that a ferrite-pearlite pattern formed with extremely small grains (Vill, 1962). These characteristics will be looked for in the resulting welds from this study.

Welding Machinery

As previously mentioned, friction welding began as a lathe process. The simple rotational and alignment characteristics of a lathe were useful for friction welding. As the process was refined over the years, alternatives to lathes were needed. The large rotational speeds required for small diameter bars and the large axial forces required for large diameter bars often exceed capabilities of common lathes. Another constraint was the stopping capability. Most commonly, the friction welding process needs to quickly stop. Lathes do not often have this feature. The increase in friction welding led to the development and manufacture of friction welding specific machines. These machines often operate along the same lines as a lathe. The axes of the welded components are horizontal, and typically one piece is held rigid while the other rotates. Developing friction welding specific machines has led to a large amount of control over the process. Rotational speed, axial pressure, upset, duration, and alignment can all be carefully controlled.

There are several companies that manufacture and commercially distribute friction welding machines. Most of the discovered companies were based in the United States or the United Kingdom. Some companies perform welds commercially, while others sell and distribute friction welding machines. Some US companies include NCT Friction Welding, MTI Welding, American Friction Welding, and Spinweld Inc. Several UK based companies include Thompson Friction Welding and Friction Welding Systems.

The general development of friction welding machines has been presented, but here the focus is drawn to the study at hand. A piece of equipment needs to be used to

perform all the testing. The facilities at Montana State University currently do not have a friction welder. There are several lathes and mills, but it is crucial that they can be controlled enough to adequately collect data. The following consideration is what led to the final machine selection, and a similar process would typically be done when beginning any friction welding process.

There are both operational and design requirements to consider. The operational requirements should sound familiar. The machine needs to have rotational speed and load capabilities for the specific process; the machine needs to have control of the upset; pressure needs to be easily controlled; the machine needs to be able to stop instantaneously; the system should have sufficient data logging capabilities. Design requirements are a little less tangible. The load carrying components of the machine need to be rigid. A failure of the machine before the samples are finished welding is intolerable. The machine needs to adequately grip the specimen. If the samples can't be gripped, then they may begin to freely rotate once contact is initiated. It is also a good idea to minimize rotating mass of the machine. The less that is rotating, the easier it will be to stop. With these considerations in mind, a three axis mill was selected.

Applications

Friction welding has applications in many manufacturing industries. It can be used for making stepped longitudinal shafts. Typically, shafts of this sort, perhaps axles for an example, have been manufactured with a lathe. This results in a large waste of material and time. With friction welding, different diameter sections can be efficiently

welded together with minimal waste. There would be a little bit of post processing to remove the collar, and the weld would be complete.

Long bolts can be easily manufactured with this process as well. Instead of manufacturing the bolt out of one piece of metal, the rod could simply be friction welded to the nut. The friction weld would guarantee a complete cross section weld, so the nut/rod interface would be secure. Then, some threads could be put on the opposite end of the rod, and the bolt would be complete.

In a similar manner, tools can be replaced easily with friction welding. For tools that undergo a lot of wear, complete replacement is often necessary. The entire tool would not need to be replaced if friction welding was implemented. The damaged piece, often the cutting edge of the tool, could be cut off. A new cutting edge could be friction welded onto the base of the tool. This is most commonly done with drill bits. Obviously there are many instances where replacing the entire tool is best, but in some situations friction welding can be applicable.

Stud welding is another important application of friction welding. This involves welding a cylindrical piece to a flat plate. “Friction Welding of Metals” gives a guideline for this method. For an optimal weld, the thickness of the plate should be less than or equal to one quarter of the diameter of the rod (Vill, 1962).

Perhaps the greatest application of friction welding is joining dissimilar materials. Many different metallic combinations are possible. Traditional welding methods can’t weld materials with different melting temperatures very efficiently. Since friction only brings materials into a high plastic regime, many different combinations can be achieved

(ASM, 1985). The following figure gives a good description of materials that can be friction welded together.

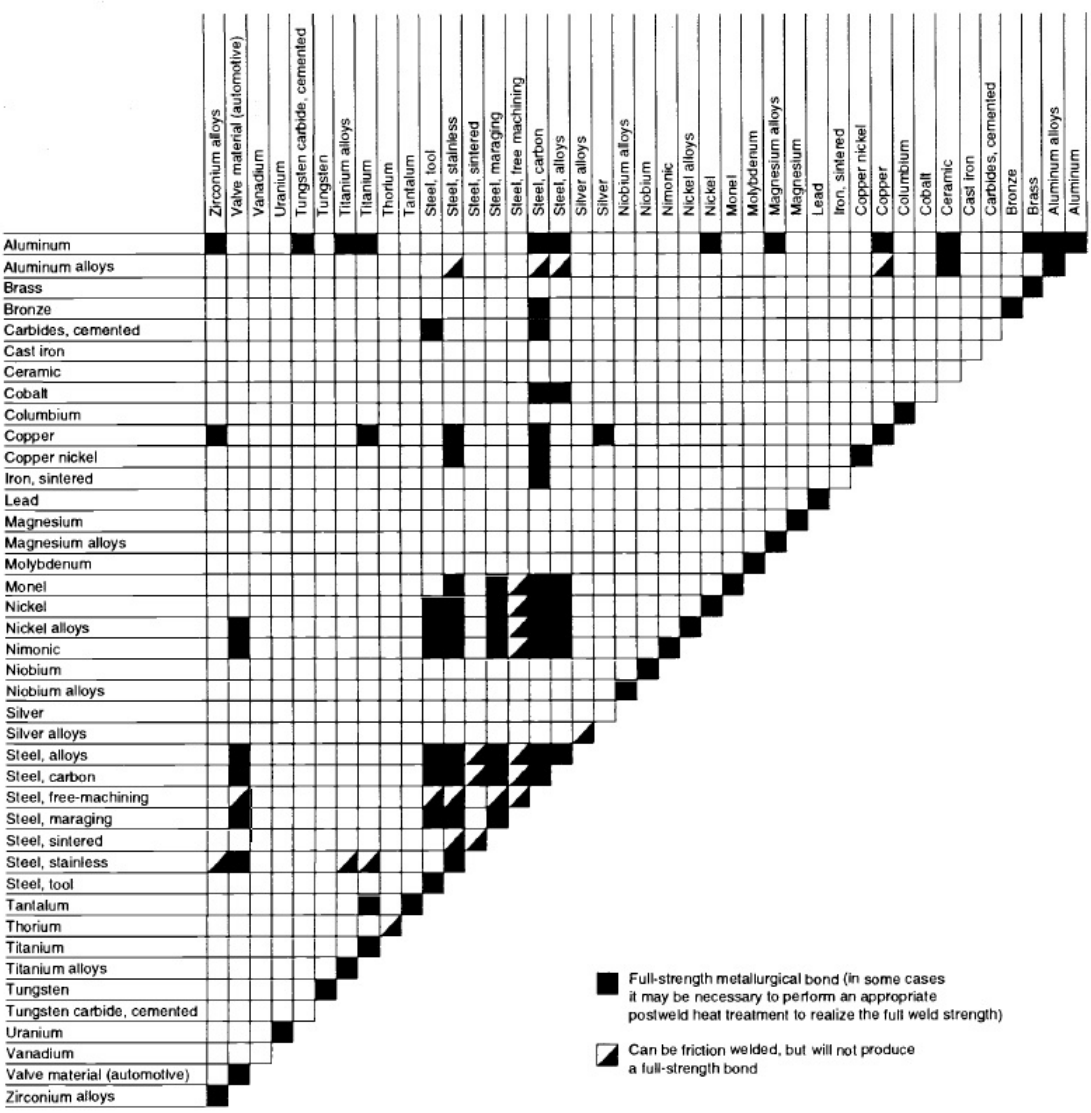

Figure 9: Possible friction welding combinations (ASM, 1985).

It should also be mentioned that some plastics can be friction welded as well. Linear friction welding is commonly used for packaging. Friction welding can be used for many more applications as well. Although it doesn't eliminate the need for traditional welding

methods, friction welding should be considered when cylindrical components need to be welded together.

EXPERIMENTAL SETUP

Preliminary Considerations

Heat Liberation

An analytical perspective to the friction welding design was taken before an experimental setup was developed. An analytical solution would help predict parameter values. The weld temperature distribution and heating rates can be collectively lumped into a term known as the heat liberation. Heat liberation is a very important concept in friction welding. Heat liberation is a measure of the heat generated in the process and a characterization of how that heat is distributed through the body (Vill, 1962). The heat liberation in a system directly relates to the power lost in the system. Experiments have been performed to calculate this power. One suggested relationship is:

$$N = 1.02 * 10^{-6} * M * n \qquad [1]$$

Where N is the heat power in the system, M is the moment on the contact surfaces from friction force, and n is the rotational speed in rpm. The moment can be solved for in the following way.

Consider analysis on a solid cylindrical rod. In the friction welding application, there will be frictional force acting on the contacting surfaces. To analyze this force, begin with a differential area. The following figure demonstrates this.

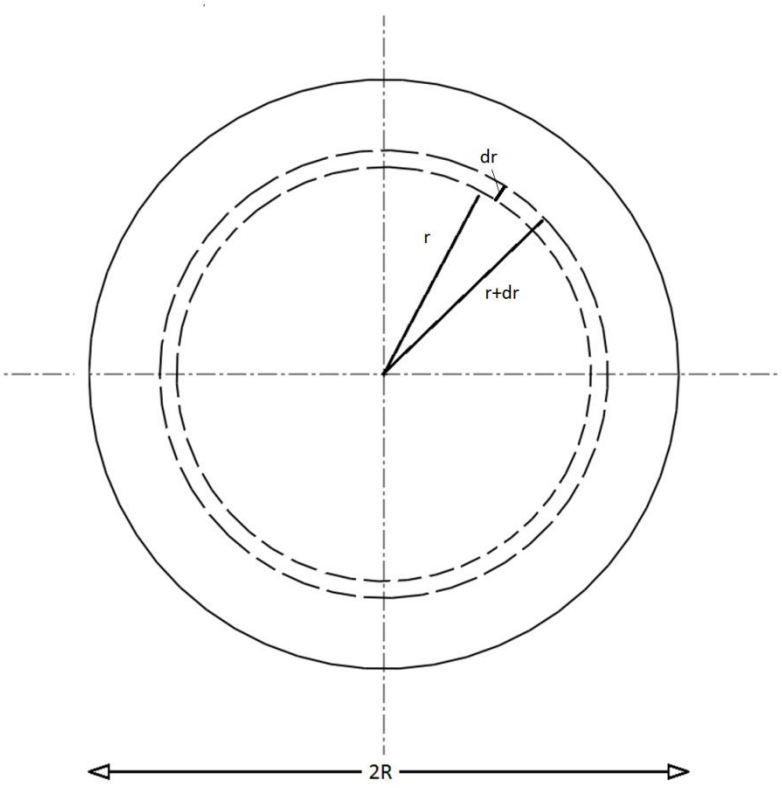

Figure 10: A differential area for heat liberation calculation.

The area from r to dr can be defined as:

$$dA = 2\pi r dr \qquad [2]$$

The normal force acting on this area is the result of the applied pressure multiplied by this area:

$$dF = P * dA = 2\pi r P dr \qquad [3]$$

The friction force acting on the area is related to the normal force by the friction coefficient:

$$F_f = dF * f = 2\pi r P f dr \qquad [4]$$

Then, the moment resulting from the friction force is:

$$dM = r * dF_f = 2\pi r^2 P f dr \qquad [5]$$

Integrating the moment from zero to the outer radius gives the total moment acting on the surface:

$$M = \frac{2}{3}\pi R^3 P f \qquad [6]$$

In this analysis, P is the applied pressure, A is an area, r is a variable radius, R is the outer radius, F is a normal force, F_f is a friction force, f is the friction coefficient, and M is the moment.

Unfortunately, the friction factor is not a constant throughout the duration of the process. The friction coefficient is dependent on several different factors related to the welding procedure (Vill, 1962; Sluzalec, 1990). These are:

1. The relative speed of motion of the friction surfaces
2. The temperature of the friction surfaces
3. The nature of the material and presence of surface films
4. The magnitude of the normal pressure force
5. The rigidity and elasticity of the friction surfaces

Each of these factors can cause a significant change in the friction coefficient. Several of these factors will be changing throughout the process. The friction coefficient clearly can't be defined as a single value. To give an expression for a governing equation for the friction factor would be extremely complicated, as well as very optimistic.

Furthermore, note the second factor. The friction coefficient is dependent on temperature. Recall that this process is attempting to define heat liberation. The heat liberation in the process will be used to determine temperature through the body. This is a

problem. The heat liberation is dependent on the friction factor, but the friction factor is dependent on the temperature as well as many other qualities. Interrelationships such as this one between the friction factor and the temperature result in a very difficult problem. Understanding friction welding from an analytical sense quickly becomes very difficult, and it appears as though physical testing is probably the best way to go about solving this problem.

Published Welding Guidelines

Specific guidelines for friction welding are difficult to find. Most commonly, tables of parameters that worked for certain situations are given. The study at hand is looking at materials of a size that has not been tabulated. Most existing literature outlines parameters for materials getting down to 2 cm in diameter. If there are any published full range parameters, they would be important to know about.

The American Society of Metals has a handbook that gives some friction welding guidelines. ASM handbook Volume 6, Welding, Brazing, and Soldering is the particular volume of interest. The following looks at these guidelines and observes how they apply to the study at hand.

Stainless steels have nearly the same values of operating parameters as carbon steels. The ASM handbook outlines three stages to the welding process. The initial phase is when contact is introduced and the friction heating process begins; the second phase is the bulk of the friction heating process; the third phase is the upsetting/forging phase. For the second phase, applied pressures are between 83 and 166 MPa for carbon steel. The upset pressure is between 166 and 332 MPa. The first phase is variable, but it is typically

10-20% of the second phase. Surface maximum tangential velocities typically range from 75 to 180 m/min.

The above parameters can then be applied to the samples used in this study. These parameters can be used to calculate operational rotational speeds as well as operational forces. The rotational speed is:

$$\omega(rpm) = \frac{S}{\pi * OD * \frac{1m}{100cm}} \quad [7]$$

Where S is the tangential velocity in m/min, and OD is the outer diameter of the sample in centimeters. Applying this to the samples yields:

$$\omega_{min} = \frac{75\ m/min}{\pi(.317cm) * \frac{1m}{100cm}} = 7{,}500\ rpm \quad [8]$$

$$\omega_{max} = \frac{180\ m/min}{\pi(.317cm) * \frac{1m}{100cm}} = 18{,}000\ rpm \quad [9]$$

The samples have an inner diameter of .14 cm. This is used to back out the applied force.

$$F = P * A \quad [10]$$

Where F is the applied force (N), P is the applied pressure (MPa), and A is the area (cm^2). For the upset pressure, the following is the range of applied forces.

$$F_{max} = 332MPa * \left(\frac{\pi}{4}(.317cm^2 - .14cm^2)\right) = 2{,}100\ N \quad [11]$$

$$F_{min} = 166MPa * \left(\frac{\pi}{4}(.317cm^2 - .14cm^2)\right) = 1{,}050\ N \quad [12]$$

On first glance, the parameters calculated with the ASM guidelines seem large. The rotational speeds are very high. The minimum rotational speed is 7,500 rpm. This

speed is larger than what common mills and lathes are capable of. These speeds beg the question of the validity of the ASM guidelines. Although it is not specified in the handbook, there is a possibility that the guidelines do not apply to the range of dimensions in this study. Furthermore, ASM suggests that the rotational speeds should be slightly increased for tube-to-tube welds; the previous guidelines were for bar-to-bar welds.

Statistical Design

Running experiments with many variables can be a daunting task. In this study, there are many parameters that can be set to many different levels. The overall goal of this study is to optimize several physical characteristics of the weld. One option to investigate this process would be to vary each parameter one at a time. In this study there are seven different parameters. Changing these one at a time would be very time consuming. It would also be expensive; the amount of samples needed for these test would be quite large. Instead of pursuing this path, a statistical testing approach was used.

Orthogonal Arrays

Extensive research in the past has been performed with the interest of running experiments efficiently. One of the most dominant statistical methods begins with orthogonal arrays. Consider two arrays with one column and eight rows apiece. Each array only contains either the number 1 or the number 2. When these arrays are placed

next to each other, there are four possible numeric combinations: (1,1), (1,2), (2,1), and (2,2).

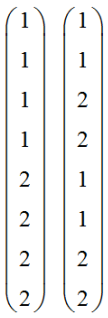

Figure 11: Two orthogonal arrays.

When these combinations "appear with the same frequency, we say that these two columns are balanced, or orthogonal" (Taguchi, 1987). The arrays in Figure 11 are orthogonal to each other.

Applied to a testing system, each array represents a parameter, or factor. Each factor has a predetermined high and low value. The optimal value for each factor needs to lie within this range of the high and low values. From the figure above, each row of orthogonal arrays represents a singular test. The first and second rows indicate tests run with each parameter at its respective low value. The third and fourth columns represent tests run with the first factor low and the second factor high. If the pairs are looked at in each row, it can be seen that the combinations (1,1), (1,2), (2,1), and (2,2) all occur twice. The repeated combinations in Figure 11 are redundant, but they help set up an expansion.

For every new factor, a new column is added. A set of orthogonal arrays for the factors used in this study would look like Figure 12.

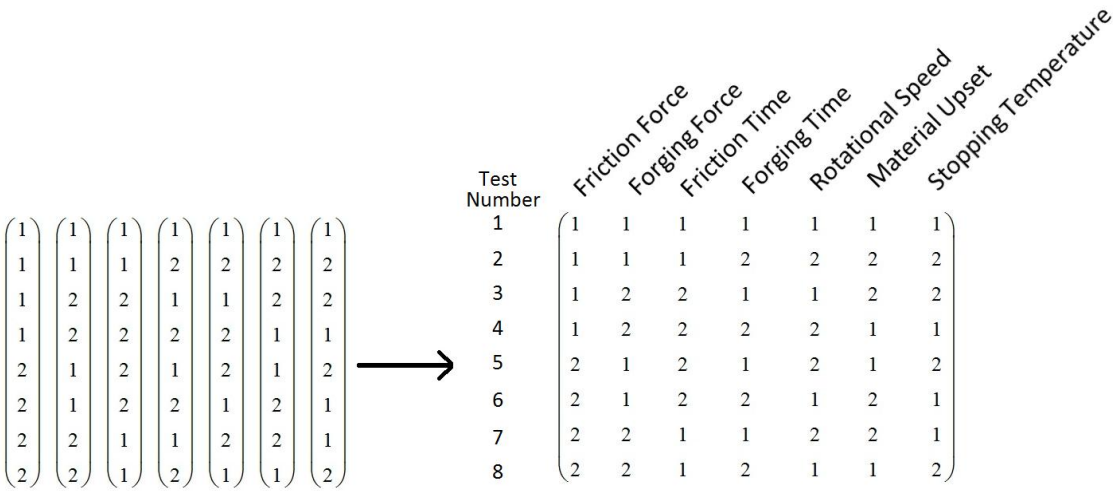

Figure 12: A set of orthogonal arrays to test all the parameters at high and low values. Each row represents one test.

Each test, 1-8, has various levels of each different factor. Preliminary testing was performed in order to reduce the above testing matrix. The DESIGN OF EXPERIMENTS chapter gives a thorough explanation of the reduction of variables, and a simplified version is presented here.

Consistently varying all the process parameters could be a difficult task. If several of the parameters could be seen as less important than others, a reduced set of orthogonal arrays could be developed. The friction time, material upset, and maximum temperature are all related to each other. Controlling one will leave the other two to be measured values. This can remove two columns this process will not be optimized based on time, so the forging time could be set to a constant value. The theory used in this study was that the friction stage is responsible for getting the process to a certain state (upset, temperature). Different combinations of friction force and rotational speed could do this, but setting these as constant values would be appropriate. Furthermore, it has been suggested that rotational speed was not a crucial factor; different levels can achieve

similar results (Vill, 1962). The resulting set of orthogonal arrays looks like the following.

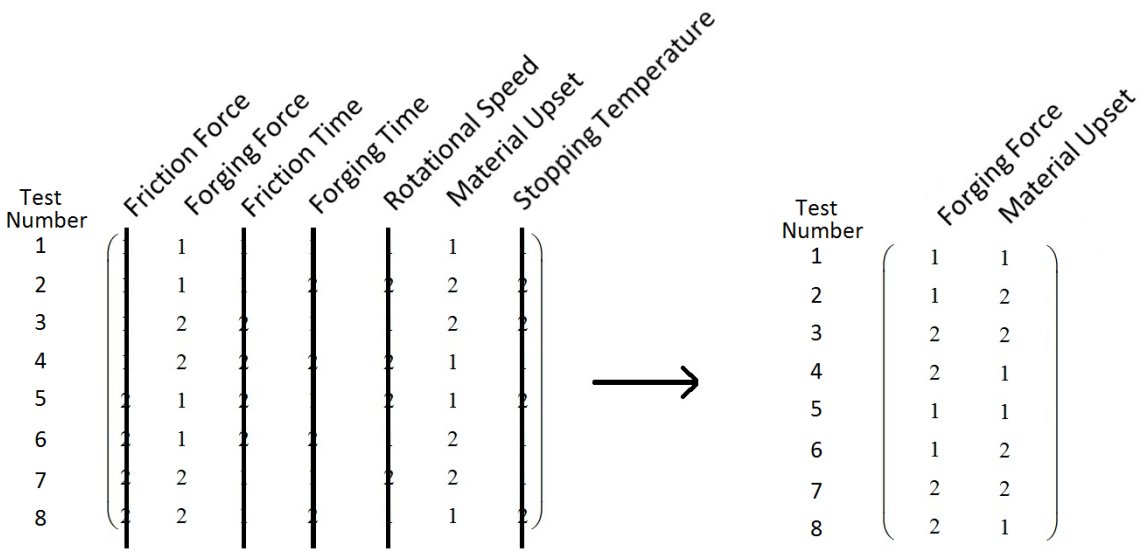

Figure 13: Assuming some parameters can be left constant and others will simply be measured, the orthogonal arrays can be simplified.

The system is back to two arrays, and the redundant combinations still exist. The redundant combinations can be removed from the arrays, and two truncated arrays remain. These arrays represent four different tests. These four tests can be presented in a rearranged testing matrix.

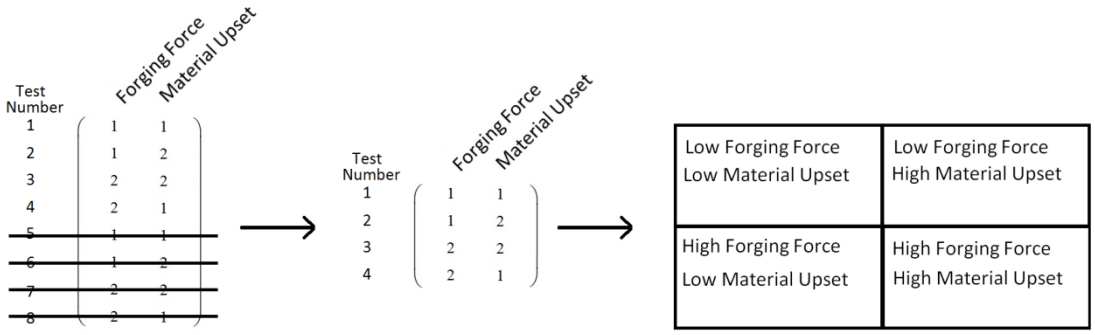

Figure 14: Final development of a sample testing matrix.

Main Effects and Interactions

The goal of running experiments with orthogonal array design is to efficiently understand how different parameters affect the results. Some of the most important outcomes from the orthogonal array design are the main effects of the factors. The main effect of a factor "is the mean of the effect by that factor on the experimental values, taken over the various levels of the other factors." (Taguchi, 1987). The main effect of a factor A is the difference between results when A is high and when A is low.

Take a step back from the friction welding variables, and introduce factors A and B. the testing matrix changes to look like Figure 15.

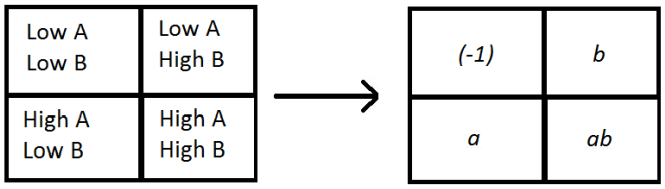

Figure 15: The variables (-1), a, b, and ab have been used to generalize the effect calculations.

The letter combinations *a*, *b*, *ab*, and *(1)* represent the totals over n tests with factor A high, B high, A and B high, and A and B low, respectively. The main effects of A and B can be represented mathematically.

$$main\ effect\ of\ A = \frac{a + ab}{2n} - \frac{b + (-1)}{2n} = \frac{1}{2n}[a + ab - b - (-1)] \quad [13]$$

$$main\ effect\ of\ B = \frac{b + ab}{2n} - \frac{a + (-1)}{2n} \qquad [14]$$

$$= \frac{1}{2n}[b + ab - a - (-1)]$$

Another advantage to this method is the ability to observe the interactions between variables. The interaction is found by taking the averaged differences of the diagonal terms of the testing matrix.

$$AB\ interaction\ effect = \frac{ab + (-1)}{2n} - \frac{a + b}{2n} \qquad [15]$$

$$= \frac{1}{2n}[ab + (-1) - a - b]$$

The interaction looks at how the results vary when one factor is held constant and the other is allowed to vary this can perhaps be explained easier graphically. The high and low values will be represented by (+1) and (-1) instead of (2) and (1).

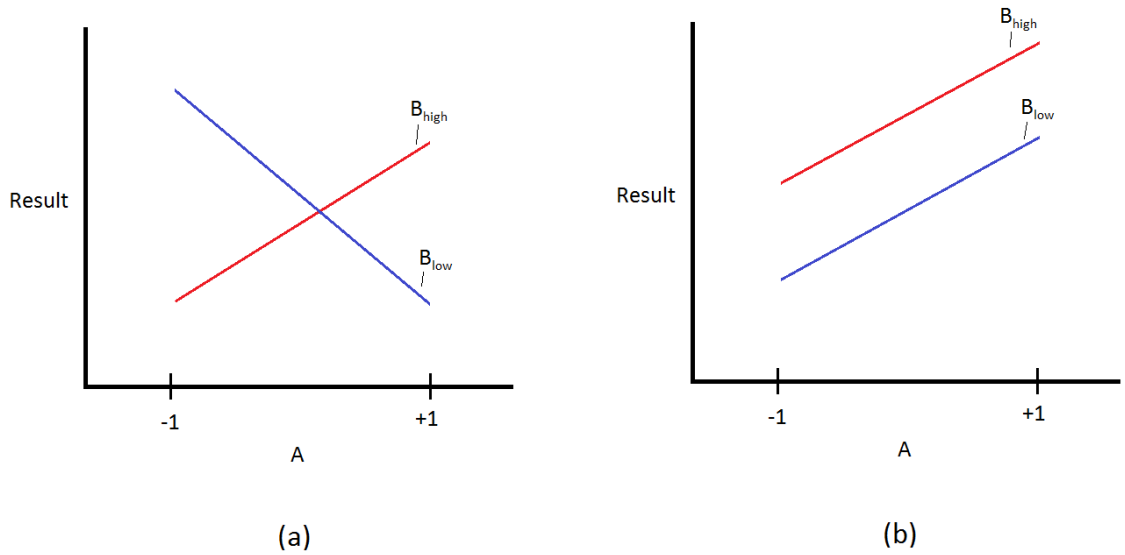

Figure 16: An example of effects. (a) shows a lot of interaction, while (b) shows no interaction.

In the above figure, (a) has a lot of interaction, while (b) has no interaction. In (a), the effects on the result from factor A change when B is changed from low to high. In (b), the effects of A are not changed when B is changed. The result increases as A increases, no matter the level of B. understanding interactions can help lead to a better understanding of the overall system.

Result Verification

Each effect needed to be statistically checked to see if it was valid. This was done by analyzing the variances of the data. The variance is essentially how far each sample deviates from the sample mean. Then, the overall variance of each test was the average of the sample variances. Most tests were run at four operating conditions, so the overall variance was the average of these four sample variances. Then, the estimated standard error of each effect was found (Montgomery, 2007).

$$se = \sqrt{\frac{\sigma^2}{n}} \qquad [\ 16\ ]$$

The term n was the number of samples for each operating condition; "se" represents the estimated standard error; σ^2 represents the overall variance.

The standard error was then used to determine confidence intervals for each effect. Based on a normal distribution, each level of confidence has a corresponding standard error multiplier. This multiplier represents the range of data that would satisfy the confidence interval. For example, a confidence interval of 95% has a corresponding multiplier of 1.96. This means that the interval resulting from any data point plus or minus 1.96*se will contain the sample mean 95% of the time.

The effects and interactions were compared to the possibility of zero influence. If the confidence level for an effect contained the numeric zero, the effect or interaction was determined insignificant. For example, consider effect A to be valued at 5. The standard error is 2.7. The 95% confidence level would be:

$$5 \pm (2.7 * 1.96) = \text{the range from } (-.292)\ to\ (10.292) \quad [\ 17\ ]$$

Since the confidence interval contains the value zero, it can be said that the effect A has little statistical significance.

Testing Configuration

The following is an overview of the friction welding setup used in this report. The testing was done in room 130B in the Engineering and Physical Sciences building at Montana State University, Bozeman, MT. The testing setup was used in the spring of 2013. There were several key components of the testing setup. The physical setup will be gone through in detail so it could be repeated if necessary. The physical system includes all the model numbers of each instrument. All necessary dimensions will be given. Secondly, a thorough explanation of the wiring will be covered. This includes information for every instrument used in the test setup. The setup should be able to be duplicated with reference to the wiring section. Lastly, a LabVIEW program was used to control and monitor the entire process. This will be gone through in detail as well.

Physical Setup

A load cell was used to measure the axial force through the experiment. The load cell was model 1010AJ-500-B made by Interface. It has a 2200 N (500lbf) maximum

limit. From preliminary testing, it was found that a 2200 N load limit will be sufficient for friction welding of the samples under investigation. A collet holder bracket and a base plate were both bolted to the load cell with 5/8-18 bolts. The mounting configuration can be seen in the following figure.

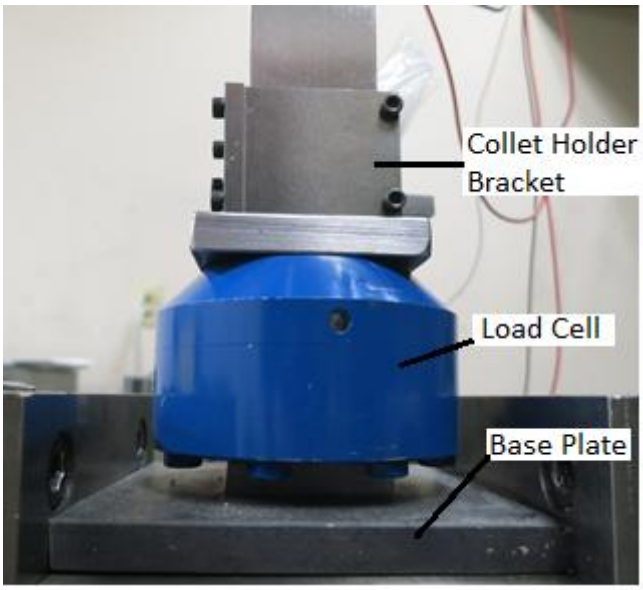

Figure 17: Load cell tower.

Displacement was measured with a linear voltage displacement transducer (LVDT). The LVDT was model number LD621-30 by Omega. It had a range of 30 mm and a sensitivity of 332.826 mv/mm (calibration sheet provided by manufacturer). The displacement in each individual test was very small, so the range of the LVDT was more than adequate. It was also found in preliminary testing that the sensitivity of the LVDT was very precise with respect to the welding experiment. The LVDT was mounted to the mill with a magnetic tool holder. The magnetic tool holder that was used was purchased as part number 1958A31 from mcmaster.com. Figure 18 shows the LVDT configuration.

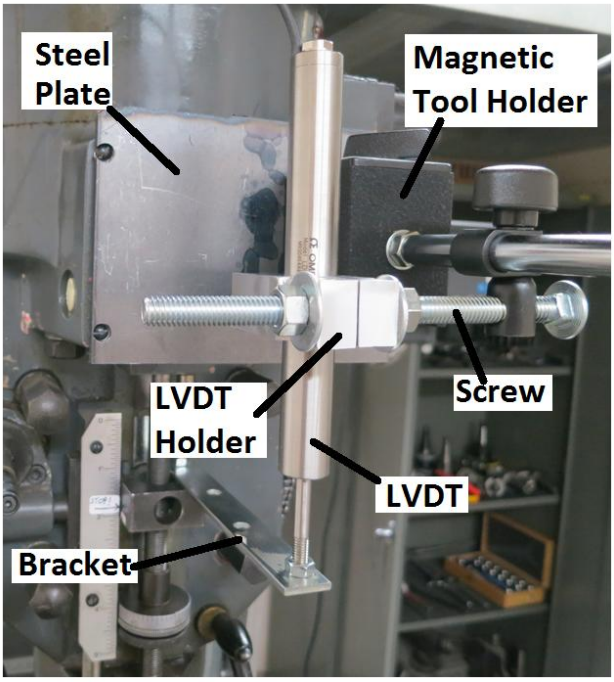

Figure 18: LVDT configuration.

The nameplate on the mill was unscrewed and replaced with a steel plate. The steel gave the tool holder a magnetic surface to adhere to. One of the mounting arms on the magnetic tool holder was replaced with a long screw. An LVDT holder was placed on this screw.

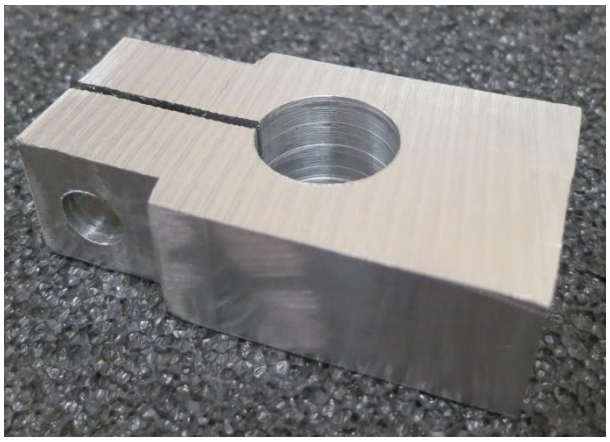

Figure 19: LVDT holder.

The LVDT holder was secured by compression from two nuts. In this way, the LVDT was held in place in a very solid fashion. A metal bracket was mounted to the vertical guide on the mill. This bracket was attached to one end of the LVDT. In this way, the LVDT recorded the displacement of the system.

Temperature throughout the experiment was obtained by infrared measurements. The tool used for this was a Raytek MI3 LTF infrared temperature sensor. A close focus lens was used in order to decrease the spot size of measurement. The optical resolution of the thermometer sensor with the close focus lens can be seen below. Due to the small size of each sample, it was very important to have a consistent location of the sensor. Figure 20 shows how the temperature sensing head was set up.

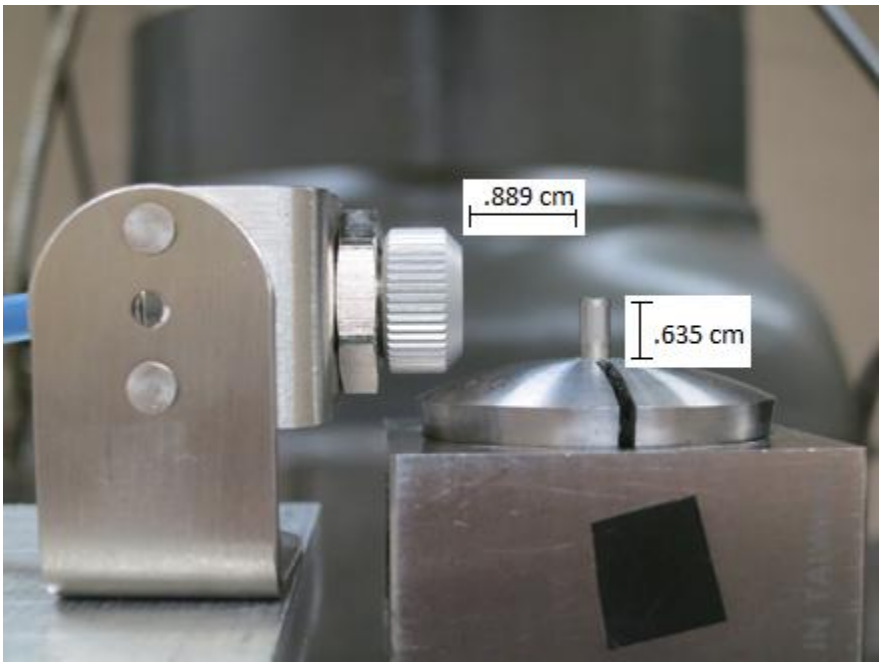

Figure 20: Configuration of the optical thermometer.

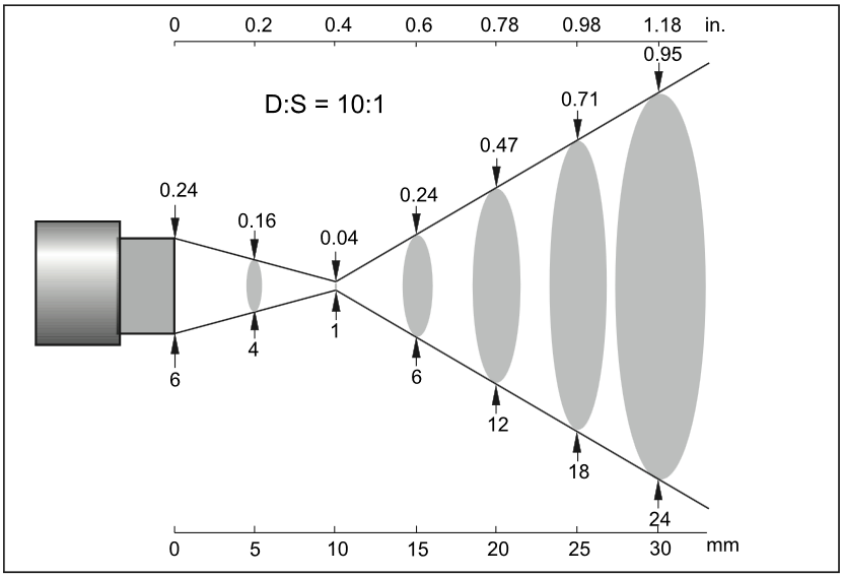

Figure 21: Optical chart provided by the manufacturer. This is with the close focus lens.

The emissivity and transmissivity were controlled on the communication box included with the temperature sensor. The emissivity was set to .6; this significance will be discussed later. Ordinarily the transmissivity would be set to around 1, but with a close focus lens attached, the transmissivity setting was .75.

A DC electric gear motor was used to control the amount of force axially applied to the friction welding. By controlling the current available to the motor, the output torque was controlled. This torque was run through a gear ratio to apply a torque to the activation arm axis of the mill. Pictures of this process will be shown shortly. The motor used was ordered as part number 6409k26 from mcmaster.com. Important information regarding the motor includes 25 rpm max, 24 VDC, 5.65 Nm torque, and 1.08 amps at full load. The motor and the sprockets were mounted to a bracket made in-house. The sprockets that were used were both ordered from mcmaster.com. Part numbers were 2737T2 and 2737T332. The following table gives the dimensions of the sprockets.

Table 2: Sprockets for the Axial Load Application

	No. of Teeth	Bore Size	Outer Diameter	Hub Diameter
2737T2	10	.64 cm	2.34 cm	1.27 cm
2737T332	54	1.59 cm	11.28 cm	5.08 cm

The hub diameter on the larger sprocket had to be turned down to 2.54 cm; the hub had to fit into a hole in the mill. This process was done on a lathe. Both of the bore sizes of the sprockets had to be increased slightly in order to fit around the shafts of the mill and the DC electric gear motor. This procedure was done with drill bits on a separate mill. Assuming no losses due to friction or internal resistance of the mill, the following gives an outline of the axial force range of the setup.

Constant torque was applied to the mill activation arm, and the resulting axial load through the load cell was recorded. This was done by hanging weights at a designated position on the mill activation arm. These weights resulted in a torque about the activation arm. The loading scenario can be seen below.

Several data points were collected, and a linear trendline was developed.

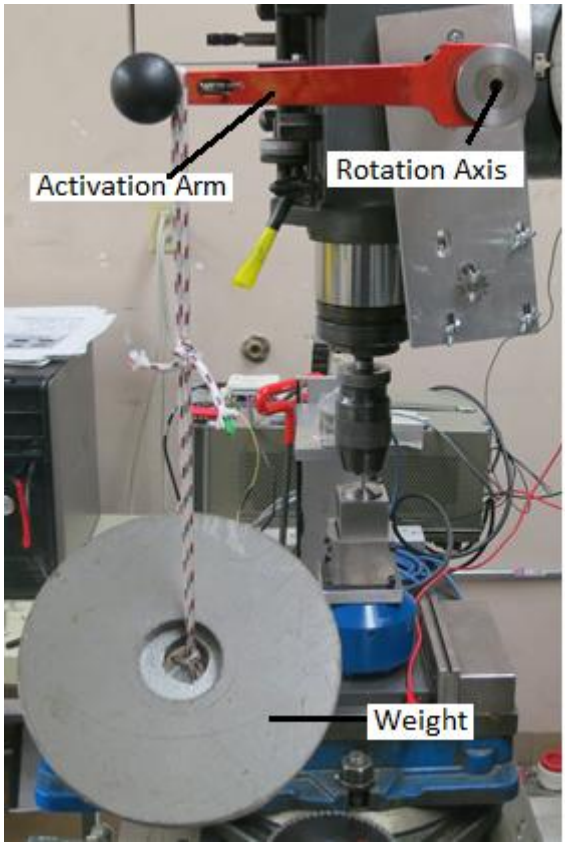

Figure 22: Developing a relationship between torque and axial load.

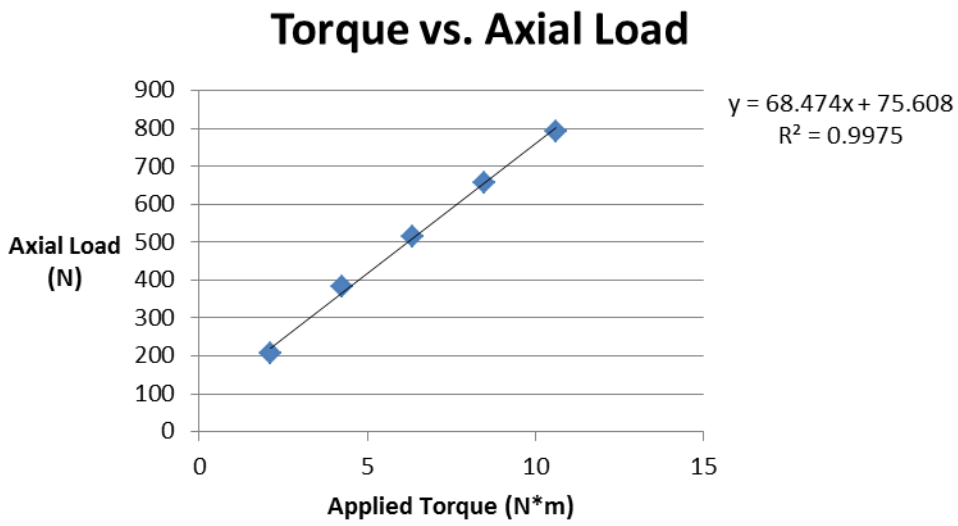

Figure 23: A linear fit was found between the torque about the activation arm axis and the applied axial load through the samples.

As can be seen from the above figure, the relationship between applied torque and axial load is very linear. The resulting linear relationship was used to determine the maximum axial load that the motor could provide to the friction welding sample.

$$axial\ force = 68.474\frac{1}{m} * torque + 75.608\ N \qquad [\ 18\ ]$$

$$\max torque\ available: 5.65\ Nm$$

$$gear\ ratio: \frac{11.3\ cm}{2.3\ cm}$$

$$maximum\ axial\ force =$$

$$\left(5.65\ Nm * \frac{11.3\ cm}{2.3\ cm} * 68.474\frac{1}{m}\right) + 75.608\ N \qquad [\ 19\ ]$$

$$= 1980\ N$$

Based on manual preliminary testing, this axial force will be adequate. In order to get a better picture of the entire sprocket system, several pictures are provided below.

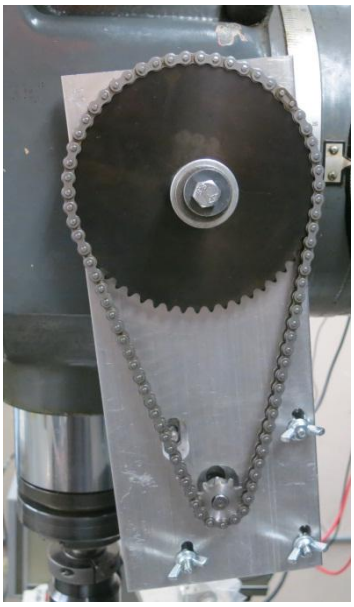

Figure 24: The torque from the motor was amplified.

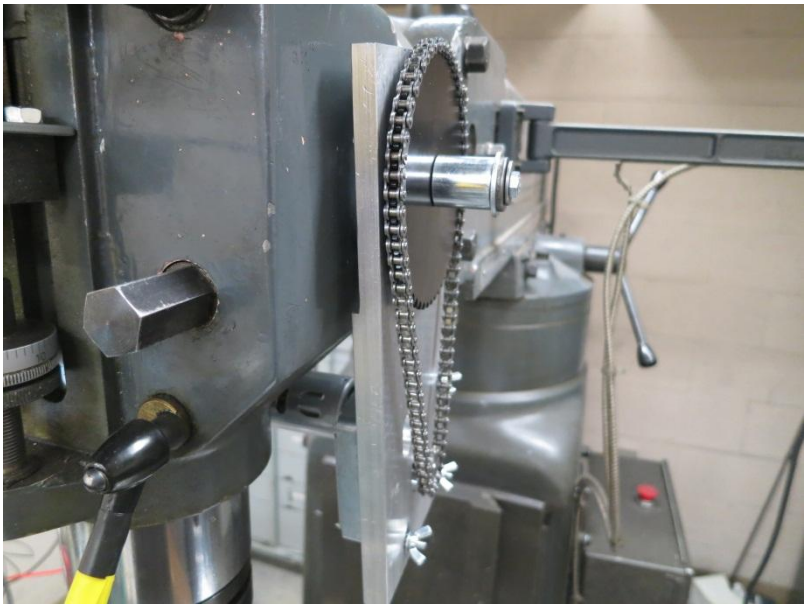

Figure 25: The motor can be seen on the backside of the mounting bracket.

Slight modifications to the mill had to be done in order to mount the sprockets. The rotational axis where the large sprocket rotates about was the same axis that the manual application lever rotated about. The manual control arm was removed. Several spacers were used in order to align the sprocket in the correct position. A picture showing the spacer assembly is shown below. This setup was for the large sprocket.

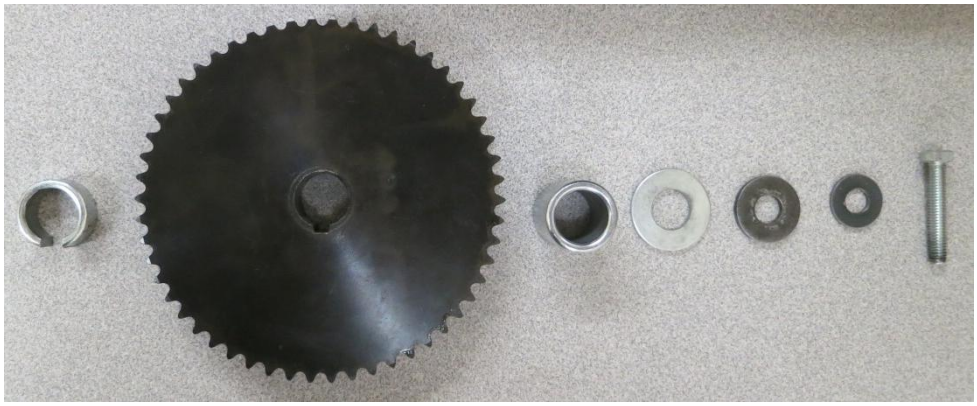

Figure 26: Disassembled spacers.

Figure 27: Assemble large sprocket.

The small sprocket was simply mounted onto the drive shaft of the DC electric motor. It was held in place with a set screw.

The mill used was a Republic Lagun Deluxe three axis mill. Only one axis was of importance for this study. It had a variety of rotational speed settings. The range of interest for this study was between 500 and 1800 rpm; the mill met these requirements. One critical factor about the mill was the alignment. It was of utmost importance that the two samples were perfectly aligned and perfectly parallel. The mill had rotational adjustments to adjust the head of the mill in two rotational directions (back and forward and side to side). These adjustments were made in order to get a perfectly parallel system.

A dial gage was placed on the drill chuck in the head of the mill. Then, the gage was run up and down the square edge of the collet holder to see if the gage changed readings. At first the gage would change substantially. The mill head was rotated and adjusted so that the dial gage would read a constant value when moved along the entire

length of a sample. The rotational adjustments on the mill were used to get close to accurate. For fine adjustments, small aluminum spacers were strategically placed under the base plate of the load cell. See Figure 28 for a visual of the gauge alignment method.

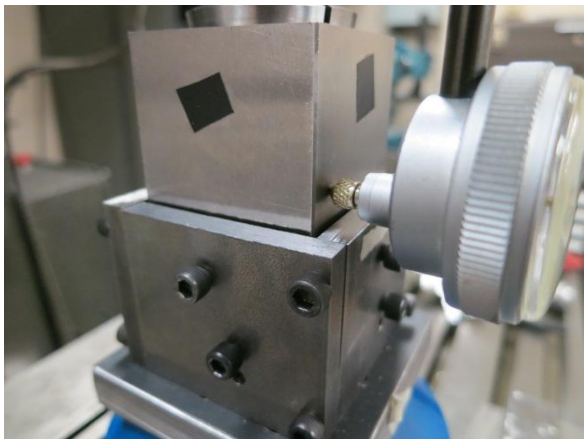

Figure 28: Ensuring the samples were properly aligned.

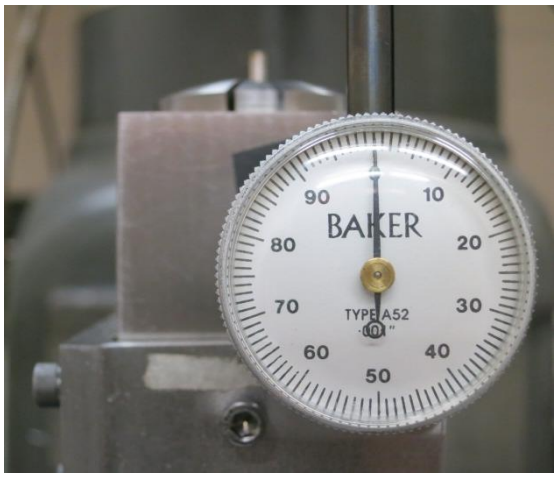

Figure 29: The samples were aligned when the dial didn't move as the vertical position changed.

The top and bottom sample will be held in slightly different manners. The bottom sample was held in place with a 5C .317 cm (1/8 in) collet. This collet was placed in a

collet holder and secured with some threading. This assembly can be seen in the following figure.

Figure 30: Collet assembly.

A collet bracket was made to hold the assembly in place. It was made slightly larger than the assembly so that the collet assembly could easily slide in and out of the bracket. The assembly was held in place with set screws. A steel spacer was used to prevent the sample from slipping in the vertical direction. This spacer rests against the bottom of the collet bracket.

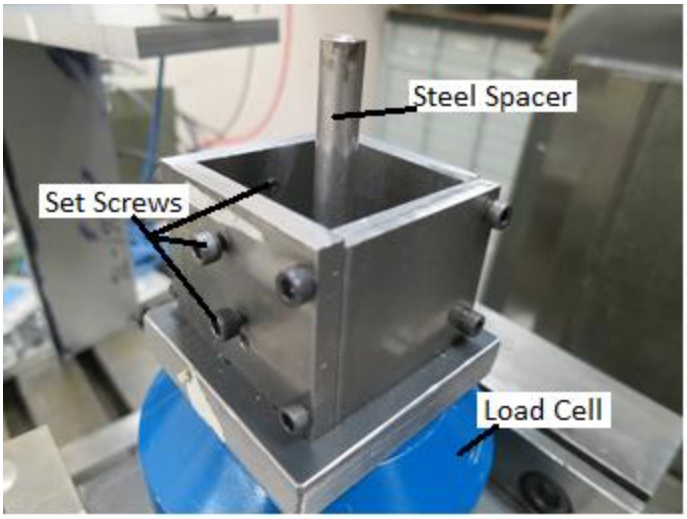

Figure 31: Collet bracket.

The top sample was held with a drill chuck. A spacer was used to prevent this sample from slipping upwards. This configuration can be seen in Figure 32.

Figure 32: Assembly to hold the upper sample in the drill chuck.

The drill chuck was tightened by hand, and the sample in the collet was tightened with a collet wrench. Both of these sample holding methods went through several iterations of design, and the presented design was the most efficient and effective.

A signal conditioner was necessary to amplify the voltage output from the load cell. The conditioner that was used was model DMD4059 from Omega. The signal conditioner was powered by a wall outlet. It then powered the load cell with 0-10 VDC. The load cell had an output rating of 1.0 mV/V input, so the load cell would be outputting voltages in a range of 0-10 mV. To use the signal conditioner as an amplifier, several rotary switches on the side of the conditioner had to be set. The switches were set to code AA03. This meant that inputs were in the range of 0-10 mV, and the conditioner would scale these values to outputs in the range of 0-10V. These voltages were then read by LabVIEW.

The DAQ that was used was a National Instruments USB-6008. This DAQ had 8 analog input channels and 2 analog output channels. The inputs were used to collect

information from the LVDT, temperature sensor, and load cell. One output channel was used to send an output voltage to a power supply.

The power supply used was a Hewlett Packard 6033A. This was the tool that sent a current to the DC electric motor. It would send a current that was proportional to the controlled input voltage. Essentially, LabVIEW would send the power supply a voltage. The power supply would respond by sending a proportional amperage to the DC gear motor.

Lastly, one small component that was used was a 16-23 VDC power converter. This was plugged into a wall outlet and would provide a constant VDC voltage. This voltage was used to power both the temperature communications box and the LVDT. The power converter was made by Omega; the part number was PSU-93.

Wiring Detail

Many wiring connections were used in this study to connect various instrumentation components. Also, many of the instruments used in this study have extra terminals that were not used. Figure 33 gives a general wire diagram for the entire electrical setup used. For each instrument, only the terminals that were used are shown. The colors indicated on the inside of the instrumentation boxes are related to permanent fixtures in each instrument. Colors that are indicated on top of wires are to show wiring colors.

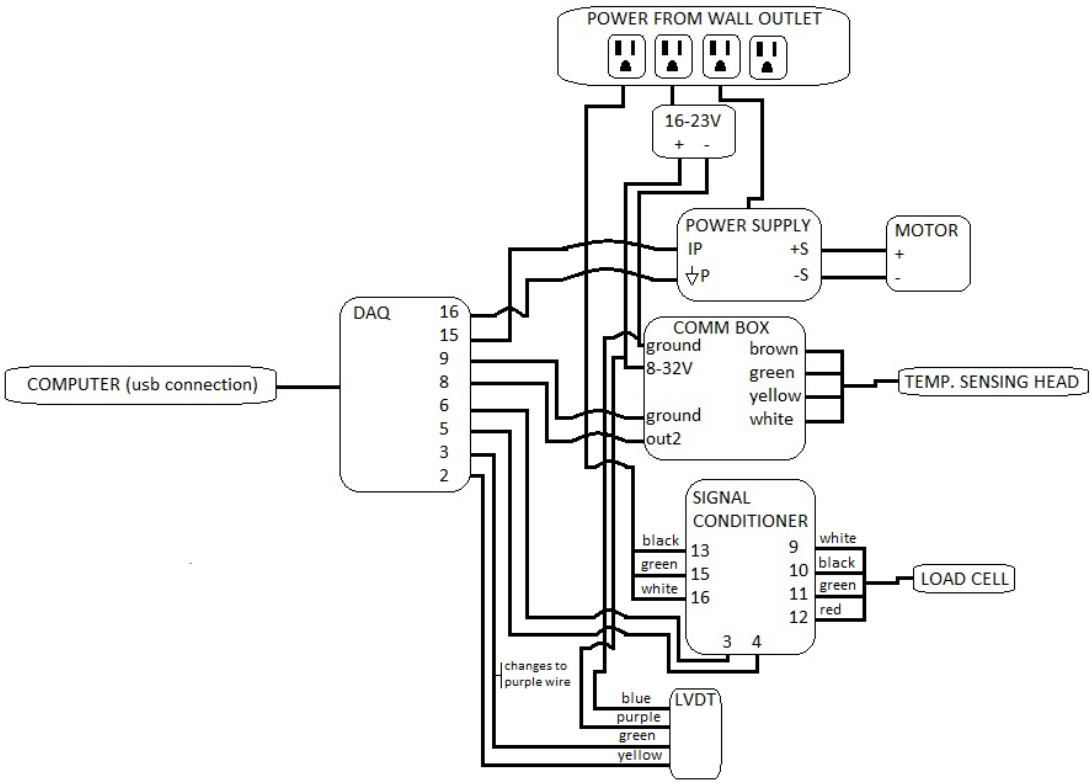

Figure 33: Wiring detail for the control and monitoring aspects of the friction welding procedure.

The general flow of the wiring diagram should be fairly straightforward. Start at the top and work downward. A power strip is used to provide three outlets. One wire from the power strip goes to the signal conditioner, one has the Omega 16-23 V device plugged into it, and the last one has some wires connected to the large power supply. The Omega 16-23 V device outputs a constant output voltage and sends this to the COMM box and the LVDT. This is the power supply for both of these devices. At this point, all the devices have power.

Next, start with the DAQ and work left to right. The output voltage channel uses ports 15 and 16. This output channel sends a controlled voltage to the power supply.

Then, the power outputs a proportional amperage to the motor. In this way, the torque of the motor was controlled. Three input channels were used. One channel was used for the LVDT, one for the signal conditioner, and one for the COMM box. The DAQ then connects to the computer via a USB cable. In this way, both controlling and monitoring systems were implemented in the test setup. Table 3 gives a concise description of what models were used for different instruments.

Table 3: Summary of Equipment Used

Diagram Label	**Brand and Model Number**
Computer	Dell Running Windows Vista and LabVIEW 8.5.1
DAQ	National Instruments USB 6008
16-23 V	Omega PSU-93
Power Supply	Hewlett Packard 6033A
Motor	Molon CHM-2425-1M
Comm Box	Raytek MI3COMM
Signal Conditioner	Omega DMD4059
LVDT	Omega LD621-30
Load Cell	Interface 1010AJ-500-B
Temp. Sensing Head	Raytek MI3LTF with close focus lens

LabVIEW Program

The entire friction welding process for this study was controlled and monitored by LabVIEW version 11. Three primary VI files were used. Time control, upset control, and temperature control based tests all had their own VI programs. All three programs were run with a PID control loop to monitor and apply forces. Measurements of each system included temperature, force, displacement, and time. The following gives a somewhat brief presentation of the controlling codes. The three programs used were all similar. The

time control system will be covered in more significant detail. Then, necessary modifications to utilize a temperature or upset control method will be highlighted.

Time Control System. Figure 34 shows the block diagram of the time control system.

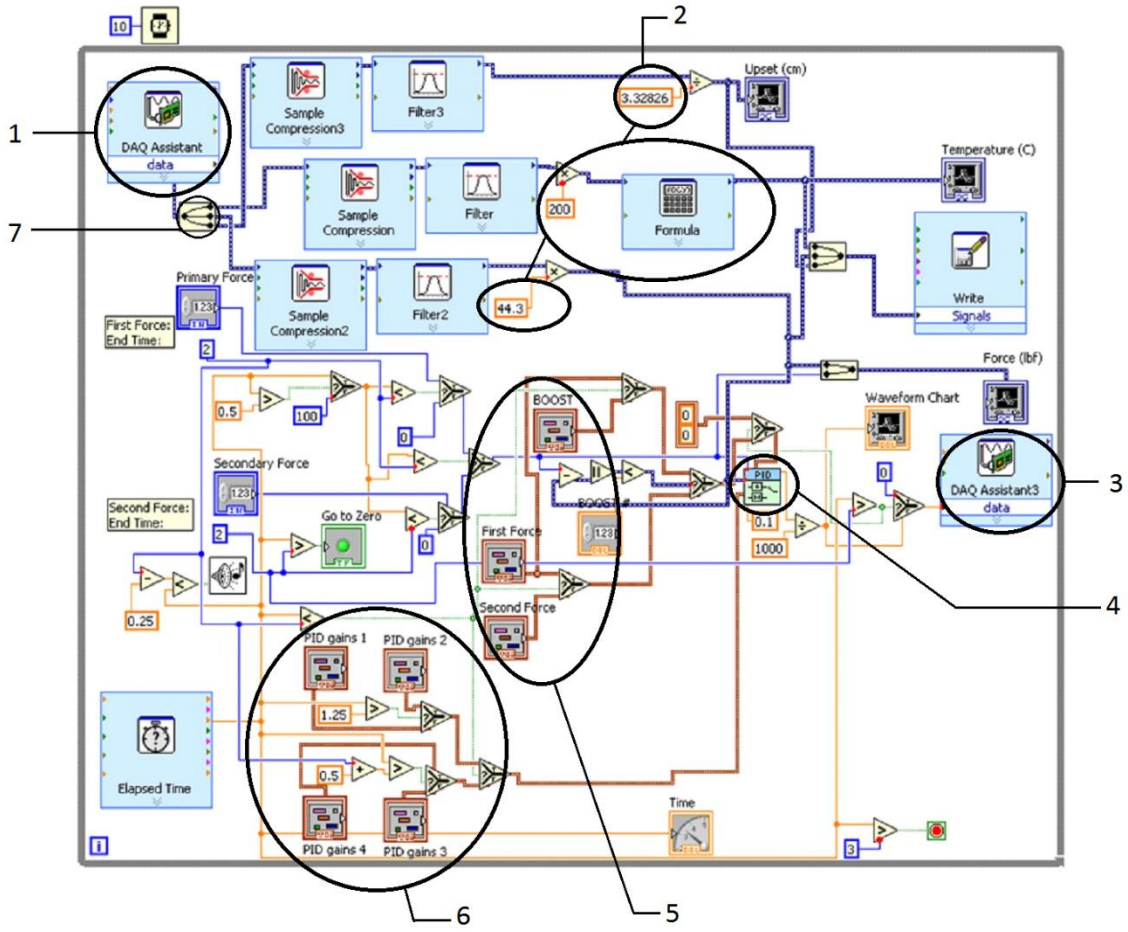

Figure 34: LabVIEW block diagram for a time control system.

Figure 35 displays the accompanying front panel for the time control.

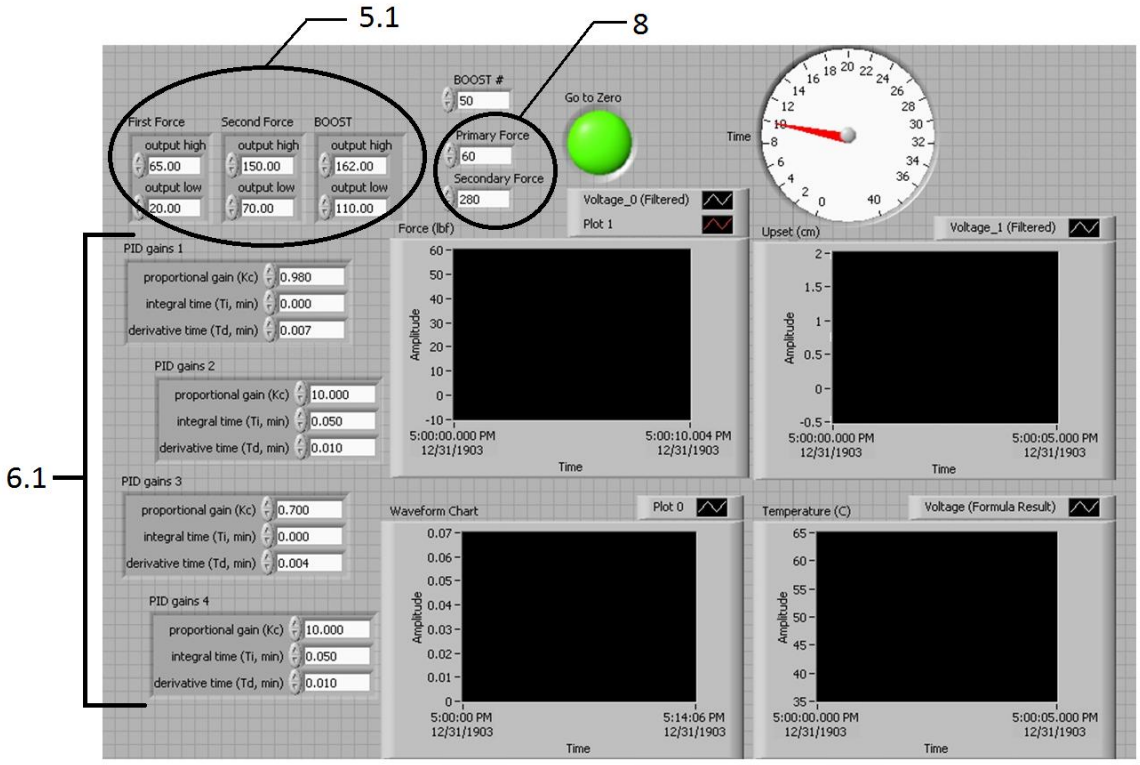

Figure 35: Front panel for the time control system.

Reference numbers in the above figures will be used for further discussion. In Figure 35, the labels 5.1 and 6.1 correspond to labels 5 and 6 in Figure 34. There were three essential elements used in this system: DAQ Assistant (1), PID (4), and DAQ Assistant3 (3). The DAQ Assistant (1) records and receives data from the system. Three differential channels were used on the DAQ itself. These channels, in order, are Temperature, Force, and Upset. The DAQ Assistant sent the data to a signal splitter (7). Data from each channel got filtered and compressed. Each string of data got adjusted based on calibration factors (2). Then, each string of data was sent to both a display chart and a text file output. The text file was used later for data analysis purposes. The remainder of the VI was used for the PID control loop.

The PID control (4) has several inputs and outputs. As can be seen in the figure below, there are several defining inputs that dictate the operation of the PID control loop.

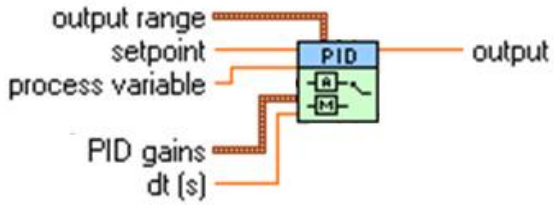

Figure 36: PID control VI

The PID available in LabVIEW had several other input options as well, but none of the other options were used. They were removed from Figure 36 for clarity purposes. The setpoint is the desired value. In this case, it was the desired force level. Force levels were set in the front panel (8). Load cell readings were delivered into the process variable port. PID gains control how the PID reacts to differences between the setpoint and the process variable. The PID gains can be seen as labels 6 and 6.1 in Figure 34 and Figure 35, respectively. An output value was then sent from the PID control. For this study, the outputs correspond to the level of current given to the gear motor. Different output ranges can be seen as labels 5 and 5.1 in Figure 34 and Figure 35, respectively. Different stages of the welding process required different gains and output ranges.

A time value was needed for PID calculations; this value came from the dt input in the PID schematic. Often times the input here is left blank, and the dt used is the system loop time. Best controlling results were achieved by fixing the dt and varying sampling rates and other PID parameters. The output from the PID program was then sent to DAQ Assistant3 (3). This DAQ Assistant then sent out a voltage to the motor power

supply. This process was continuously looping and making necessary adjustments to achieve appropriate force levels.

Temperature Control. Peviously, force levels, PID gains, and PID output ranges were all dictated by time. Several conditional statements carried out this logic by comparing the current time to constant times. For instance, the user could decide the forging force should be applied after five seconds. Once the current time exceeded five seconds, the forging force would be applied. This was fairly easy to do for time control. The time was always increasing, so once a threshold was achieved, there was no chance of the system reverting back to the original parameters. Friction Force

Complications with this method presented themselves when temperature control began. Basic comparisons had flaws. Consider the following. Once a certain temperature was achieved, say 500 °C, the force should increase to the forging force level and the rotation should stop. The forging force was applied, but the temperature began to decrease due to the rotation stopping. Once the temperature was below 500 °C, the code would try to reduce the force and apply the friction force. Solving this problem was one of the main modification necessary to run a temperature control system. The solution to this problem can be seen in Figure 37.

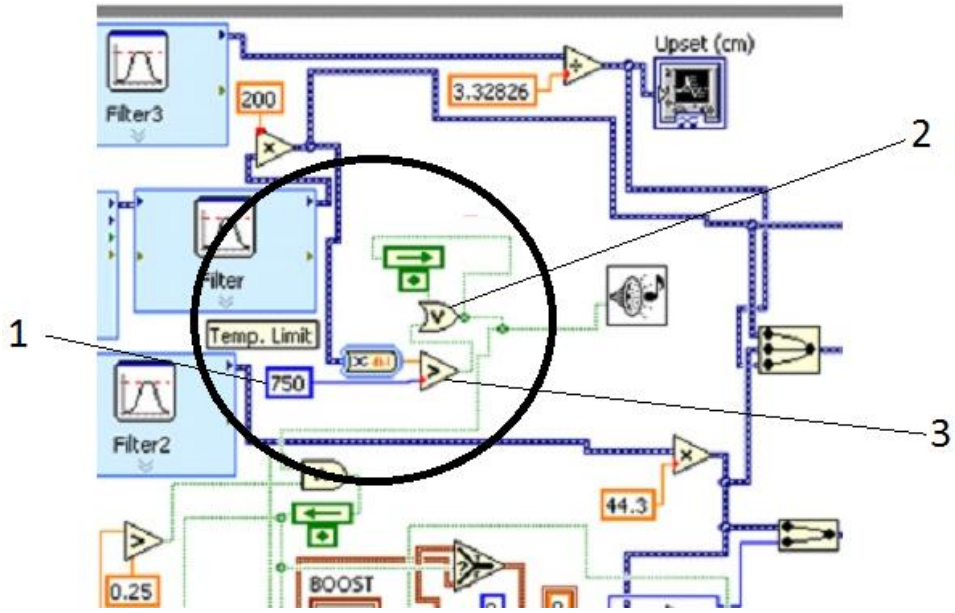

Figure 37: Using a looping OR gate for the temperature control program.

In Figure 37, item (1) is the desired stopping temperature. Item (2) is an OR gate. This gate has two inputs and one output. If either of its inputs are “true” it will output “true”. Notice that the output splits, and one split reconnects into an input port. The other input port is the temperature comparison. When the program starts, a “false” signal is transmitted through the wires. Once the temperature exceeds the temperature limit, the OR gate outputs “true”. This “true” signal the gets looped back into an input in the OR gate. Now the OR gate will infinitely output a “true” signal, and the force levels will not drop back to the friction force level.

Upset Control Several simple modifications to the temperature control had to be made in order to use an upset control. In figure 38, the same OR gate strategy was used (1).

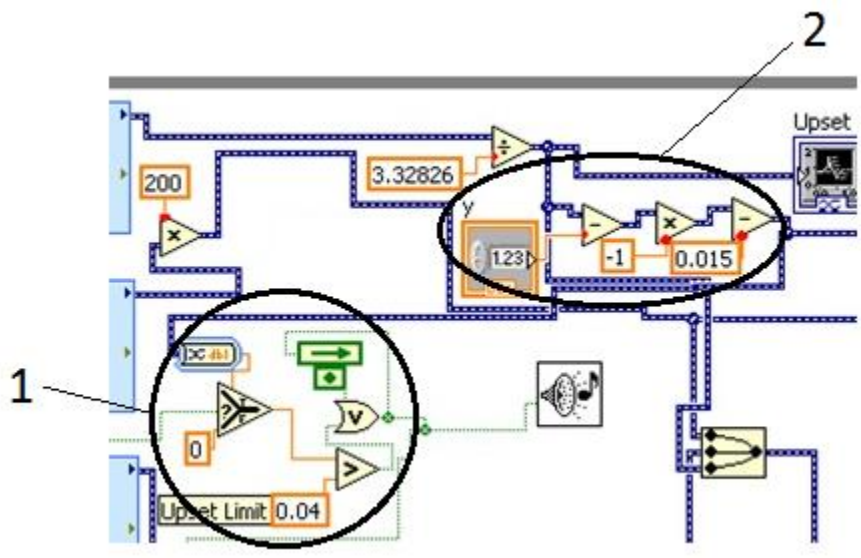

Figure 38: Modifications to enable upset control.

Upset was measured by an LVDT recording displacement. The LVDT starting position had to be subtracted from the recorded data (2). This zeros out the upset measurement. Every time the tests were run, a preliminary LabVIEW code was quickly used to determine the current position of the LVDT. The user then input this value as "y" (2). Based on the physical configuration of the LVDT, its measurements had to be negated. Lastly, the initial distance separating the two samples was also accounted for. With these adjustments, the upset value was sent to the OR gate, and upset control was achieved.

Calibration

Load Cell

The load cell had a range from 0 to 2200 N (500lb). A voltage was sent to the LabVIEW program; this voltage was proportional to a force. A correlation was developed between the output voltage and the axial force applied to the load cell. Weights were put

on the load cell, and the measured force was compared to the force of the weights. After a little trial and error, a scaling factor was found that accurately measured applied forces.

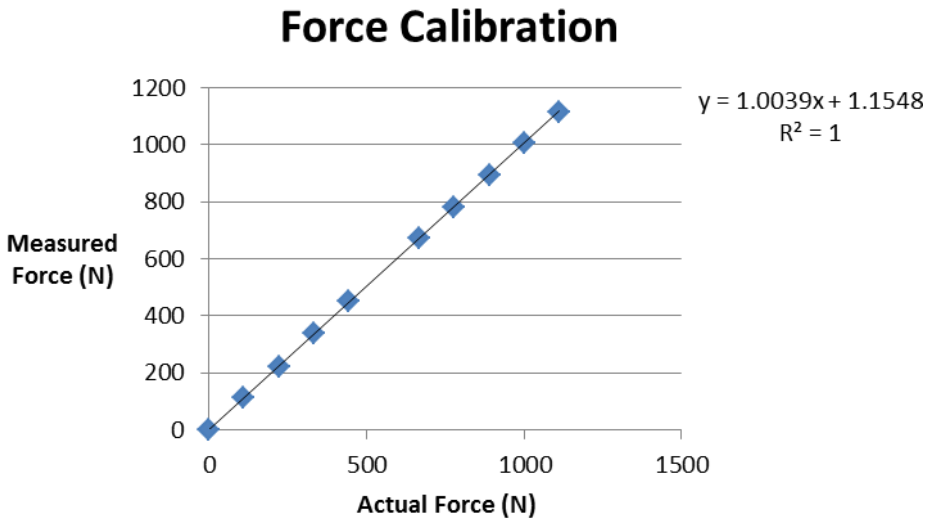

Figure 39: Calibrating the load cell.

LVDT

The LVDT came with some calibration paperwork. It had been tested by the manufacturer, and a sensitivity relating mV output to cm of displacement was available. This sensitivity was used. It was checked several times, and it was proven to be accurate.

Emissivity

Emissivity determination was complex. Emissivity values for samples are of utmost importance when measuring temperatures with infrared thermometers. For more information on infrared measurement theory, reference Introduction to Engineering Experimentation (Wheeler, 2003). In simplest form, the emissivity value characterizes how well materials emit infrared electromagnetic waves. Many infrared thermometers

have adjustable emissivity settings to accommodate the measurement of different materials. The thermometer used in this study did have an adjustable emissivity.

A very small amount of infrared measurement theory will be discussed here. The trends and implications of the emissivity setting on the thermometer need to be understood. “If a higher than actual emissivity value is set, the output will read low, provided the target temperature is above its ambient temperature” (Raytek, 2010). The emissivity setting is a correlation between the amount of energy seen and the reported temperature. If the setting is too high, the sensing head will be expecting to see more energy for the temperature of the sample. It won’t see all the energy that it would be expecting, so it will report a lower temperature. This is easier to understand and explain graphically:

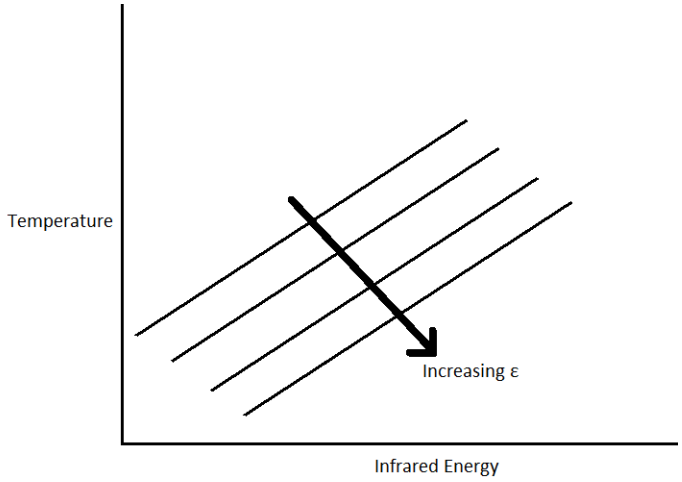

Figure 40: Trends in infrared temperature measurement.

For a given amount of energy seen by the sensing head, the reported temperature will increase as the emissivity setting on the sensing head decreases. The correct temperature

is found after the emissivity setting has been calibrated. The following paragraphs go through calibration tests.

Temperatures drastically increase throughout the friction welding process. It was important to check the emissivity of the sample as it became hotter. There has been some published information about how the emissivity of stainless steel responds to changes in temperature. A paper written by Roger (Roger, 1979) suggests that the emissivity of stainless steel increases as the temperature increases. This is also suggested by tabled values in Incropera (Incropera, 2007). In the studies just mentioned, the stainless steels under investigation were all more polished than the stainless steel used in this study. For this reason, the emissivity values in the studies were substantially lower than those used in this study. There weren't any papers found that outline emissivity and temperature relations for the same style of stainless steel used in this study. Testing was done to determine applicable values.

It should be noted that determining emissivity based on a changing temperature could be a study in and of itself. That being said, an approximation was developed to accurately read temperatures. Two different methods were used to find an acceptable temperature reading. First, some samples were heated up in a controlled furnace. This furnace was set to several different temperatures ranging from 250 ˚C to 1000 ˚C. The samples were heated at these temperatures for several minutes. One at a time, the samples were taken out of the oven and placed in front of the infrared thermometer. Several tests were run with different temperatures and different emissivity values on the thermometer.

A thermocouple was placed on the samples once they were removed from the oven. The thermocouple temperature was taken to be the true temperature. The

differences between the infrared temperature and the thermocouple temperature were used to determine proper emissivity values. This testing showed general trends, but it was not a very precise method. It was also difficult to replicate results. Once the samples start cooling down, the surface oxidizes quickly. This then changes the surface of the samples dramatically. By the time the thermocouple heated up to the sample temperature, the oxidized layer was in full effect. This led to an inaccurate emissivity prediction. An alternate method was used for temperature analysis.

The same furnace was used for this second method. Samples were heated to different temperatures from 400 ˚C to 1000 ˚C. The samples were each cooked for about twenty minutes to make sure that they reached a steady state oven temperature. Then, the samples were quickly placed in front of the infrared thermometer. A rigid sample holder was used to ensure the samples were placed exactly the same distance away from the infrared thermometer each time. The time elapsed from taking the samples out of the oven and putting them in the thermometer position was about half a second every time. The thermometer then recorded the cooling of the samples.

The first several seconds of the cooling process were then plotted and fit with a trendline. The idea here was that the trendline was fit to the data before the samples had a large oxidation effect. Then, the trendline was used to find the predicted temperature of the sample when it was in the oven. A half a second was subtracted from the time of the first temperature data point. This time was determined to be when the sample was at the true oven temperature. This time was plugged in to the trendline equation, and a corresponding temperature was recorded. Differences in the predicted temperature and the oven temperature were used to make a correlation between the infrared sensor and the

true temperature of the samples. For all of this testing, the emissivity was set to a constant value of .6.

Note that this analysis turned out to be a study on the system; this was not a study on emissivity values of stainless steel. The results of this analysis can be seen in the following figure.

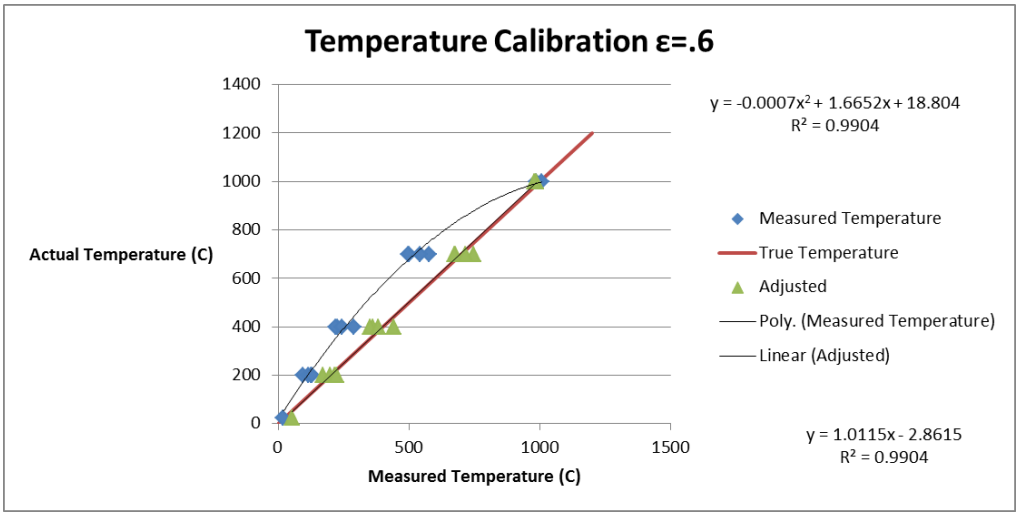

Figure 41: The success of the temperature correcting equation can be seen.

The x axis represents the temperature measured from the infrared thermometer. The y axis represents the oven temperature. The calibration here is similar to the calibration used for the load cell. The blue diamonds are the data points from the testing. The red line is the y=x line; this is the true temperature line. A trendline was fit to the data, and a second order polynomial equation was found. It can be seen that the infrared temperatures are all lower than the oven temperatures. A fitting equation will be used to add temperatures in order to fit the measured data to the actual oven temperatures. The difference between the infrared temperatures and the oven temperatures was found by subtracting one from the other.

$$correction = -.0007x^2 + 1.6652x + 18.804 - x \quad [20]$$

$$correction = -.0007x^2 + .6652x + 18.804 \quad [21]$$

The correction equation was then added to every data point recorded from the infrared thermometer. This correction was added straight into the LabVIEW program. The green triangles on Figure 41 represent the adjusted temperatures. The interesting shape of the trendline is discussed below in the concerns section.

Post Processing

After the welds were completed, several physical qualities were inspected. The amount of material displaced to the center of the hole was analyzed with an area reduction analysis. Weld leak rate was found using a pressurized testing setup. Lastly, ultimate tensile force was found using an Instron load frame.

Hole Reduction Analysis

A simple method was used to identify the through-hole reduction. A photograph looking through the hole was taken of each finished weld. Then, Solidworks was used to trace an area around the remaining hole. Another area was traced around the original hole.

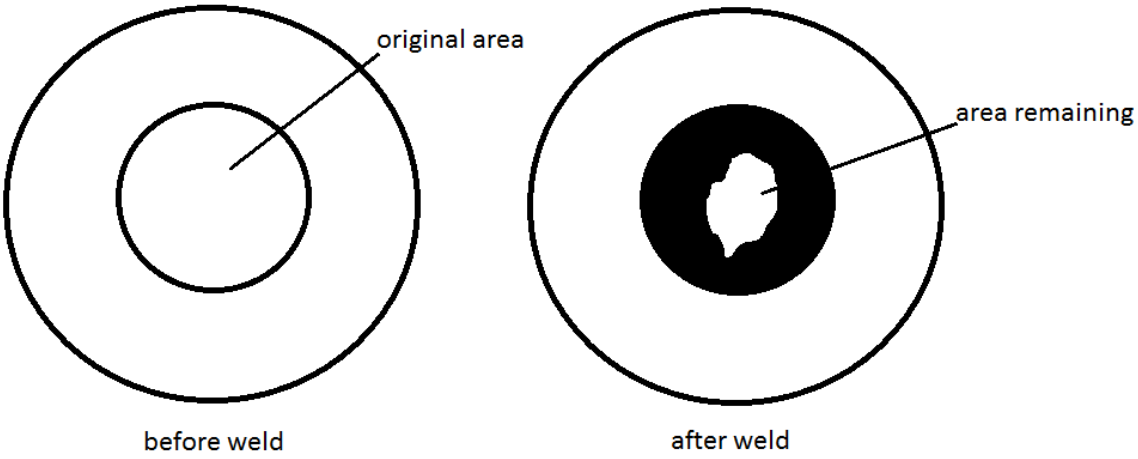

Figure 42: Through-hole reduction percentage analysis.

The ratio of these areas was then used to determine the percent area reduction.

$$Reduction\ Percent = 100 * \left(1 - \frac{area\ remaining}{original\ area}\right) \quad [\ 22\ ]$$

Leak Testing

A series of pipe fittings was used to measure the leak rate of the weld. Helium was used at 103.4 kPa (15 psi) in this system.

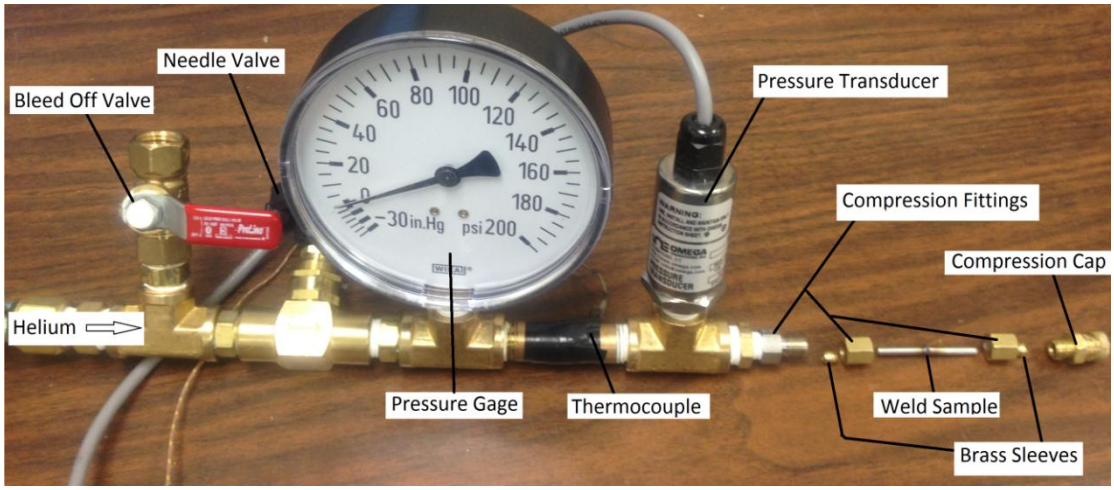

Figure 43: Leak testing configuration.

Once 103.4 kPa (15 psi) of helium was in the system, the needle valve was closed off. The bleed off valve released the back pressure in the system. The pressure transducer had a range of 0-300 psi. This was not ideal; a tighter pressure range would have been better. It was still good enough to provide decent accuracy. Pressure measurements from this transducer were recorded by a LabVIEW program. Also, the thermocouple recorded the temperature of the outside of the piping system. This was in order to observe any strange temperature effects or the possible temperature influence from the room. This temperature was recorded in LabVIEW as well.

The pressure drop was multiplied by the internal volume of the measuring container (13 cm^3). Slight temperature fluctuations were noticed, so a modifying equation was used to account for some temperature variations. This was done because it was found that the room temperature had more impact on the thermocouple reading than the pressure of the gas. For instance, consider a reported pressure drop with a correlating temperature drop. It was assumed that part of the pressure drop was due to the temperature drop, and part of the pressure drop was due to a leak. The modifying equation only altered the reported leak rates slightly; it can be seen in Appendix B. Helium was treated as an ideal gas due to the low pressure.

Tensile Testing

An Instron load frame was used to perform tensile testing. This was done after the welds had been pressure tested. To be removed from the pressure testing setup, the ends of the samples had to be cut off. This resulted in short samples. The Instron was still

capable of gripping the samples, but each sample was gripped right near the weld. In this way, the strength of the weld was isolated.

Figure 44: A sample is loaded in the Instron. This was where fracture testing was performed.

Tests were run until the samples completely fractured. Every test was run with a displacement rate of .089 cm/min. Ultimate tensile force was recorded and compared for every test. The modulus, yield strength, and other properties were not used for comparisons.

Concerns

Emissivity Trendline

Based on the provided theory in the previous section, the emissivity increases as the temperature increases. This implies that the difference between the infrared measurement and the true temperature should decrease as the oven temperature increases.

Instead, a unique trend occurs. There is little difference between the two temperatures when both are at room temperature. As the oven temperature increases, the difference between temperatures increases. This trend happens until about 400 ˚C. Then, the expected trend happens. The temperature difference decreases as the temperature increases. This implies that the emissivity is increasing.

Something strange is happening here, and it should be addressed. At room temperatures, the thermometer was not very sensitive to changes in emissivity. When it was run at a minimum and maximum emissivity value (.1 to 1), the corresponding temperature difference was only about thirty degrees Celsius. At larger temperatures, this operational window grew much larger. Since the possible range of output temperatures was small at room temperature, the temperature difference between the two readings could not possibly have been very large. This phenomenon continued up until the 400 ˚C oven temperature. At 400 ˚C, the possible output temperature window allowed the infrared temperature to vary largely with respect to the oven temperature. As the temperatures increased above 400 ˚C, the emissivity of the sample increased as well.

It was still a possibility that the emissivity of the sample increased throughout the entire test. It just so happened that it was not very sensitive to temperatures around room temperature. Once temperatures increase above 400 ˚C, the expected trend is seen in Figure 45. As the temperature increased, the emissivity increased as well.

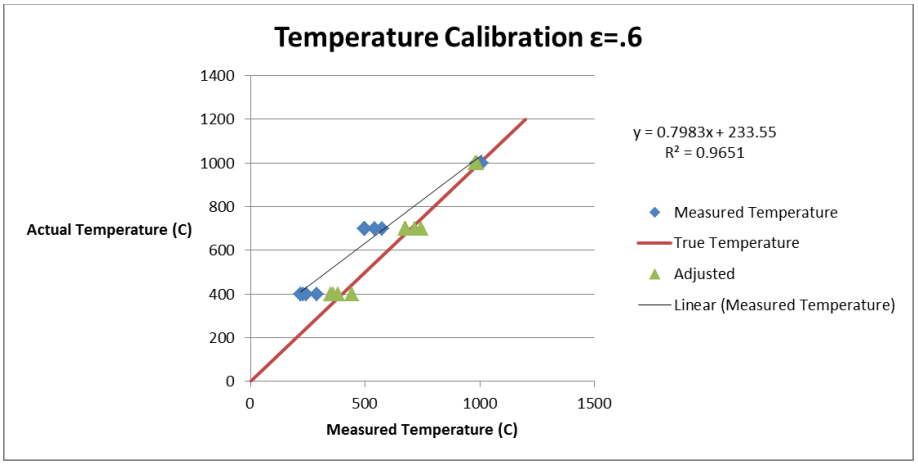

Figure 45: A modified plot of the true and measured temperatures helps understand the effects of emissivity.

These comments further show that this emissivity determination only applies to this study. It is not clear from this data exactly how the emissivity value behaves from room temperature to 400 ˚C, but a characterization of this specific experiment can be found and used. For the study at hand, it appears that the emissivity starts high, decreases, and then increases again. This is not confirmed, but this temperature trend was safely used to predict temperatures.

Torque on Load Cell

Torque on a load cell is always a concern. The load cell used in this study was designed for only axial loads. On off-axis load or an applied torque to the load cell could potentially cause errors in the load cell readings. This load cell manufacturer addresses this problem in their specifications sheet. The load cell used has both torque and moment compensation characteristics. The following figure shows the compensation values. The series used was 1000.

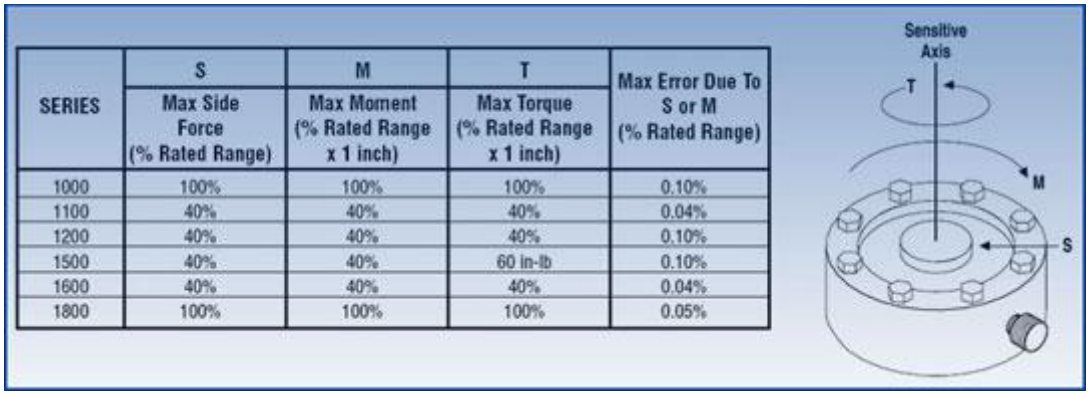

SERIES	S Max Side Force (% Rated Range)	M Max Moment (% Rated Range x 1 inch)	T Max Torque (% Rated Range x 1 inch)	Max Error Due To S or M (% Rated Range)
1000	100%	100%	100%	0.10%
1100	40%	40%	40%	0.04%
1200	40%	40%	40%	0.10%
1500	40%	40%	60 in-lb	0.10%
1600	40%	40%	40%	0.04%
1800	100%	100%	100%	0.05%

Figure 46: The load cell compensated for both moments and torques.

The load in the study was applied essentially as an axial load directly aligned with the axis of the load cell. There was a chance that the alignment was slightly off. To see if small misalignments were acceptable, consider a very simple example.

The maximum load in the study was less than 1800 N; use 1800 N as an axial load to overestimate the applied moments. If there was a misalignment of .317 cm (large overestimation), then the resulting moment would be:

$$Moment = radius * \ axial\ force \qquad [\ 23\ ]$$

$$Moment = .317cm * \ 1800N \qquad [\ 24\ ]$$

$$Moment = 5.7\ Nm \qquad [\ 25\ ]$$

The maximum rated moment can be seen from the above figure. The load cell had a 2200 N (500 lb) rating, so the maximum moment would be:

$$Moment\ Max = 2.54cm * \ 2200N \qquad [\ 26\ ]$$

$$Moment\ Max = 56\ Nm \qquad [\ 27\ ]$$

The overestimated applied moment is ten times smaller than the maximum allowed moment. Based on this analysis, the moments resulting in the system were not a problem. A similar analysis was done for the torque.

The torque developed in the study resulted from a friction force. Again, the values used in this short example are for overestimation purposes. A friction coefficient of .9 results from the connection of the two samples. The friction coefficient will only be used when the materials are spinning. The maximum force for the initial stage could be overestimated to be 900 N. The following quickly works out the torque applied to the load cell. The outer diameter was used for further over-approximation.

$$T = \frac{d}{2} * F_f \quad [28]$$

$$F_f = F_n * \mu \quad [29]$$

$$T = \frac{d}{2} * F_n * \mu \quad [30]$$

$$T = \frac{.317cm}{2} * 900N * .9 \quad [31]$$

$$T = 1.3\ Nm \quad [32]$$

Similar to the moment compensation characteristics, the maximum allowable torque is 56 Nm. The calculated torque above is less than 3% of the maximum allowable value. Based on this approximation, the torque compensation characteristics of the load cell are more than adequate. Both the moments and the torques created in the duration of the testing will be far below their rated values.

Thermometer Positioning

The position of the infrared sensing head was of critical importance. The spot size of the thermometer was very small. In order to read accurate measurements, the spot had to be in the same position every time. This introduces potential errors in four physical degrees of freedom: proximity of the sensing head to the sample, vertical height of the sensing head relative to the sample, and two rotational degrees of freedom. Each of these degrees of freedom had to be easily controlled from test to test.

Horizontal distance between the sample and the sensing head was controlled with a bracket mounted on the mill deck. A bracket was bolted to the mill deck so that the thermometer tower could slide up against it. The thermometer tower had to be slid out of position every time the samples were exchanged. With the stopping bracket in place, the tower could be slid out of position and back into position very easily.

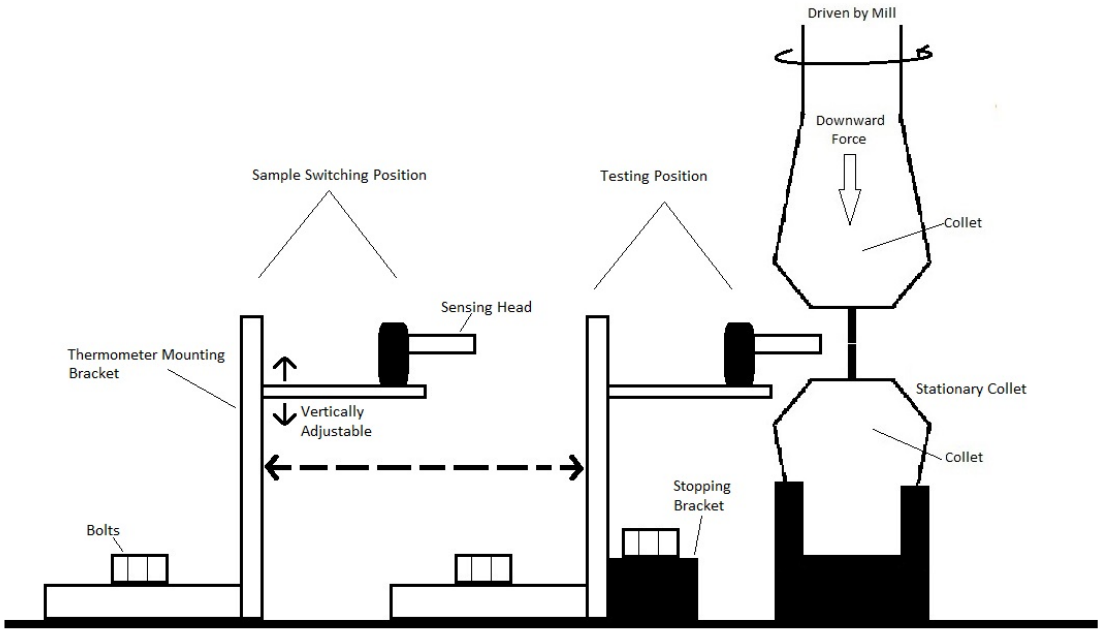

Figure 47: Horizontal position of the thermometer was controlled with a stopping bracket.

This ensured a constant position in the horizontal direction. The horizontal distance was very critical in order to regulate the spot size. The sensing head was set to be .889 cm away from the samples. This distance was regularly checked to make sure the spot size was being controlled. Reference Figure 21 for a spot size diagram.

Vertically, the position of the sensing head was locked in place with some bolts. Once testing began, the vertical position of the tower was held constant. The height of the samples was then controlled by using consistent samples. The spacer in the stationary collet was used for every test. This height plus the height of the samples resulted in a consistent height for every test.

Rotationally, the sensing head can be rotated up and down or left and right. These are the last two degrees of freedom to be controlled. The up and down rotation component was set once for the duration of the testing period. It was set so that the sensing head was perpendicular with the testing samples. It was important that the head be at a perpendicular angle in order to reflect the true emissivity of the samples.

Lastly, the side to side rotation needed to be controlled. Unlike the previous three degrees of freedom, this component was continuously adjusted for every test. The sensing head needed to be facing the sample at a perfectly perpendicular direction. There was no laser or other guiding technique on the sensing head, so a makeshift method was used. The user would place their hand behind the sample. If the sensing head was out of alignment, it would read the temperature from the users' hand. The rotational position of the sensing head would be adjusted until the effects of the users hand were not seen in the temperature reading. This can be visualized in the following figures.

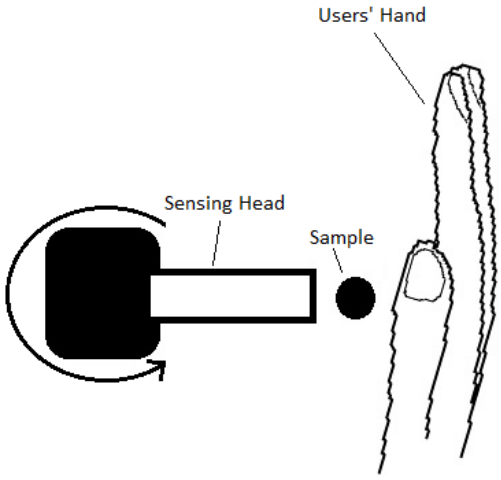

Figure 48: Rotational alignment techniques for the temperature sensor.

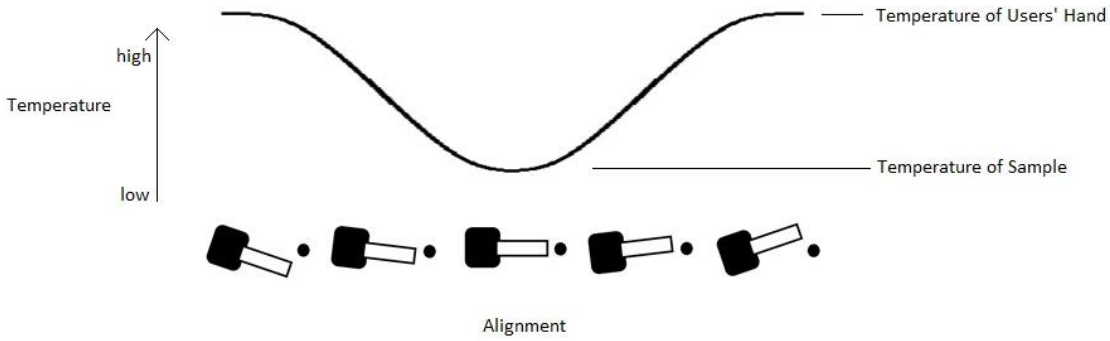

Figure 49: As the alignment was perfected, the temperature reading would decrease.

These methods proved to work very well for the thermometer alignment. They were quick and effective.

Experimental Samples

Properties and Dimensions

Stainless steel 304 was used in this study. This was the only material used. The following table gives the material properties and composition of this metal (MatWeb, 2013).

Table 4: Stainless Steel 304 Mechanical Properties and Chemical Composition

Mechanical Properties	
Tensile Strength, Ultimate	505 MPa
Tensile Strength, Yield	215 MPa
Modulus of Elasticity	193-200 GPa
Chemical Composition	
Carbon, C	≤.08%
Chromium, Cr	18-20%
Iron, Fe	66.345-74%
Manganese, Mn	≤2.0%
Nickel, Ni	8.0-10.5%
Phosphorous, P	≤.045%
Silicon, Si	≤1.0%
Sulfur, S	≤.03%

Using the above yield and ultimate stress values, the expected yield force and ultimate force were 1000 N and 3200 N, respectively. Sample testing revealed that unwelded samples had a yield force of 1850 N and an ultimate strength of 4600 N. These values are considerable larger than those predicted by MatWeb. The tensile testing configuration in this study used very shot sample lengths. Only about 1 cm of material was exposed between the load frame grips. This short length likely resulted in an apparent strengthening. For comparisons later, the actual values from testing were used.

Only one size tube was used in this study. For some tests, a bar was also used. Dimensions can be seen in the following table.

Table 5: Sample Dimensions

	Outer Diameter	**Inner Diameter**	**Length**
Tube	.317 cm (.125 in)	.14 cm (.055 in)	1.905 cm (.75 in)
Bar	.317 com (.125 in)	-	1.905 cm (.75 in)

Surface Finish

Several different methods were investigated to prepare samples. The final sample finish was achieved from a manual lathe. The tubular samples were purchased from a machine shop. A drawing used showing flatness tolerances can be found in Appendix C. The bar samples were successfully made in-house; they were also finished with a manual lathe. There were no chemicals or cleaning agents used to clean the surface before welding.

Control Methods

There were three potential methods to control the friction welding process. A system based either on temperature, time, or upset was available. In traditional friction welding procedures, either time or upset are used. In this way, one controls and the other is dependent on the process variables. The third option, temperature control, is not commonly used. This is most likely due to difficulties in temperature measurement. For this system, temperature control is an option.

All three control methods operated in the same way. Once the process reached a certain value (temperature, upset, or time), the rotational speed stopped and the forging force was applied. All three methods have various advantages and disadvantages. It was originally decided that a time based system would be the easiest to monitor and control consistently.

For the first round of testing, the goal was to heat the samples up to different temperature ranges. In order to control this process by time, a time-temperature relationship was needed. Several tests were run to find this relationship. A friction time of about 6 seconds would heat the samples to a 500-600 °C range, and a time of about 7.5 seconds would heat the samples to a range of 800-900 °C. This relationship can be seen in the Figure 50.

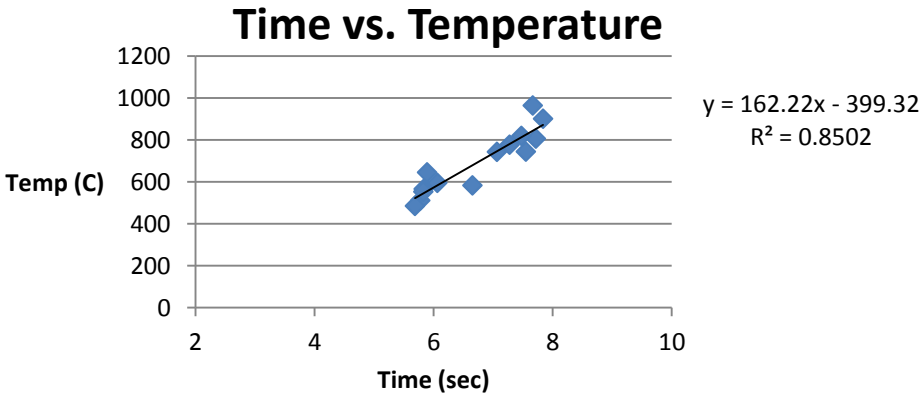

Figure 50: A relationship between time and temperature was originally used for time controlled testing.

The above relationship was used to run several tests in the first design matrix (DESIGN OF EXPERIMENTS chapter). However, temperatures achieved were becoming inconsistent. It was taking several welding attempts to achieve desired test

results. The above time-temperature plot was populated to a larger degree, and the correlation between the two parameters began to drift apart (Figure 51).

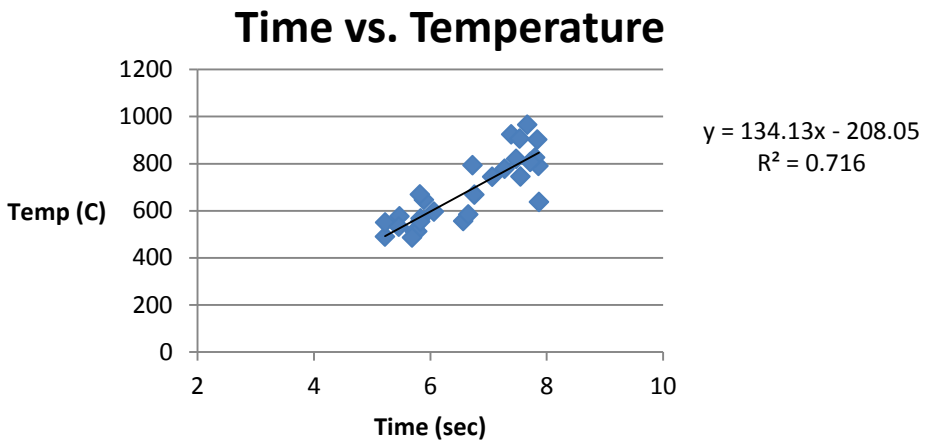

Figure 51: The correlation between time and temperature became less precise as more data points were added.

Slight variations in surface finish likely cause this lack of a concrete relationship, but there is still a basic correlation. As the time generally increases, the temperature generally increases. With the correlation becoming weaker, an adjustment was made in the testing process.

The remainder of the first design matrix tests were run with a temperature controlled process. Temperature goals were the same as those with the time based system. Tests were run to get to the temperature ranges of 600-750 °C and 850-950 °C. A much higher rate of consistency from test to test was achieved with this control system. As will be presented in later sections, the results from the first design matrix showed that upset values were very important to the success of a weld. Due to this fact, an upset control method was then created.

The LVDT shown previously directly measured the upset in each test. The position of the mill chuck was known throughout the entire duration of the test. In this way, once the mill chuck displaced a certain amount, the rotation stopped and the forging force was applied. The upset control method proved to be both successful and reliable. Upset control was used for much of the testing.

DESIGN OF EXPERIMENTS

Parameter Selection

Variable and Constant Parameters

Recall, the parameters governing the friction welding process include friction time, forging time, stopping temperature, friction force, forging force, rotational speed, and material upset. Performing an optimization procedure with all of these parameters as variables would be exhausting and potentially unnecessary. In order to simplify the optimization process to a more reasonable task, several of the above parameters will be held constant.

Consider the friction process of the welding procedure. The initial theory used here was that the process needs to reach a certain temperature in order to weld successfully. The rotational speed, friction force, and friction time all affect the operating temperature of the system. The goal was to eliminate two of these variables and just concentrate on one of them. It has been shown in literature that rotational speed is often a low order variable (Vill, 1962); rotational speed will be held constant throughout the process. A decision was also made to hold the friction force constant. Based on the nature of the physical control of the friction welding process used in this study, it was much easier to control one force for various temperatures than to control different force levels. The friction force was set to one constant value, and the stopping temperature was varied.

To help clarify further discussion, the friction time and stopping temperature can almost be considered equal. It was decided to vary the stopping temperature by running the tests for different times. This was based on a correlation between temperature and

friction time. Once it was found that this correlation was weak, the control system was modified to be based on temperature. The similarity is that both the temperature and time control systems had the objective of getting the process to a specified temperature. With this in mind, further parameters need to be declared constant or variable.

Friction time, stopping temperature, and material upset are all closely related in this process. When one of them is held constant, the other two become dependents. As previously mentioned, the initial goal was to operate at a certain temperature. This made the friction time and the material upset dependent values. They were not necessarily controlled parameters; they were more just left to be a measured result of each test. Alternatively, upset control methods were used in some instances in later testing. This would result in letting stopping temperature and friction time become dependents.

Lastly, forging force and forging time have not been addressed. This study focused on optimizing physical properties of the welds. It was not attempting to optimize a welding time. For this reason, the forging time was held at a constant value. On the other hand, the forging force could certainly have some effect on the weld quality. It is not interrelated to other parameters like the friction time, stopping temperature, material upset, and friction force. The forging force was then chosen as a variable parameter. The following figure summarizes these decisions.

Table 6: Constant, Variable, and Measured Parameters

Constant Parameters	**Variable Parameters**	**Measured Parameters**
Rotational speed	Stopping temperature or material upset	Material upset or stopping temperature
Forging time	Forging force	Friction time
Friction force		

Constant Parameter Values

The constant parameters have been decided, and now the constant values themselves need to be obtained. The rotational speed, forging time, and friction force all need to be set. Applicable values were determined from both literature suggestions as well as from preliminary testing results.

Initial testing was performed to get a general range of applicable parameters. Rotational speeds in the range of 960-1500 rpm proved to be adequate. Higher rotational speeds resulted in decreased stability of the system. Rotational speeds below this range were not very effective at heating up the samples. Rotations in the middle of this spectrum more consistently produced decent welds. Friction forces between 180 and 530 N created enough heat to initiate a weld, and forging forces between 530 and 1250 N finished up the weld nicely. Comparing these values to those suggested by ASM, they were all a little lower.

Table 7: Welding Values Predicted by ASM

	Maximum	Minimum
Friction Force	1,060 N	528 N
Forging Force	2,110 N	1060 N
Rotational Speed	18,300 rpm	7,600 rpm

It is likely that the ASM values were suggested for larger pieces of metal. The dimensions of the samples used in this study were much smaller than typical use. The ASM data provided a decent starting place, but values outside the suggested range proved to be more adequate. In fact, other publications also suggest using values lower than those from ASM. In many publications, a friction pressure is used instead of a friction

force. Adjusted to the samples used in this study, the friction forces used in literature are in the range 125 N to 380 N. Forging forces are in the range of 380 N to 830 N (Sluzalec, 1990; Sahin, 2005; Paventhan, 2012; Satyanaraya, 2004). This indicates that using values lower than those suggested by ASM will not be a concern.

A range of values for rotational speed and friction force has been presented. From here, tests were run at different levels to analyze how the system itself responded to various levels. The friction force was varied between 270 and 360 N; the rotational speed was varied between the three levels of 960, 1200, and 1500 rpm. Tests were run at these different combinations while other variables were held constant. The force control system was much more precise when controlling 270 N. Vibration induced from the mill was observed to be minimalized when a rotational speed of 1200 rpm was used. After performing several of these preliminary tests, it was found that the system responds most consistently and appropriately when a friction force of 270 N and a rotational speed of 1200 rpm was used. From here, these values were used as constants.

The forging time was chosen primarily by observation. When the rotational speed stopped and the forging force was applied, the samples cooled very quickly. Once the samples cool, the effects of the forging force will begin to become negligible. After running many preliminary tests, it was decided that a forging time of six seconds would be sufficient. This was set as a constant value for all the tests run in this study.

Table 8: Constant Parameter Settings

Parameter	**Constant Value**
Friction Force	270 N
Rotational Speed	1200 rpm
Forging Time	6 sec

Variable Parameter Values

In a similar fashion to the constant parameter values, the variable parameter ranges needed to be defined. The factorial design experiments that were run in this study require a high level and a low level for each variable. High and low values need to be set for the stopping temperature, the forging force, and, eventually, the material upset. The goal of the first round of tests was to bound the welding problem around maintaining a through-hole in the finished weld.

Several tests were run to observe results of different stopping temperatures. The high and low levels were determined from welds that had the highest and lowest through-hole area reduction percentage. Low temperatures resulted in the through-hole maintaining a decent integrity. Higher temperatures resulted in the through-hole becoming completely filled. The low value for stopping temperature was chosen as the temperature that still allowed a weld to bond, but the through-hole integrity remained quite good. The high bound was chosen from preliminary tests that had either a tiny hole through the center, or they were just barely filled in all the way. The low temperature range was approximately 600-750 °C. The high temperature range was approximately 850-950 °C. The temperature had a more tangible effect on the through-hole than the forging force, so the forging force range was chosen in a different way.

Discovering a maximum value to use for the forging force was based on the capabilities of the system. Originally, it appeared that the maximum applied force the system was capable of was 1980 N. This held true based on impulsive forces. The system could start at a low value and then quickly send an impulsive force and reach around 1980 N. However, this force was not sustainable. If the applied force level began to drop

from 1980 N, the system did not have the power to maintain this high level. Essentially, there wasn't much control with this large of a force. Instead, the maximum sustainable force was sought after. It was found that an applied force of 1250 N could be maintained throughout a full test. A force of 1250 N actually fits into the range suggested by ASM. Although 1250 N is lower than the original expectations of the system, it should still suffice as a high level for forging force.

A low end for the forging force was chosen as 530 N. This force level fits into both the suggested ranges provided by ASM as well as other literature. A force at this level was also proven to be effective in preliminary testing. Lastly, this value is about twice the value of the constant friction force chosen (270 N). Doubling the value of the friction force is not strictly necessary, but it was seen as a convenient starting place.

Upset bounds were also needed for later testing. These levels were set during the testing period that was not concerned with maintaining the through-hole integrity; the importance of a leak free weld was stressed in these tests. Results from the temperature controlled testing showed an upset value of at least .095 cm was necessary to eliminate leaks. An upset value of .1 cm was chosen as a lower bound. An upset value of .2 cm was then chosen as an upper bound. With a .1 cm gap between bounds, the importance of material upset was sure to be found. Also, when tests were run with values larger than .2 cm, the system became unstable. The samples began to rotate out of axis and bend. The following figure summarizes the high and low bounds for the variable parameters. Keep in mind that when the stopping temperature was controlled, the upset as a measured output, and when the upset is controlled, the stopping temperature as a measured output.

Table 9: Constant Value Settings

Parameter	**Low Value**	**High Value**
Stopping Temperature Range	600-750 °C	850-950 °C
Forging Force	530 N	1250 N
Material Upset	.1 cm	.2 cm

Note that the above values are guidelines more than exact, achievable values. The nature of the testing system resulted in slight fluctuation in parameter values. The majority of the data ranged by about 10% of the desired values. The temperature control and measurement could have included some slight error resulting to slight misalignments.

Measures were taken to run tests as consistently as possible, but this does not mean errors were eliminated. To help remedy this, each weld was also filmed with a camera. This helped for categorizing high and low temperature tests. Forces also varied slightly. The feedback system used to control the forces relied on measuring a force error and making adjustments as necessary. The force levels would hover around the desired values, but they were often off by plus or minus 50 N or so. The large differences in high and low values could afford these changes.

Factorial Design

The following presents the design matrices used for this study. Although the following tests were not done strictly in chronological order, results from one group of tests led to decisions about further tests to run. In general, testing was done with two different trains of thought. At first, maintaining a through-hole was sought after. Parameter values were chosen in order to bound the problem around an intact through-

hole. Most of these welds were found to leak. After this design matrix was completed, the second rationale of testing was implemented. The through-hole was considered to be of secondary importance, and tests were done to optimize weld integrity. This new design matrix sought to find welds that were both strong and leak free. Both of these testing rationales had other small variations as well.

With Respect to Maintaining the Through-Hole

The first design matrix used stopping temperature and forging force as the two variables. The individual tests are shown in each cell in the matrix. For full data detail on each test, visit Appendix A.

Table 10: Initial Testing Matrix

	Low Temperature	**High Temperature**
Low Forging Force	D14, E14, F14, E21, A22, B22	A15, B15, E15, F17, B18, B19
High Forging Force	C16, D16, E16, B17, A21, C21	C17, D17, E17, F19, C20, F20

The through-hole was compromised in all the above tests. Some of them still had a decent amount of it left, but all of the tests filled in the through-hole somewhat. In order to try to avoid this problem further, several tests were run with beveled samples. These samples all had slightly beveled ends. The idea was that the material would deform into the voids created by the bevel. It was later shown that the forging force did not have a large effect on the through-hole reduction. Friction duration had a much larger impact. Using this information, a reduced testing matrix for beveled samples was used.

Table 11: Beveled Tubed Tests

	Low Upset	**High Upset**
Low Forging Force	C30, D30, C31, F31	A32, A33, C33, D33

The beveled tube testing was done late in the experimental process. It was done at a time when the upset control was being effectively used for other tests. For this reason, the above design matrix was categorized by upset rather than temperature.

With Respect to Leak Performance

As mentioned previously, upset control was used to proceed in the testing phase. When the through-hole of the samples was maintained, the welds often leaked when they were pressure tested. Only the samples with the largest upset were able to hold a pressure. With this in mind, a new design matrix was developed in order to attempt to create welds that consistently did not leak. The following design matrix was used.

Table 12: Larger Upset Tube to Tube Tests

	Low Upset	**High Upset**
Low Forging Force	F22, A23, F35	E23, F23, B24, D24
High Forging Force	F24, B25, C25	A25, A26, B26

All these tests completely filled the through-hole. However, they did have much better leak rate and strength characteristics.

Lastly, one more design matrix was used. The upset control method was used to weld a solid bar onto the end of a tube.

Table 13: Bar to Tube Welds

	Low Upset	**High Upset**
Low Forging Force	F26, A27, B27, C27, D27	E27, F27, A28, D34, E34
High Forging Force	C28, E28, A29, B29	C29, D29, E29, B30

Further Testing

The testing setup described thus far yielded great control and flexibility. However, its weakness was rigidity. Once all the bolts were tightened and the samples were ensured to be parallel, miniscule vibration still existed in the system. The load cell tower would slightly vibrate translationally once the samples began to contact. Although this effect was minimized, it still existed in a small amount. A modified testing setup was used to compare a more rigid setup to the one used for the majority of the testing.

The tower itself was removed, and the collet holder was gripped directly in the vise of the mill. The force was applied by hanging a weight from the activation arm of the mill. This same configuration was used in Figure 22. In this way, a constant force was applied throughout the entire process. Essentially, the friction force and the forging force were held as the same value. The constant applied force was 220 N (50lbf). Due to physical constraints of this new system, temperature measurements were not taken. This setup offered limited control, but it had a high level of rigidity.

One goal of this new testing setup was to try to maintain the through-hole. A higher rotational speed was used to try and shorten the friction stage of the process. This would hopefully reduce material flow to the inside of the tubes. A rotational speed of 1800 rpm was used. These samples all left an opening in the tubes, so a drill was used

restore the tube to its original true inner diameter. Stopping criteria was determined from observation. When the samples began to glow bright orange, the rotation was stopped.

One last set of tests was run. The rigid setup was used to try and directly compare the more rigid tests to the previous tests. Tests were run at 1200 rpm, and the upset was as a control. The upset values were used to match the upset values from Table 11. Both sample sets for this last testing setup can be seen in the table below.

Table 14: Final Testing Configuration Weld Data

1800 rpm	1200 rpm	
I4, G8, H5, I5, H6, G13, H13, I13, G14	Very Low Upset:	I15, G16
	Low Upset:	I9, I10, I11, H12
	High Upset:	G9, G12

EXPERIMENTAL RESULTS

Providing the entire force, temperature, and upset profiles for each test would be excessive. Instead, several sample profiles are presented. With respect to force control, each test had a slightly different response. If the force profile from a test appeared to be very inconsistent, the weld was not accepted as valid data. Below, examples of acceptable and unacceptable force profiles can be seen.

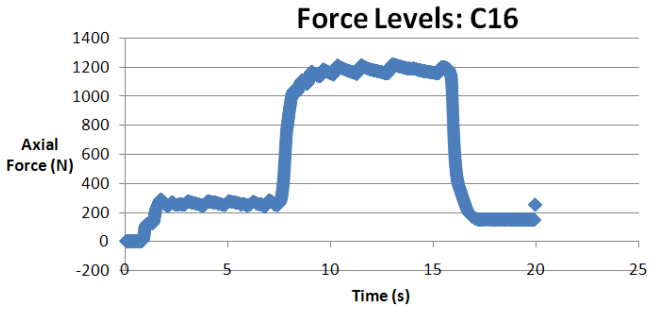

Figure 52: This force response was considered very good. The forging force was at the high level.

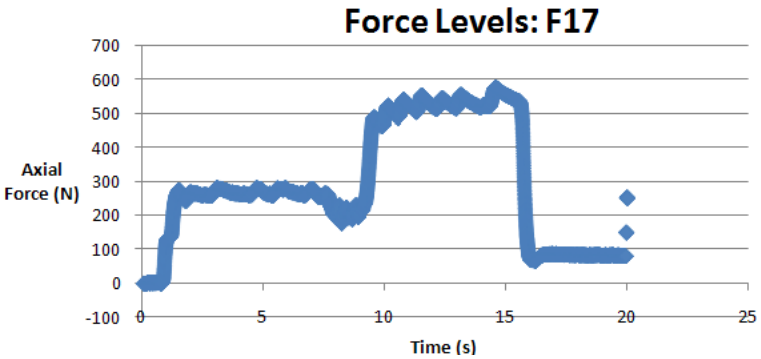

Figure 53: The forging force was set to the low level.

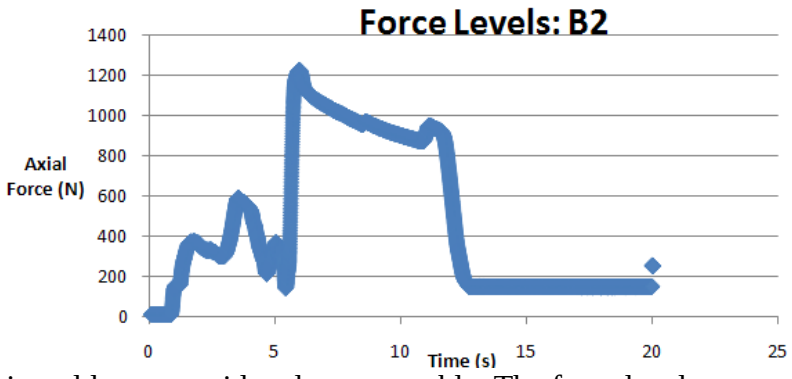

Figure 54: This weld was considered unacceptable. The force levels were very irregular.

Temperature profiles were somewhat consistent from weld to weld. The temperature quickly increased upon initial contact. The rate of temperature increase then decreased as the friction process continued. Once the weld was active for several seconds, the temperature drastically began to increase. The thermometer had a limit of 1000 °C. With the temperature adjustment formula used, this resulted in a maximum temperature reading of 984 °C. There were some tests that exceeded this temperature limit. Their temperature profiles flat-line when they are above this temperature. Maximum temperature estimations were then calculated using the cooling curve rate. Several temperature profiles appear below.

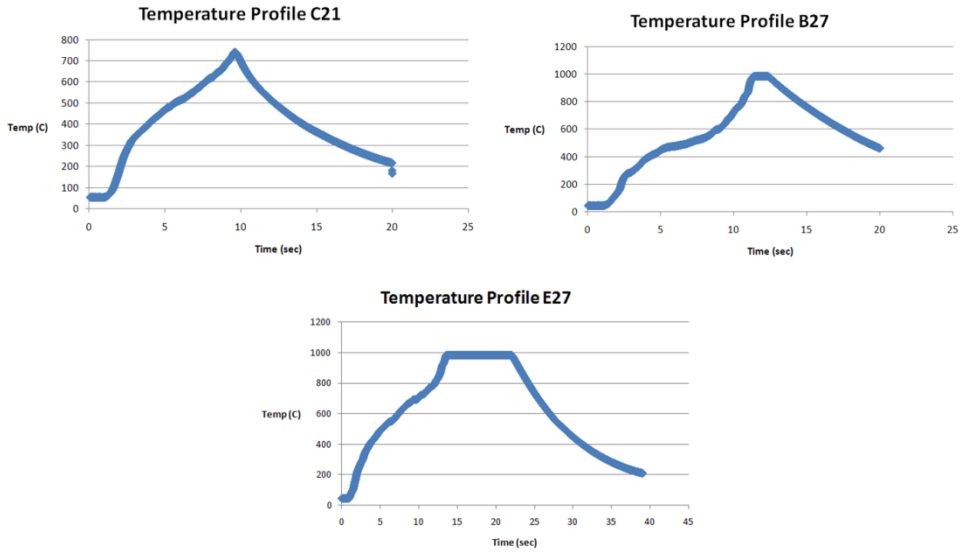

Figure 55: Different temperature responses. Weld C21 shows a typical response. Welds B27 and E27 show various temperature responses when the maximum temperature of the thermometer was exceeded.

Material upset had the most consistent profile from test to test. At the beginning of each test, the samples were .015 cm apart from each other. For this reason, the upset curve started at a negative value. Once the samples made contact, the displacement reading showed a value of zero. Upset slowly increased until the samples heated up significantly, then a large upset occurred. The upset drastically increased until shortly after the rotation stopped. Upset then slowly increased again. There appeared to be a secondary large upset section in every test. This resulted from relaxing the samples after the test is over. The displacement was from the entire welding deck lowering; it was not a material upset value.

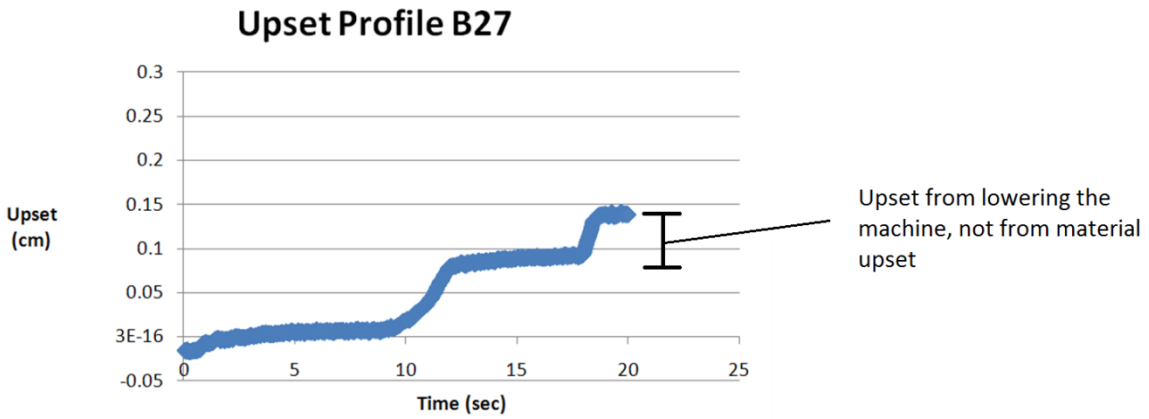

Figure 56: Typical upset profile.

Temperature, upset, and force were all related by time. Figure 47 shows all three profiles overlain on one plot. The scale for each data series has been removed.

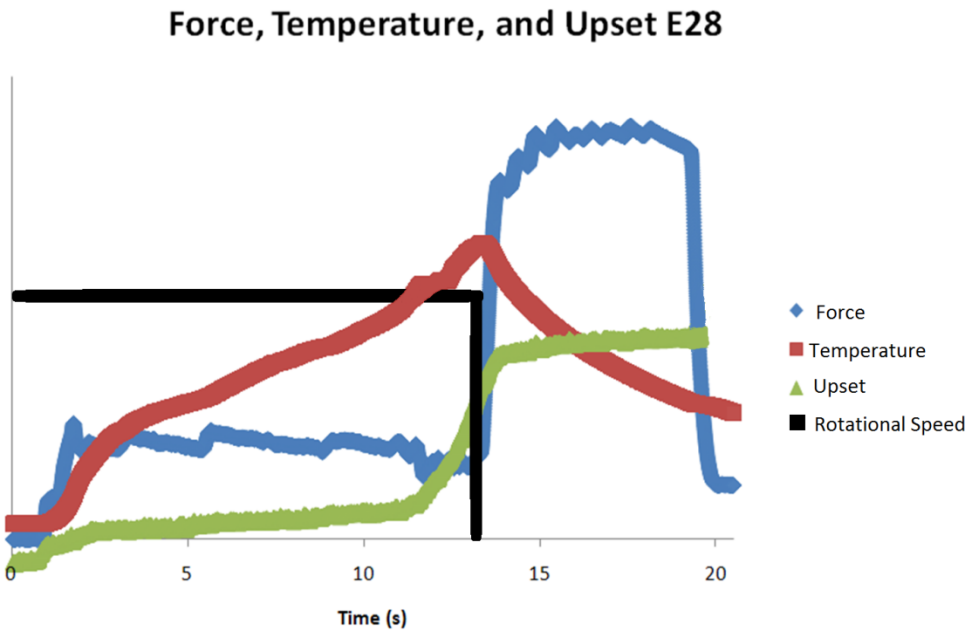

Figure 57: The temperature, force, upset, and rotational speed are all plotted with respect to time.

This study analyzed the quality of 81 welds. Of these, 64 were created with the original load cell testing configuration. Maximum temperature, force levels, maximum upset,

friction time, and post-processing results can be seen for all of these tests in Appendix A. The remaining 17 welds were made with the more rigid testing setup. Appendix A also shows their welding characteristics.

ANALYSIS AND DISCUSSION

Analysis was performed to identify effects the parameters had on weld quality. Several different sets of tests were run. In the following discussion, the testing groups are often compared to each other. Consistent nomenclature for each testing group will be used. The group names to keep in mind are “initial tests”, “beveled tubes”, “large-upset-tubes”, “bar-to-tube”, and “constant force” tests with either a high or a low speed. These names will be used throughout.

Tube to Tube

Initial Tests

The first testing matrix in this study yielded interesting results. For this testing matrix, parameters were set to bound the problem around a resulting weld with at least some percentage of the through-hole intact. Some tests were done with a temperature control and some were done with a time control. Both control methods were to create a certain stopping temperature condition. The low temperature range was around 700 °C, and the upper temperature range was around 900 °C.

Through-Hole Reduction. Material displaced to the inside of the tube for every test. However, some welds definitely performed better than others in this regard. The average through-hole reduction percentage for all the tests was about 85%. The lowest reduction occurred when the temperature was low and the forging force was high. The highest through-hole reduction occurred when both the temperature and the forging force

were high. Figure 58 shows how the forging force and temperature affected the through-hole.

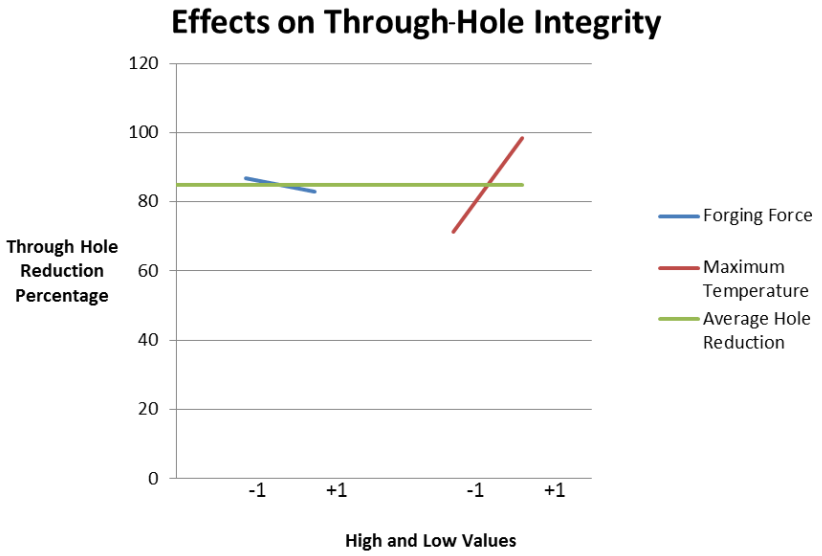

Figure 58: Effects on through-hole integrity for the initial tests. Maximum temperature had a much larger effect than forging force.

It can instantly be seen that the maximum temperature had a larger influence than the forging force. Below, the interaction between parameters can be seen.

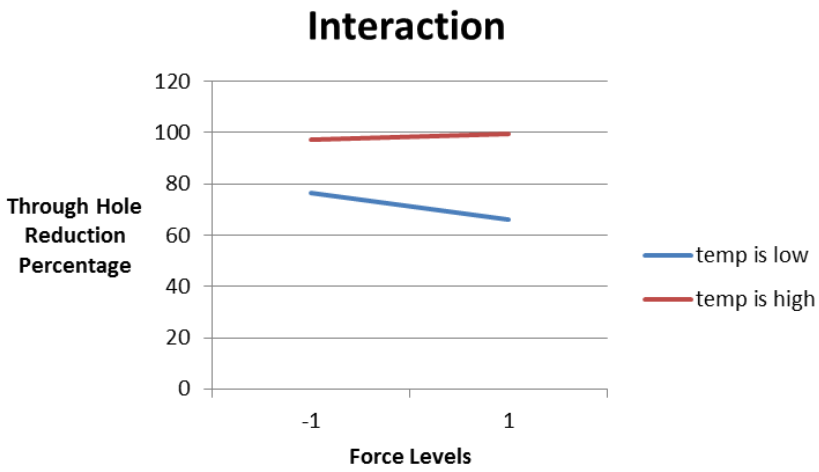

Figure 59: Interaction was low between the forging force and the temperature.

The interaction appeared to be fairly weak. Also, compared to the effect of the stopping temperature, the forging force appeared to have a very weak effect as well. A 95% confidence interval revealed that the stopping temperature was the only statistically relevant parameter.

Table 15: Statistical Significance from the Initial Tests: Through-hole Reduction Effects

Through-hole Reduction A=forging force B=temperature	
A effect ± confidence interval	-4.1 ± 7.18
B effect ± confidence interval	27.217 ± 7.18
AB interaction ± confidence interval	6.467 ± 7.18
Estimated Standard Error	3.663
Confidence Level Used	95%

The forging force did not have much of an influence on the through-hole integrity. Interaction of the parameters did not play an important role either. When the temperature was high, the reduction percentage was high no matter the level of the forging force. Lastly, the higher the stopping temperature, the more the hole filled in with material. When the metal was at higher temperatures it was more plastic. In turn, it was more capable of displacing towards the center of the hole.

Leak Rate. The leak rate results proved very poor performance. Nearly every test released all the pressure very quickly. The majority of the leak rates were on the order of

10^0 atm*cm^3/s; a leak free weld should be on the order of 10^{-7} to 10^{-8} atm*cm^3/s. With these values in mind, the effects can still be looked at.

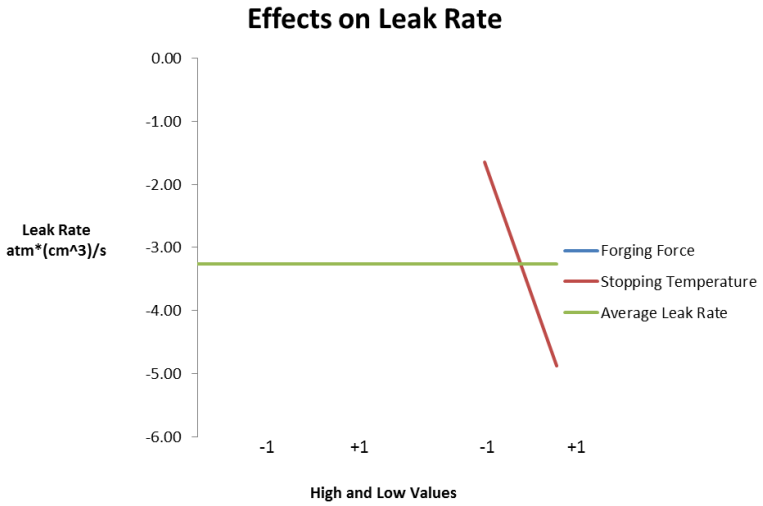

Figure 60: Effects on leak rate for the initial tests.

It appears as though the forging force was omitted from the above figure. This was not the case. The effects of forging force were so small that the line was hidden by the average leak rate line. On the other hand, the stopping temperature appeared to have some significance. It appeared that as the stopping temperature was hotter, the leak rate was larger. The interaction can be observed as well.

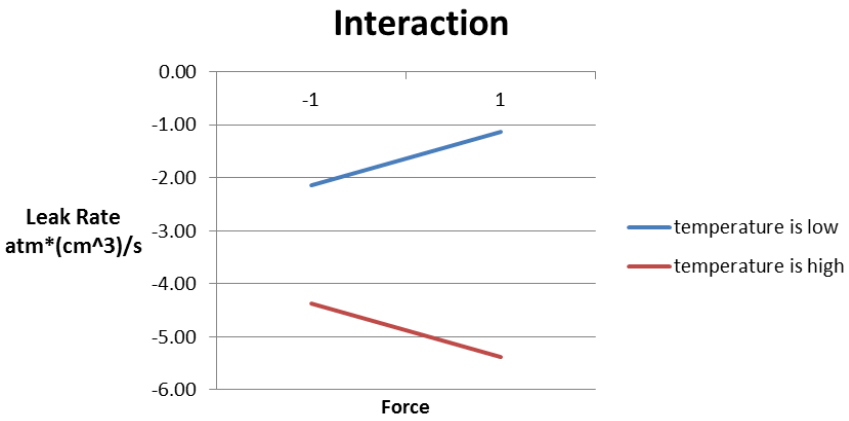

Figure 61: Interaction based on leak rate for the initial tests.

Plotting the interaction shows that the forging force and the stopping temperature interact in some way. Before analyzing it further, the statistics of the effects should be looked at. A 95% confidence interval found that the effects from the forging force and the stopping temperature were not statistically relevant. It also found that the interaction between the two parameters was not significant either. Reducing the confidence level did find that the stopping temperature had an effect on the leak quality.

Table 16: Statistical Significance from the Initial Tests: Leak Rate Effects

Leak Rate A=forging force B=temperature	
A effect ± confidence interval	-.00278 ± 2.74
B effect ± confidence interval	-3.235 ± 2.74
AB interaction ± confidence interval	-1.01 ± 2.74
Estimated Standard Error	1.657
Confidence Level Used	90%

These results should be taken with caution. The average leak rate for these welds was terrible. Any confirmed or denied effects from these tests might not hold true for welds that do hold a pressure. As has been shown, the stopping temperature appears to be much more important than the forging force. This might be true for these porous welds, but a new conclusion might very well be found when better welds are looked at.

There were two welds in this data set that leaked much less than all others. These were tests C17 and F17. Test F17 was a high temperature/low forging force test; test C17 was a high temperature/high forging force test. Useful information was gained from these samples. Tests C17 and F17 were the tests with the highest upset values out of this data set. To pursue different testing parameters, it can be seen that larger upset values will result in better leak performance characteristics.

Tensile Strength. Similar to the leak rate and hole reduction, the maximum temperature proved to be most important factor. The average ultimate tensile force was 945 N. When the temperature was low, the average force was 450 N. Welds had an ultimate tensile force of 1440 N when the temperature was high.

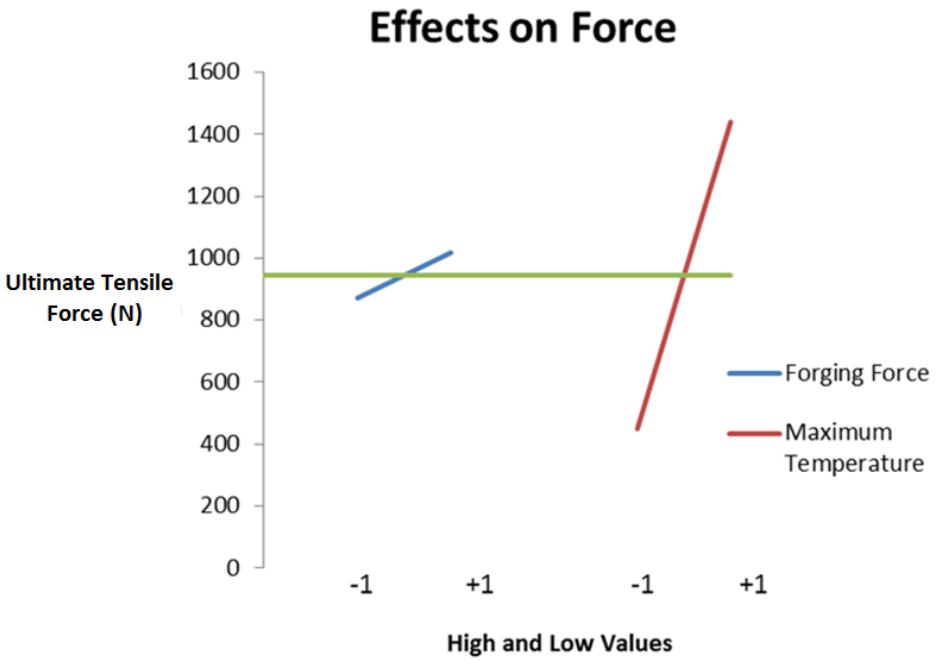

Figure 62: Effects on ultimate tensile force for the initial tests.

The larger temperatures withstood much higher tensile loads than the lower temperature welds. The forging force appeared to have little effect. Also, the interaction was minimal.

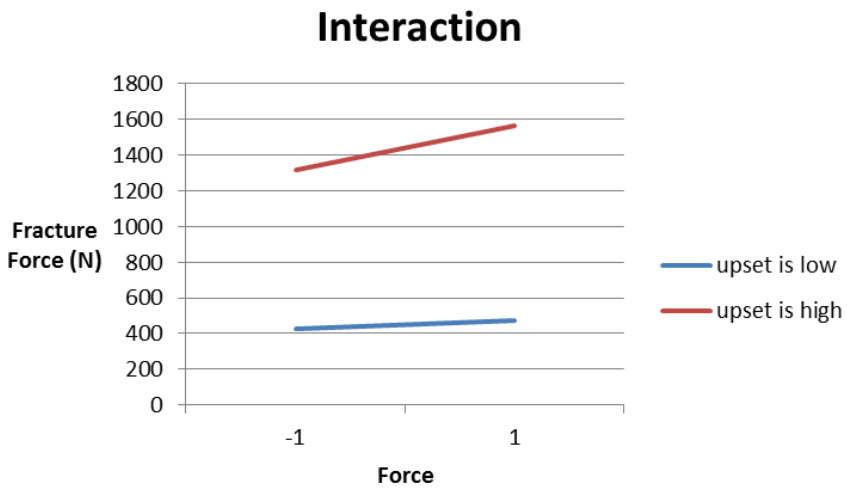

Figure 63: The interaction based on the l ultimate tensile force was weak for the initial tests.

Table 17: Statistical Significance from the Initial Tests: Ultimate Tensile Force Effects

Ultimate Tensile Force A=forging force B=temperature	
A effect ± confidence interval	149.1 ± 391.5
B effect ± confidence interval	988.5 ± 391.5
AB interaction ± confidence interval	99.8 ± 391.5
Estimated Standard Error	199.7
Confidence Level Used	95%

A 95% confidence interval indicated that the temperature was in fact the only important effect. These welds were weak though. The yield force for an unwelded tube is about 2200 N. Compared to this, these welds did not show great strength performance. It has been shown that the leak rate and the hole reduction are both problems, but putting those aside, the strength of the weld would have to be analyzed for different situations. The welds were not nearly as strong as the base metal, but they could still be used in light service. Low pressure systems do not necessarily need very high strength. If the system allows for low pressures, the strength of these tubes would likely be acceptable. However, once the strength is considered acceptable, the problems from the leak rate and hole reduction introduce themselves again.

Beveled Tubes

Beveled tubes were looked at to try and see if hole integrity could be improved. Both upset and temperature control were used for these tests. Temperature control was used initially, and then upset control was used to finish testing. It was found through other tests that upset control can sometimes be more consistent, so it was utilized in some of these tests. Tests were grouped according to upset. The upset ranges were chosen to compare to the initial tests. However, upset values for the beveled tubes were slightly higher than the regular tubes. Beveling the tubes creates a section of very thin wall. This thin wall was quickly removed during the friction welding process. Slightly larger upset values had to be used in order to still heat the tubes properly. Also, insight from previous testing was used to reduce unnecessary testing. The forging force level had little effect on the measures, so only a forging force of 530 N was used for the beveled tubes.

Through-Hole Reduction. The beveled tubes did not improve the through-hole properties of the weld. The average reduction percentage was about 91%. This is higher than the 85% average for the regular (unbeveled) tubes. When only considering the testing matrix cells with low force and low upset, the beveled tubes had an average of about 83% hole reduction. In the comparable cell for the regular tubes, the average reduction was about 77%. The hole reduction measurement system was not absolutely precise; it had a tolerance of approximately ±10%. With this in mind, the reduction percentages between the two styles of tubes can be considered similar. The beveled tubes did not improve the through-hole reduction percentage.

This can be explained. It was touched on previously, but the bevel did create a thin wall at the welding surface of the tube. Ideally the bevel section would allow for some material to flow into the void and leave the hole in a better condition. Instead, the thin wall got eaten away very quickly in the process. The rotation essentially burnt off the thin wall before high enough temperatures were achieved to create a weld. Effectively, this reduced the beveled tube to a similar geometry to the regular tubes. Then, the welds behaved in similar ways. The reduction percentages were similar, and the through-hole reduction percentage increased as both the temperature and the material upset increased. A 95% confidence interval indicates that the effect of upset was significant.

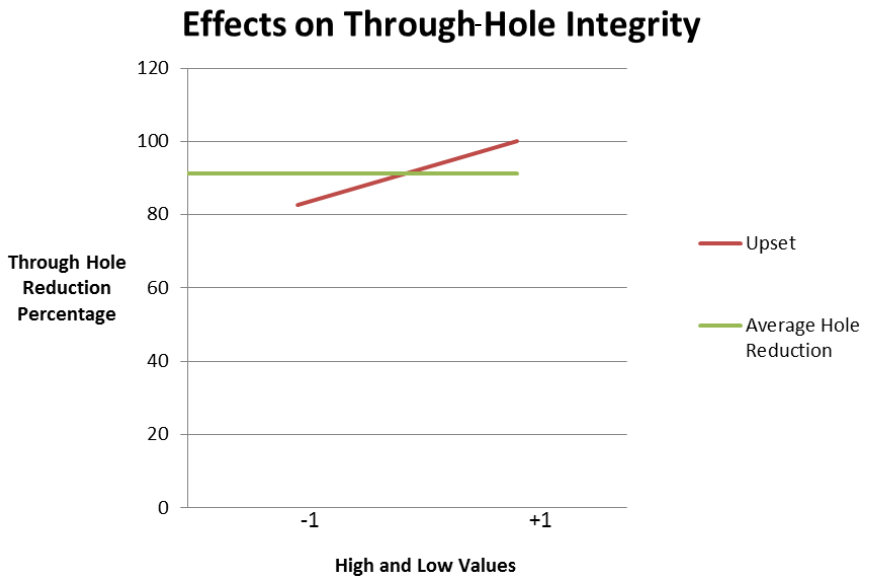

Figure 64: The upset had a positive effect on the average hole reduction.

Table 18: Statistical Significance from the Beveled Tests: Through-hole Reduction Effects

Through-hole Reduction A=upset	
A effect ± confidence interval	-4.1 ± 3.82
Estimated Standard Error	1.95
Confidence Level Used	95%

Leak Rate. The leak rates of the beveled tubes compared to the regular tubes. Most tests yielded terrible leak rates. There was one test, C33, that held a pressure, but all others had large leak rates. The leak rates in general decreased as the upset increased, but the leak rates were still large. A 95% confidence interval indicated that the upset had an effect on the leak rate. As the upset was increased, the leak rate decreased.

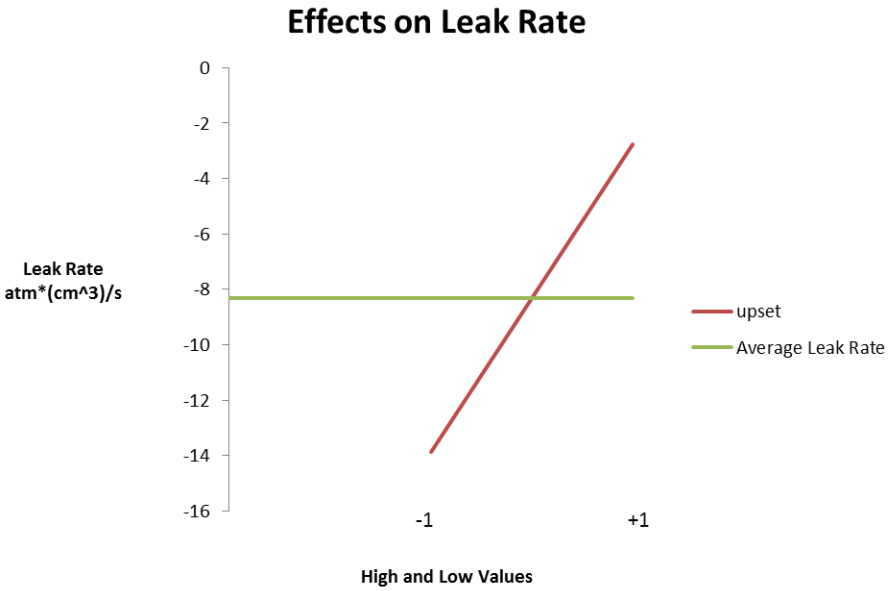

Figure 65: The upset had a positive effect on the average leak rate.

Table 19: Statistical Significance from the Beveled Tests: Leak Rate Effects

Leak Rate A=upset	
A effect ± confidence interval	5.559 ± 4.35
Estimated Standard Error	2.219
Confidence Level Used	95%

Tensile Strength. The tensile strength of the beveled tubes was very similar to that of the regular tubes. The regular tubes had an average ultimate tensile force of 945 N, and the beveled tubes had an average ultimate tensile force of 887 N. In both scenarios, the increase of temperature and upset resulted in stronger welds. A 95% confidence interval shows that the upset significantly affects the tensile strength of the weld.

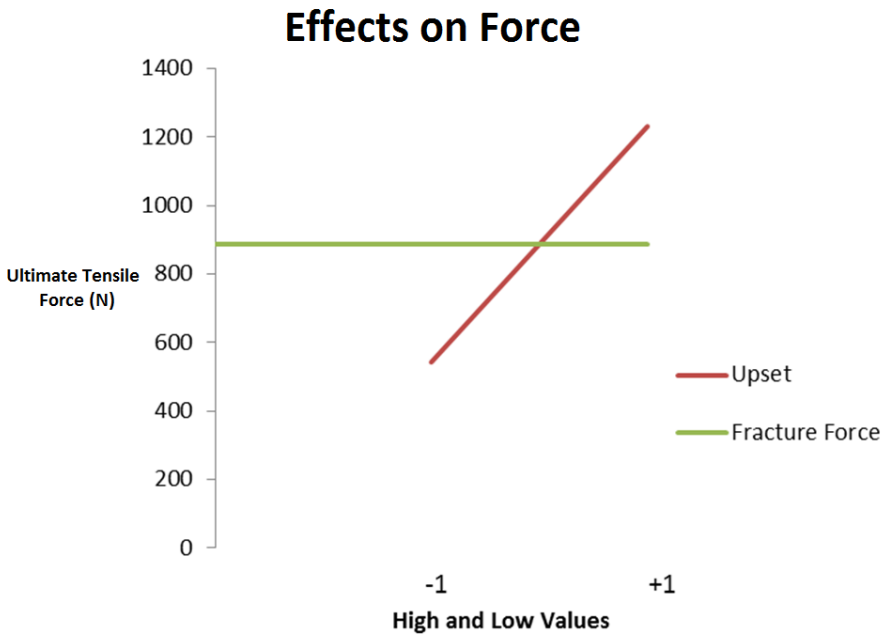

Figure 66: A larger upset value resulted in a stronger weld.

Table 20: Statistical Significance from the Beveled Tests: Ultimate Tensile Force Effects

Ultimate tensile force A=upset	
A effect ± confidence interval	344.2 ± 342.6
Estimated Standard Error	174.8
Confidence Level Used	95%

Large Upset Tubes

Results from the tube-to-tube testing led to a testing matrix designed around an acceptable leak rate. The only tests that held a pressure in the regular tube-to-tube testing were those that had the highest upset values. Larger upset tests did result in much better leak performance. At the same time, the hole integrity was compromised. All of the large upset tests completely filled in the hole. From the previous tests, an upset value of .1 cm

resulted in a very low leak rate. This value was used for a lower bound, and an upset of .2 cm was used for an upper bound in the forthcoming data set. Drilling out the center of some welds was attempted. Even with carbide drill bits, this did not work. The large-upset-tubes were left with the through-hole completely filled in.

Leak Rate. The average leak rate for all the large upset tests was -5.865e-6 atm*cm^3/s. A larger upset worked much better to achieve a low leak rate. This value is still not as low as desired, but it will be seen later that it can be considered to be the same as the base rate of the test setup. It was found that the parameter effects and the interaction were all negligible. Even at a confidence level of 90%, both effects and the interaction were shown to not be significant.

Table 21: Statistical Significance from the Large-Upset-Tubes: Leak Rate Effects

Leak Rate A=forging force B=upset	
A effect ± confidence interval	-1.32e-7 ± 5.36e-6
B effect ± confidence interval	3.78e-6 ± 5.36e-6
AB interaction ± confidence interval	6.99e-7 ± 5.36e-6
Estimated Standard Error	3.24e-6
Confidence Level Used	90%

All the leak rates for these tests were very low. It could be that the observed leaks were just the base leak rate of the system. Several unwelded test samples were loaded

into the testing device. Their leak rates do indicate that the welded rates might be similar to the system leak rate. A two-sample t-test was performed to test the null hypothesis that the leak rates of the welds were the same as the leak rates from the system. The following table is a representation of leak rate data used for the t-test.

Table 22: A t-test Compares the Leak Rates of the Welds to the Base Rate

Tube to Tube Tests ($atm*cm^3/s$)	Unwelded Sample Leak Rates ($atm*cm^3/s$)
-6.78E-06	-5.73E-06
-7.46E-07	-3.14E-06
-1.45E-05	-1.23E-06
-6.76E-06	-2.87E-06
-1.66E-05	-3.39E-06
-1.16E-06	-1.44E-07
-1.23E-06	-1.16E-05
-4.02E-06	-3.1E-06
-7.52E-06	
-3.59E-06	
-1.02E-06	
-6.46E-06	

Microsoft Excel was used to perform the t-test. An alpha of .05 was used, and the test was run assuming unequal variances. The resulting data follows.

Table 23: t-test Results

t-Test: Two-Sample Assuming Unequal Variances		
	Variable 1	Variable 2
Mean	-5.9E-06	-3.9E-06
Variance	2.69E-11	1.23E-11
Observations	12	8
Hypothesized Mean Difference	0	
df	18	
t Stat	-1.00711	
P(T<=t) one-tail	0.163614	
t Critical one-tail	1.734064	
P(T<=t) two-tail	0.327229	
t Critical two-tail	2.100922	

The most important values in the above table are the “t Stat” and the “t Critical two-tail” values. In order to reject the null hypothesis that the two leak rates are the same, the absolute value of “t Stat” would have to be larger than the “t Critical two-tail” value. This is not the case, so it can be seen that the two leak rates can be considered the same. The null hypothesis is accepted. Significant implications can be taken from these findings.

A leak rate goal of 10^{-8} atm*cm^3/s was specified by the National Laboratory. The tubes could be used in service if they met this standard. The measuring equipment used in this study could not measure to the specified precision. Instead, it could be said that the welded samples leak no less than the leak testing system itself. They still may be able to meet a lower leak rate specification. Due to limits of testing equipment, the welds can be classified to be better than the order of 10^{-6} atm*cm^3/s.

Tensile Strength. Tensile testing this group of regular tube-to-tube samples led to interesting results. Similar statistical analysis used previously helps show important effects. The average ultimate yield force was about 2050 N in tension. These welds were about twice as strong as the initial tests. Also, this is comparable to the yield strength of the base metal.

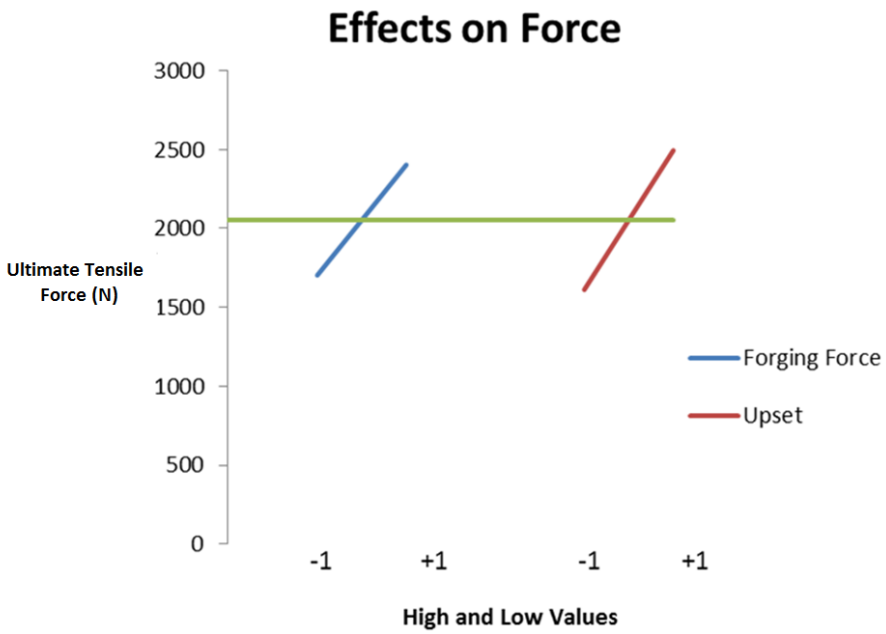

Figure 67: The forging force and the upset both affect the ultimate tensile force.

Both the forging force and the upset have positive effects on the ultimate tensile force. As the forging force and upset are each increased, the ultimate tensile force increases.

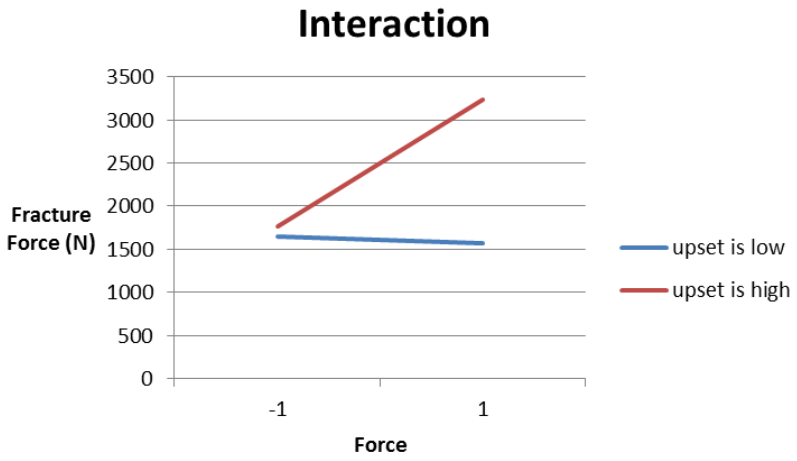

Figure 68: Interaction between the upset and the forging force appears to be significant.

Unlike previous interaction plots, figure 68 clearly shows interaction between effects might be significant. When the upset is low, the ultimate tensile force will be low. When the upset is high and the forging force is low, the ultimate tensile force will also remain low. It was not until both the forging force and the upset were at the high levels that a large ultimate tensile force was achieved. The above interaction graph can be visualized better with the following matrix available.

Table 24: The Interaction Explored Further

Interaction Graph Data, Average Ultimate tensile forces		
	Low Upset	High Upset
Low Forging Force	1647 N	1762 N
High Forging Force	1573 N	3231 N

Three cells in the above matrix contain very similar values. Only the cell with the high upset and high forging force appears different than the others. Furthermore, this high/high cell has an average ultimate tensile force about twice that of the other cells. From this, several conclusions can be made. A decent tensile strength can be achieved with various levels of upset and forging force. In order to obtain a significantly larger tensile strength, both the upset level and forging force level must be increased. Simply increasing one or the other will not result in a significant increase in tensile strength.

Unfortunately, the statistical significance of the results discussed above is in question. A 95% confidence interval reveals that none of the above trends are statistically significant. At a 90% confidence level only the upset effect can be determined

significant. It is not until an 85% confidence level is used that both effects and the interaction can be determined significant.

Table 25: Statistical Significance from the Large-Upset-Tubes: Ultimate Tensile Force Effects

Ultimate tensile force A=forging force B=upset	
A effect ± confidence interval	697.5 ± 696.1
B effect ± confidence interval	886.9 ± 696.1
AB interaction ± confidence interval	771.5 ± 696.1
Estimated Standard Error	483.4
Confidence Level Used	85%

Confidence levels this low have not been used so far in this study. It is believed that the effects shown in this data set are still of importance. In this data set, each cell of the testing matrix was populated with only three tests. A sample set of three tests will yield a much larger sample standard error than a set of four tests. This results in a higher difficulty to accept effects and interactions.

An 85% confidence interval is not terribly low, and for a small sample size, the results here were still considered significant. The data in this section can be used to point to the following conclusion. Both the upset and the forging force can be increased to increase the ultimate tensile strength, but maximum strength is produced when both parameters are increased simultaneously.

Bar to Tube

Previous testing has shown that a leak free weld is possible. This possibility was explored further. A bar was welded to a tube in order to cap a system. The goal of this procedure would be to create a leak free weld between the bar and the tube. The same upset and forging force values from previous testing were used for the bounding parameters for these tests.

Leak Rate

The leak rate results for this section were very similar to those in the large upset tube-to-tube section. All the tests proved to have a leak on the same order as the system leak rate. The leak rates were all on the order of either 10^{-6} or 10^{-7} atm*cm^3/s. The average leak rate was -3.31E-06 atm*cm^3/s.

The results here compared to the large-upset-tubes. The plots were omitted for this section; neither the effects nor the interaction were determined statistically significant. At a confidence level of 90%, none of the factors can be considered significant.

To move forward, the leak rates were compared to the base leak rates of the system. A t-test was used to test the null hypothesis that the two leak rates were the same. An alpha of .05 was used to test the following data.

Table 26: Statistical Significance from the Large-Upset-Tubes: Leak Rate Effects

Leak Rate A=forging force B=upset	
A effect ± confidence interval	7.10e-7 ± 2.27e-6
B effect ± confidence interval	-1.81e-6 ± 2.27e-6
AB interaction ± confidence interval	4.83e-7 ± 2.27e-6
Estimated Standard Error	1.37e-6
Confidence Level Used	90%

Table 27: A t-test Was Used to Compare Leak Rates

Tube to Tube Tests ($atm*cm^3/s$)	Unwelded Sample Leak Rates ($atm*cm^3/s$)
-1.43E-06	-5.73E-06
-3.03E-06	-3.14E-06
-1.72E-07	-1.23E-06
-5.44E-06	-2.87E-06
-2.30E-06	-3.39E-06
-4.74E-06	-1.44E-07
-7.25E-07	-1.16E-05
-1.40E-06	-3.14E-06
-1.19E-06	
-2.05E-06	
-9.37E-06	
-6.64E-06	
-4.00E-06	
-6.67E-06	
-3.60E-06	
-2.09E-07	

Again, a two sample t-test assuming unequal variances was performed in Microsoft Excel. The key results to note are the "t Stat" and the "t Critical two-tail" values.

Table 28: t-test Results

t-Test: Two-Sample Assuming Unequal Variances		
	Variable 1	Variable 2
Mean	-3.3E-06	-3.9E-06
Variance	7.12E-12	1.23E-11
Observations	16	8
Hypothesized Mean Difference	0	
df	11	
t Stat	0.422214	
P(T<=t) one-tail	0.340502	
t Critical one-tail	1.795885	
P(T<=t) two-tail	0.681003	
t Critical two-tail	2.200985	

The t-test shows that the two leak rates can be considered the same; the null hypothesis is accepted. Leak testing of these bar-to-tube tests shows that the samples can hold a pressure as well as the testing setup. It can be concluded that these tests at least have a leak rate less than the order 10^{-6} atm*cm^3/s.

Tensile Strength

Interestingly, the tensile average ultimate tensile force for these tests was very comparable to the large-upset-tubes. The average ultimate tensile force for the bar-to-tube testing was 1945 N. Again, this average is approaching the yield strength of the base metal. The force levels for the bar-to-tube were less widespread than those of the regular tube-to-tube tests. A maximum averaged strength was achieved when the upset was low

and the forging force was high. The lowest averaged strength occurred when the forging force was low and the upset was high.

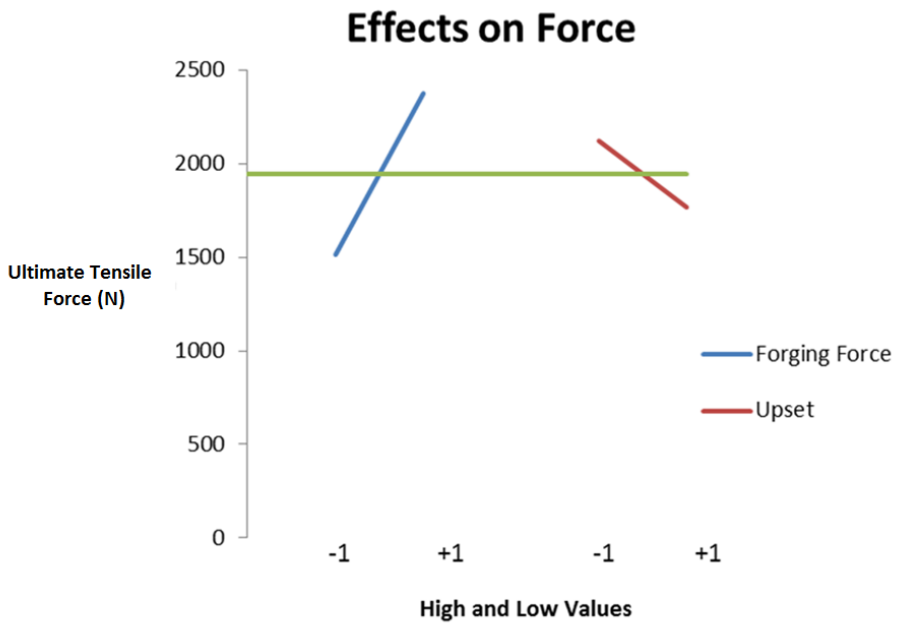

Figure 69: The forging force greatly affected the strength of the welds.

Conversely to the large-upset-tubes, an increase in upset appears to decrease the ultimate tensile force. An increase in the forging force still shows an increase in ultimate tensile strength. The interaction also indicates that a larger forging force will create a stronger weld.

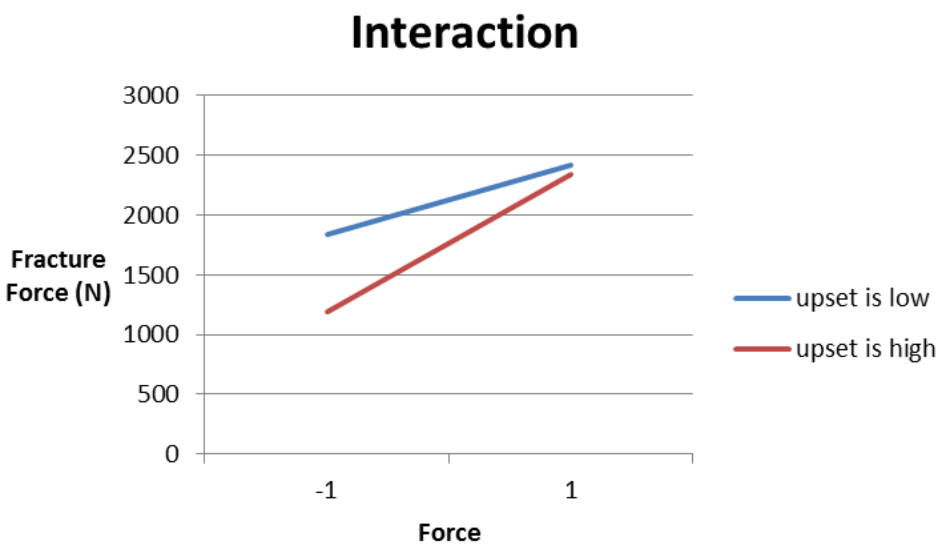

Figure 70: The interaction between upset and forging force was found to be insignificant.

Both effects and the interaction failed to appear significant under the scrutiny of a 95% confidence interval analysis. When a 90% confidence level was used, it became clear that the forging force was the only factor that led to a significant change in ultimate tensile force.

Table 29: Statistical Significance from the Bar-to-Tube Tests: Ultimate Tensile Force Effects

Ultimate tensile force A=forging force B=upset	
A effect ± confidence interval	867.4 ± 863.2
B effect ± confidence interval	-360.3 ± 863.2
AB interaction ± confidence interval	282.4 ± 863.2
Estimated Standard Error	521.9
Confidence Level Used	90%

Constant Force Testing

Recall, this set of testing was performed to compare a more rigid testing configuration to the one used for the majority of testing. Tests were run at two levels. A higher rotational speed was used for one group, and the same rotational speed used throughout all above tests was applied to another group of samples. This second group was controlled with upset values.

High Speed Testing

Testing here was performed with a rotational speed of 1800 rpm. There were nine tests performed here. Test G8 was used for microstructure analysis, so there were eight ultimate tensile force data points and nine leak rate data points. The average ultimate tensile force was 1900 N. This value compares to the yield strength of an unwelded sample. The unwelded test resulted in a yield strength of 1850 N, so the average ultimate tensile force just beat that. This shows considerable strength. -5.865×10^{-6} atm*cm^3/s

With the high speed used in these tests, controlling the process by upset or time didn't allow a quick enough reaction time. Instead, the test was controlled by observation. A decent level of consistency was produced from this control. The average measured upset value was .0344 cm. The lowest upset was .018 cm, and the largest was .059 cm. It was found that the ultimate tensile force and upset were related to each other for these tests. As the upset increased, the ultimate tensile strength increased as well.

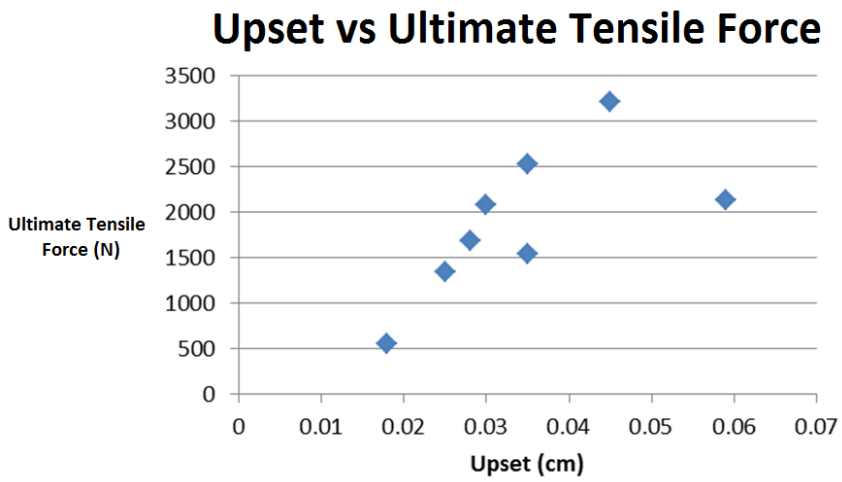

Figure 71: Upset and ultimate tensile force had a positive relationship in the high speed constant force testing.

Tests from this method resulted in variable leak performance. It was found that most of the samples were holding a pressure very well. Most of them showed a leak rate that was on par to the leak rate of the pressure testing system. However, there were others that had a more severe leak. A leak-free success rate of 66.67% was found. Six out of nine welds were able to meet the leak rate of the pressure testing system.

Regular Speed Testing

This set of samples was performed in order to directly compare results from the rigid test setup to the original test setup. The goal here was to imitate upset data from the Large Upset Tests section. Ultimate tensile strength data was then used to compare the two data sets. Six tests were performed with an upset value of about .1 cm, and two tests were completed with an upset value of about .2 cm.

These tests, unlike the high speed testing welds, were done with specific high and low upset values. For this reason, the statistical analysis used previously can be applied

here. The average ultimate tensile force was found to be 1673 N. A positive correlation between upset and ultimate tensile force was also found.

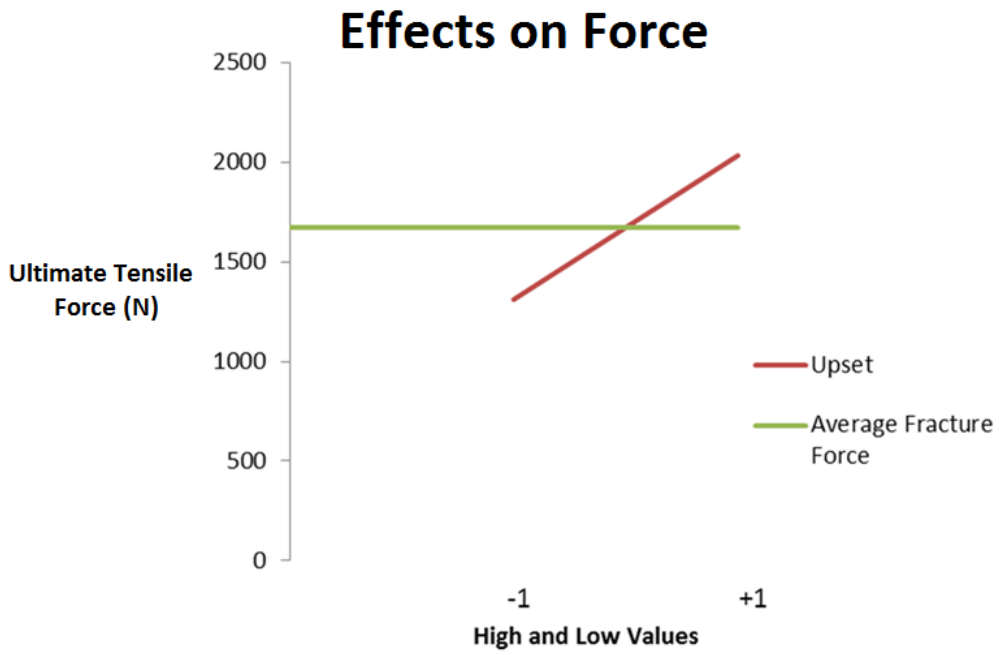

Figure 72: The upset had a positive correlation to the ultimate tensile force.

A 95% confidence level was used to show the above effect was statistically significant.

Table 30: Statistical Significance of the Upset

Ultimate tensile force A=upset	
A effect ± confidence interval	363.5± 202.1
Estimated Standard Error	103.1
Confidence Level Used	95%

Further Discussion and Comparisons

Thus far, the results have been primarily looked at in their own groups. Here, comparisons across testing matrices are made. Also, microstructure analysis is introduced. This helped determine how complete the welds were.

Microstructure

Three different welds were analyzed under a microscope. Welds B24, D34, and G8 were all looked at. Weld B24 was in the large-upset-tubes category. It was welded with a low forging force and a high upset. Weld D34 was a bar-to-tube weld. It was performed with a low forging force and a high upset. Weld G8 was a high speed weld. The other high speed welds were post drilled to reproduce a through-hole. This was not done with weld G8 so that the true result from the weld could be observed. Several of the following figures are composed of several images stitched together; this causes the variation in coloring.

Figure 73: Weld B24, 50x.

Possibly the first quality noticed in Figure 73 is that the weld does not successfully bond through the entire wall thickness. This could be a concern. It appears most of the bonding occurs on the inner part of the tube. The material centered in the tube most likely adds a high level of structural integrity. Looking more closely at the right leg, the grain orientation can be observed.

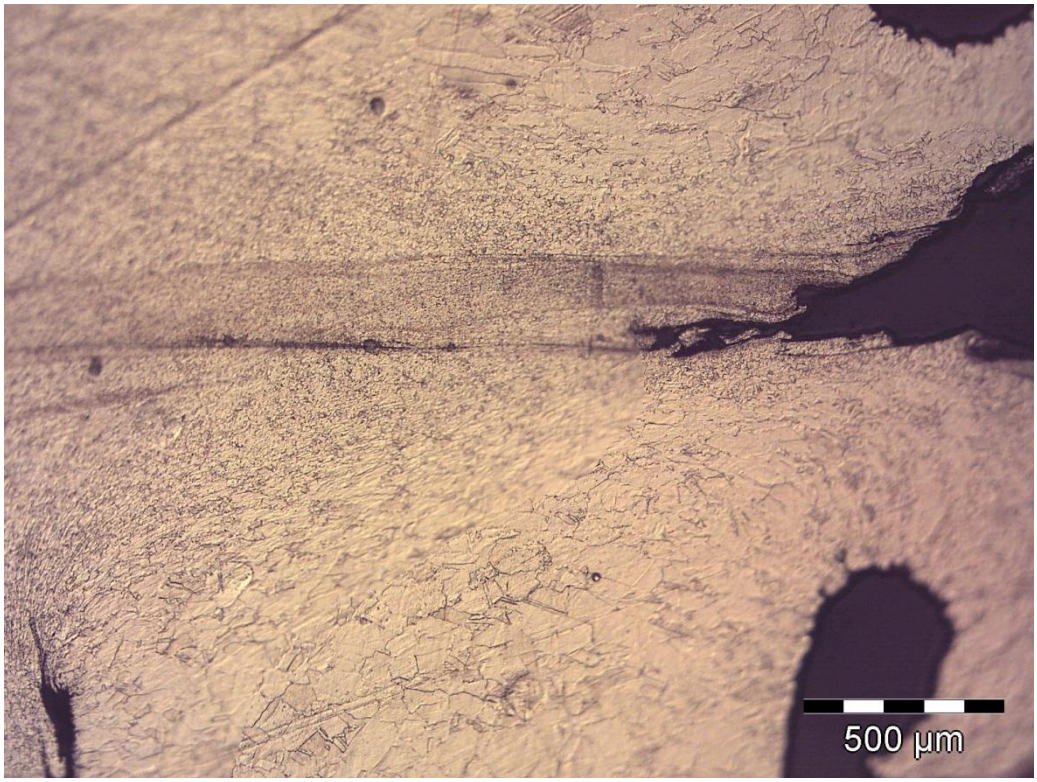

Figure 74: Weld B24, 100x.

There still appear to be some gaps in the weld, but the grain structure indicates welding behavior. At the extremities of Figure 74, the grains look consistent and of moderate size. Closer to the weld interface, the grains begin to squish together and reorient themselves. Immediately contacting the weld interface, the grains are quite small. They have been squished together under the axial forces of the process.

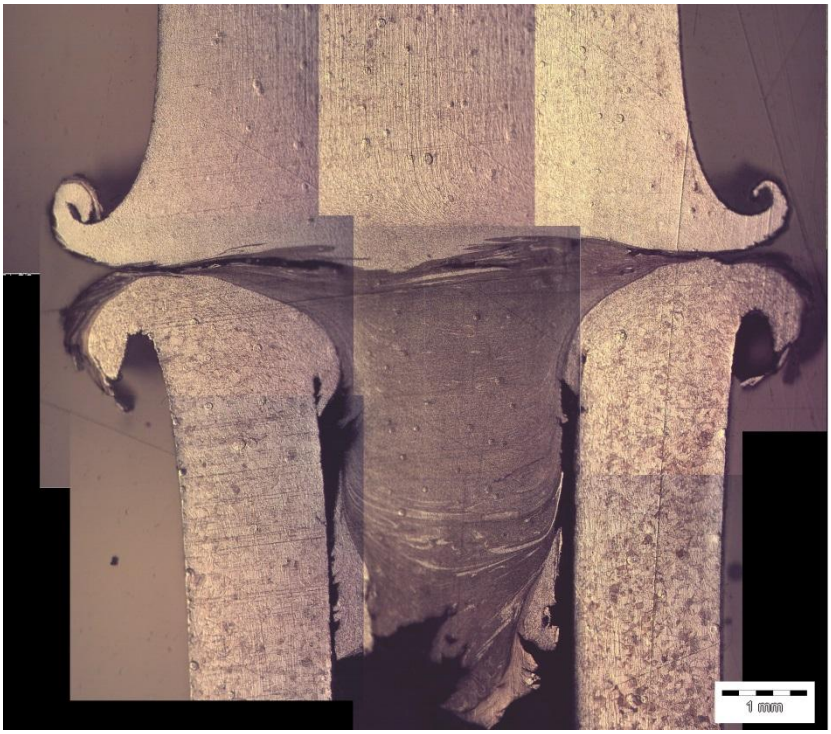

Figure 75: Weld D34, 50x.

Weld D34 also shows some bonding concerns. There appears to be several void spaces in the weld. Also, the material joining the bar to the tube appears to be different than the base material. This is likely a hardened section of metal resulting from the high temperatures in the weld. There could be a simple explanation for this behavior.

It looks as though the heating rate and force levels were not ideal for this weld. The metals likely heated quickly to create a soft section of metal. Then, the applied forces pushed this softened section into the hole of the tube. The softened section separated itself from the base metals, but then it refused everything together during cooling.

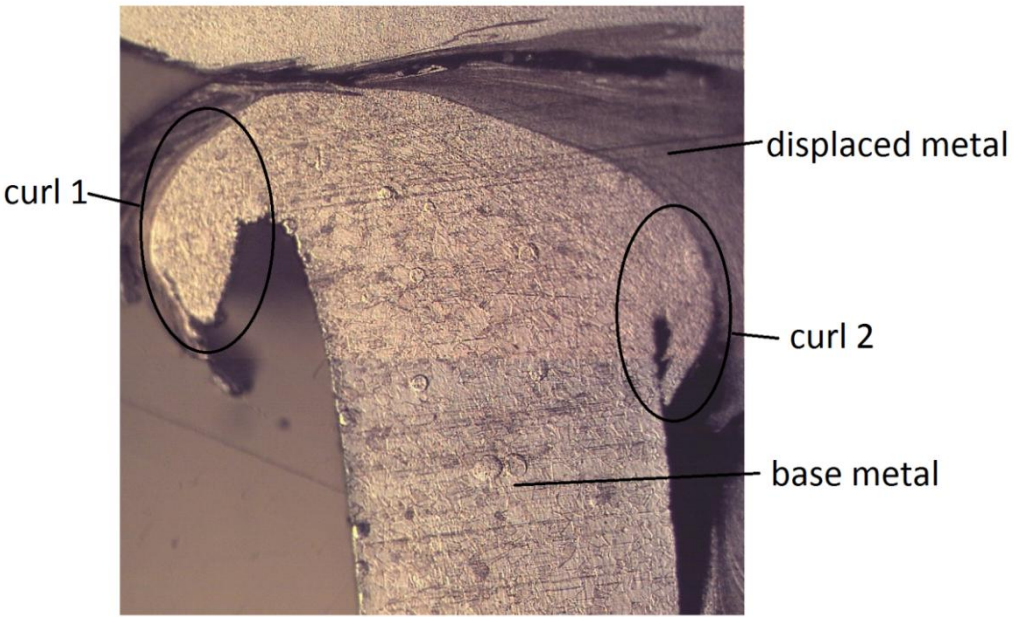

Figure 76: Weld D34, 50x.

Ideally, only curl 1 would be visible. Curl 2 should have bonded into the weld, but it clearly exists in the above figure.

Aside from this strange effect, other weld qualities can be observed from weld D34.

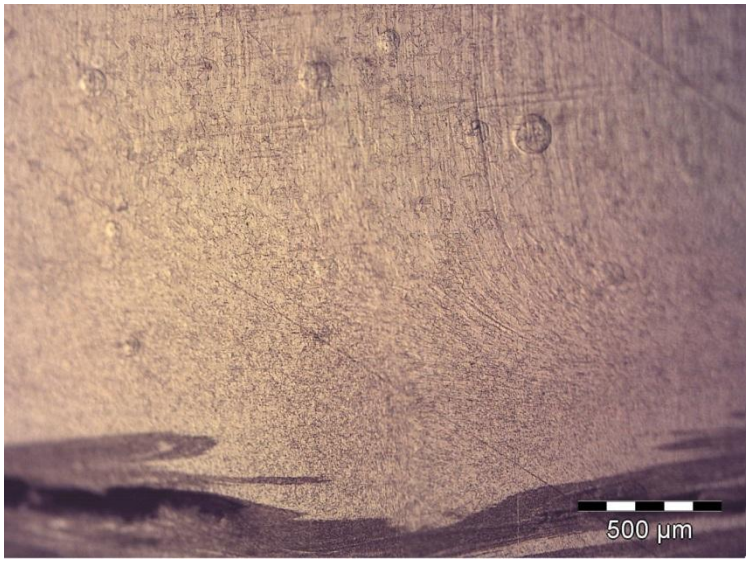

Figure 77: Weld D34, 100x.

Figure 77 shows the center of the bar immediately above the weld interface. The grains are larger at the top of the figure, and they begin to decrease closer to the weld interface. Furthermore, the grain structure begins to curve closer to the weld. This was from the rotation of the bar. This part of the bar was definitely experiencing welding transformations, but the primary bond was to the intermediate material instead of the tube itself.

Lastly, the high speed weld was studied under a microscope. This weld had some of the same problems as the others above, but it also showed a progress in quality.

Figure 78: Weld G8, 50x.

Left undrilled, weld G8 still shows a decent quality of through-hole retention. The curls on the interior of the weld could be easily removed with a drill after the weld was completed. It appears as though the removal of the curls would not reduce the physical characteristics of the weld.

As mentioned, problems still exist with weld G8. Voids clearly exist in the weld interface on both legs. Wall thickness quality becomes reduced especially on the left leg.

The weld interface itself looks better than the previous two welds. Again, grain size was moderate at a significant distance away from the weld.

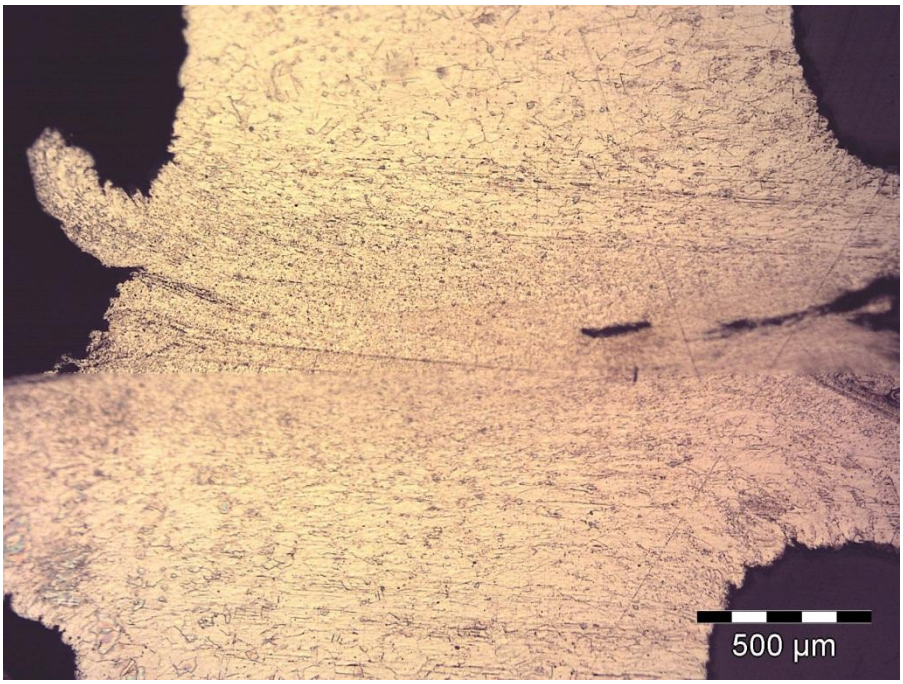

Figure 79: Weld G8, 100x.

Grains closer to the weld become smaller and more compressed. When looking closely at the weld interface, it is difficult to differentiate the top sample from the bottom.

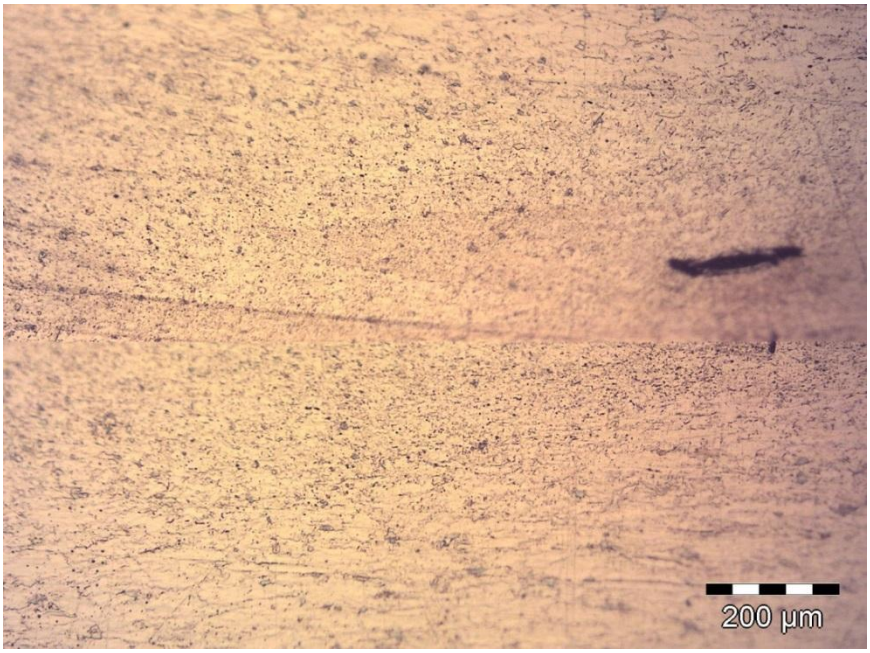

Figure 80: Weld G8, 200x.

The weld interface goes right the middle of Figure 80. The large void indicates a section of this interface. Metal directly above and below this area looks very similar. Looking to the left of this void but at the same vertical level, it is very difficult to determine the weld line. This helps indicate strength. The grain size has been reduced from the base metal, but uniformity in the weld zone has been achieved.

All three of the welds presented above show flaws. There are two important questions to consider. Are these welds adequate indicators of all samples? Do the flaws matter? Both questions do not have a straightforward answer. To the first question, all three of these welds held a pressure at the highest level achievable in this study. Unfortunately, they weren't tensile tested (for obvious reasons). If tensile testing found them to be weak, perhaps they would not be adequate representations of their populations. To best answer this first question, many samples would need to be studied

under the microscope to find trends. Unfortunately, this is beyond the scope of this study. Based on leak performance, there is a decent chance these welds represent their respective populations.

Do the defects matter? A first impression of these photos might cause a large amount of concern. However, all hope is not lost. This study was conducted based on optimizing physical sample qualities. All three welds come from sample sets that performed well in physical testing. Each weld, based on testing of similar samples, can hold a tensile force larger than the yield force of the base metal. The choice then comes down to the user and the application. All three weld sample groups have been shown to be strong and leak free, but there certainly are weld defects.

Lastly, the rigid testing setup created welds with the best microstructure quality. The large-upset-tubes had decent size voids and the bar-to-tube weld showed strange bonding. The high speed weld showed the best bonding of the actual base material. This could be due to various things (higher speed, constant force, etc.), but the rigid testing setup configuration could possibly have been the cause for this success. Perhaps other welds would look slightly different in a different setup. The validity of the original setup will be discussed immediately in the following section.

Ultimate Tensile Strength

Recall, the yield strength of the base metal was found to be 1850 N. The ultimate force was found to be 4600 N. These values will be important to keep in mind when analyzing ultimate tensile force levels of the welds.

Interesting results can be found when comparing ultimate tensile strengths across different testing configurations. The following table concisely summarizes relevant ultimate tensile strength data.

Table 31: Strength Summary of All Welds

Sample Set	**Total Average Ultimate Tensile Strength (N)**	**Highest Average Ultimate Tensile Strength**	
		Value (N)	**Testing Conditions**
Initial tests	945	1560	High temp, high forge force
Beveled tests	887	1233	High upset, low forge force
Large upset tubes	2050	3231	High upset, high forge force
Bar to tube	1945	2417	Low upset, high forge force
High speed, constant force	1900	2491	Upset ≥ .03cm
Low speed, constant force	1673	2037	High upset
Low speed, constant force, very low upsets to mimic initial tests	974	-	-
Unwelded sample:	Yield Strength: 1850 N	Ultimate tensile force: 4600 N	

The initial tests and the beveled tests had very similar strength data. These two data sets made up the weakest welds in variable force study. Even their maximum strength conditions result in a fracture failure quite far below the yield stress of the base metal. These welds were considered to be weak.

Proving to be the strongest welds, the large upset tubes demonstrated a high quality of fracture resistance. It took an average of 2050 N to fracture those welds. This average possibly understates the strength potential of these welds. When the upset and the

forging force were both at the high levels, an average ultimate tensile force of 3231 N was achieved. While still sufficiently under the ultimate tensile strength of the base metal, this was nearly 1.75 times larger than the yield strength of the base metal.

In comparison to the large-upset-tubes, the bar-to-tube welds showed lower ultimate tensile strength. The average force of 1945 N compared to the large-upset-tubes, but the maximum force from the bar-to-tube welds was only 2417 N (recall the upset had low significance with the bar-to-tube strength, and when the upset and the forge force was high, the ultimate tensile force was still 2340 N). Both the average ultimate tensile strength and the maximum ultimate tensile strength of the bar-to-tube welds were above the yield strength of the base metal. This shows the bar-to-tube welds still were quite strong, but an explanation to the difference between the large-upset and bar-to-tube welds should be presented.

Looking back at the microstructure section, it appears as though the large-upset-tube welds resulted in both tubes losing equal amounts of material. The material in the middle of the tubes helps show this, but the curls on the outside are better indicators.

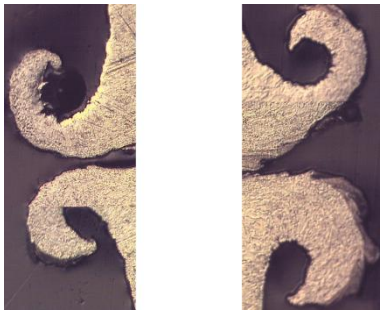

Figure 81: The curls of the large-upset-tests. Weld B24.

All four curls appear to contain roughly the same amount of material. In these tests the metal had the plastic ability to move into both the top tube and the bottom tube.

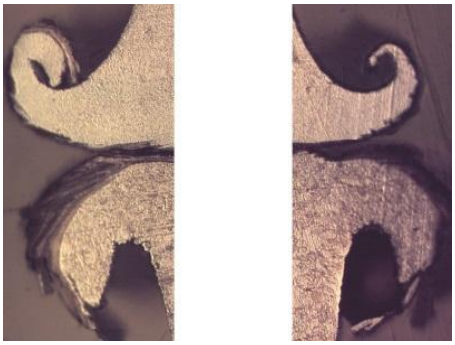

Figure 82: The curls of the bar-to-tube tests. Weld D34.

The bar-to-tube curls look unequal. The curls on the tube appear to contain much more material. This suggests that more material from the tube was plastically moving. More bonding opportunities occur when more material from each source is plastically moving and interacting. From this train of thought, equal plastic deformation in the large-upset-tubes allowed for a higher strength than the bar-to-tube.

The constant force tests had varying ultimate tensile force levels. The high speed tests had upset values comparable to the initial tests mentioned previously. It was then a surprise to see such high ultimate tensile force levels. Testing proved to show these samples had ultimate tensile strengths stronger than the yield strength of the base metal. Even with the small upset values, the high speeds allowed for adequate plastic development of the weld interface.

Constant force tests with lower speeds proved to form weaker welds. These specific welds were designed to be compared to the large-upset-tubes. System integrity was the question these tests were trying to answer; did the rigidity of the original test

setup still allow for productive testing? Both sets of welds showed upset has a positive effect on ultimate tensile strength. Also, the large-upset-tubes showed an increase in forging force results in increased ultimate tensile strength. From these trends, it was expected that the more rigid tests would have increased ultimate tensile strength with an increased upset. Also, since there was no forging force, the more rigid samples were expected to be weaker. Lastly, it would be an added comparison if the more rigid samples filled in the through-hole.

These trends were found in the data. The more rigid tests demonstrated increasing strength with increasing upset. Their ultimate tensile strength values were also lower than those found from the large-upset-tubes. Lastly, the through-hole was filled in entirely in all but one of the more rigid tests. These findings help show that the force trends found with the original setup were valid.

One last point will be made to close this section. Tests I15 and G16 were made with a very low upset and a constant force. Their rotational speed was 1200 rpm. Fractional strength was found with these two tests to see if the values compare to the initial tube-to-tube testing matrix. The average ultimate tensile force of these two samples was 974 N. This falls directly in between the high and low temperature ultimate tensile force values for the initial tests. This helps show again that the original testing setup did not compromise strength characteristics.

Leak Rate Success Percentage

The initial tests and the beveled tube tests did not have significant leak rate results, so they will not be discussed here. The concern here lies within the high speed

tests. Through-hole reduction was eliminated in these welds, but they did not always hold a pressure.

Table 32: Leak Rate Success

	Leak Rate Success Percentage
Large-upset-tubes	100%
Bar-to-tube	100%
High speed, constant force	66.67%

Pressure was held in the high speed tests strictly from the wall thickness. In the other two weld styles, the through-hole was filled in completely. The filled hole along with the weld in the wall thickness more securely prevented the pressure from leaking out. Better success percentages could likely be produced from the high speed method, but at present the success rate is far from 100%.

Population Trends

When the entire population was looked at as a whole, some final trends can be found. The following figures use data from most of the data points from the original testing setup; the samples set aside for microstructure analysis were not included in the figures. Also, only data from the original testing was included; the constant force data was left out.

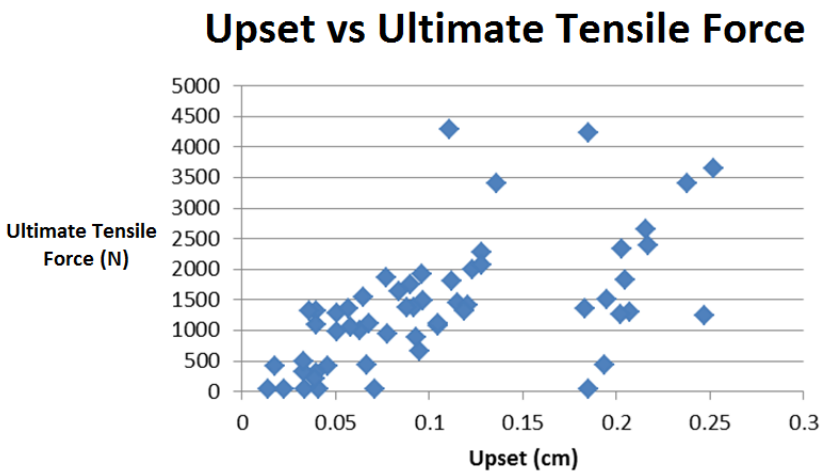

Figure 83: Throughout the sample population, a weak trend shows the ultimate tensile force increases with an increasing upset.

Throughout the entire sample population, a correlation between ultimate tensile force and upset presented itself. The data in figure 83 is quite scattered, but a general trend indicates that as the upset increases the ultimate tensile force increases. From other findings, this makes sense. As more material is displaced and capable of bonding, larger strength can be achieved.

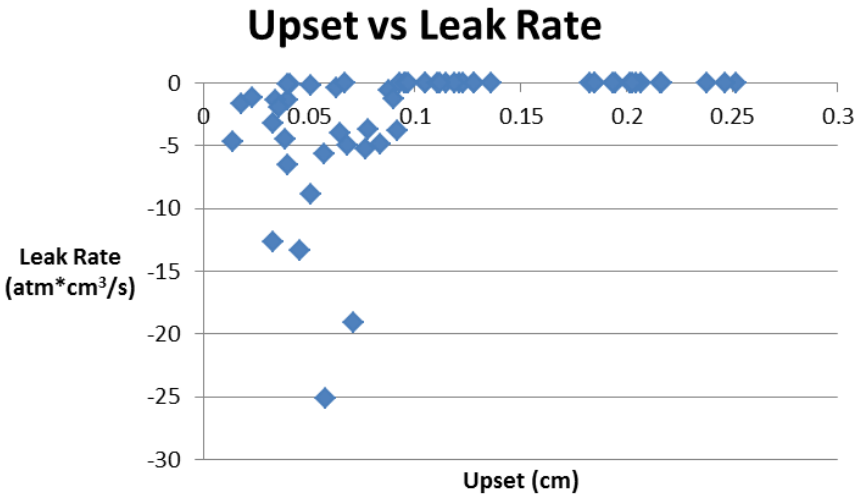

Figure 84: The upset had an effect on the leak rate when the whole population was considered.

It appears that the upset played a very critical part in leak rate quality. Some tests at low upset values were able to hold a pressure, but upset values above .1 cm greatly increased the leak rate success percentage.

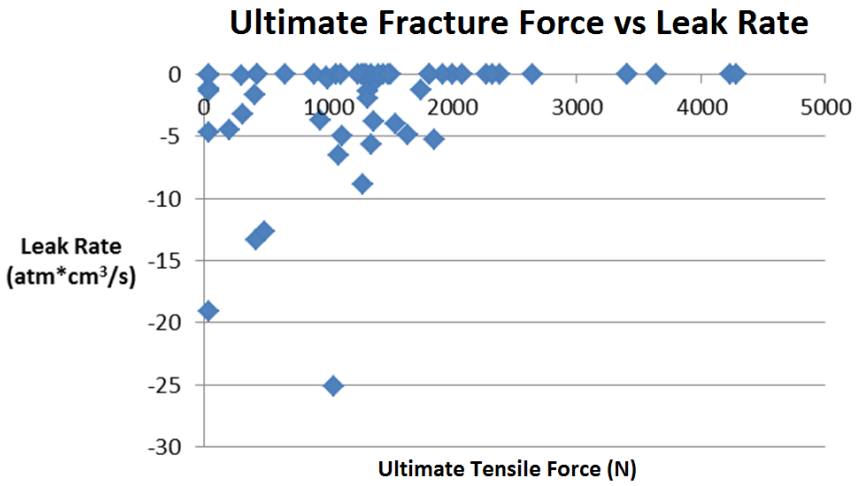

Figure 85: Only weak conclusions about the ultimate tensile force and leak rate can be made.

Figure 85 shows the comparison of two measured values. Both the leak rate and the ultimate tensile force were measured after the weld was completed. Weaker welds, with a ultimate tensile force less than 2000 N, had a variable response as to whether they would hold a pressure or not. Stronger welds held a pressure with much more success. The above figures are all in agreement with each other. Higher upset increases the ultimate tensile force; higher upsets and higher ultimate tensile forces reduce the leak rate. Strong conclusions will not be drawn from these population comparisons, but they have been presented to show general trends throughout all tests.

RESULTS SUMMARY

Parameter Effects

A large amount of information has been presented. This section is to summarize in tables the effects that were found in different welds. All discussion has been presented previously.

Table 33: Summary of the Parameter Effects

Weld Style	**Weld Quality**	**Significant Effect**	**Effect Direction**	**Confidence Interval Used**
Initial Tests	Through-hole reduction percentage	Max temp	+	95%
	Leak rate	Max temp	-	90%
	Tensile strength	Max temp	+	95%
Beveled Tubes	Through-hole reduction percentage	Upset	+	95%
	Leak rate	Upset	-	95%
	Tensile strength	Upset	+	95%
Large upset tubes	Leak rate	None	None	90%
	Tensile	Forging force	+	85%
		Upset	+	85%
		Interaction	…	85%
Bar to Tube	Leak rate	None	None	90%
	Tensile strength	Forging force	+	90%
Constant force, 1200 rpm	Tensile strength	Upset	+	95%

Leak Rate Summary

Weld Style	**Zero Leak Success Percentage**	**Comparison to System Base Rate**		
		T_{stat}	**T_{crit}**	**Leak rate = Base rate?**
Large upset tubes	100%	-1.007	2.101	Yes

Table 33 Continued

Bar to tube	100%	.422	2.201	Yes
Constant force, 1800 rpm	66.67%	-	-	-
Constant force, 1200 rpm	0%	-	-	-

Design Decision

The overall goals of this study have been met. Both tube-to-tube and bar-to-tube welds were completed. Welds showing high strength and great leak rate characteristics were created with several different methods. These results then need to transition from a research study to a real design application. What information can be taken from this study to apply to a design necessitating a rotational friction weld of these small dimensions?

The following thought process would be good to consider when implementing these friction welds into a design. First and foremost, the adjustability, control, and rigidity of the welding system needs to be analyzed and fully understood. A finished weld with the through-hole intact will require a very rigid system. Also, the weld will have to be drilled out after the weld is completed. This was an easy post-processing step with short samples, but it may be more difficult in an application. Capping a tube with either a bar or another tube (use a large upset value to fill in the hole) is possible with a slightly more flexible system.

Then, the quality of the desired weld needs to be determined. Increasing the forging force typically increases the weld strength, and maintaining a set upset proved to be the most consistent method of control. Again, using a more rigid system will most likely help reduce weld defects, but acceptable physical qualities can be achieved from

various testing setups. These considerations should help evaluate the feasibility of friction welding in a design.

Future Work

Primary future work should analyze different testing parameters in a more rigid setup. The main testing setup used in this study had a rigidity weakness, and the rigid setup used at the end of this study lacked control. Integrating both of these testing qualities in a future testing setup would be beneficial. Also, varying other parameters would be of use.

Other studies have used the friction force as a variable parameter (Sahin, 2007, Satyanarayana, 2004). It would be interesting to do this here. In fact, with an unlimited amount of time, all seven of the testing parameters could be varied. The original orthogonal array presented earlier (Figure 12) is perfectly designed this. Many tests could be run at many different levels, and a more thorough understanding of the effects would result.

Lastly, a more thorough microstructure investigation would be beneficial. Looking at several samples for each testing scenario would help establish consistency. Also, better polishing and etching would help show the grain transformations.

CONCLUSIONS

Rotational friction welding was successfully used to join stainless steel tubes of small dimensions. Parameters varied in the primary testing included maximum temperature, material upset, and forging force. Welds resulting with the least through-hole reduction were found with a rotation speed of 1800 rpm, an upset of about .03 cm, and a constant axial force of 220 N. A drilling procedure still needed to be done to remove material on the inside of the tubes; these tests also only resulted in a 66.67% success rate of preventing leaks. Tube-to-tube and bar-to-tube tests with higher upsets created a leak-free environment 100% of the time, but the through-hole of the tube-to-tube tests was filled in. The effects of the varied parameters were presented, and microstructure analysis was performed to further analyze quality. Rotational friction welding can be a very beneficial process when properly integrated into a design, but the parameter effects and system capabilities need to be understood in order to be effective.

REFERENCES CITED

Alves, E. P., Piorino Neto, F., An, C. Y., & Silva, E. C. d. (2012). Experimental determination of temperature during rotary friction welding of AA1050 aluminum with AISI 304 stainless steel. *Journal of aerospace technology and management, 4*(1), 61-68.

ASM International., ASM International. Alloy Phase Diagram Committee., & ASM International. Handbook Committee. (1985). ASM handbook *Welding, Brazing, and Soldering* (Vol. 6, pp. v.). Materials Park, Ohio: ASM International.

Houldcroft, P. T. (1977). *Welding Process Technology*. Cambridge, Great Britain: Press Syndicate of the University of Cambridge.

Incropera, F. P. (2007). *Introduction to Heat Transfer* (Fifth ed.). Hoboken, New Jersey: John Wiley and Sons.

Lancaster, J. F. (1993). *Metallurgy of welding* (5th ed.). London ; New York: Chapman & Hall.

MatWeb. (2013). 304 Stainless Steel. Retrieved 6/17/2013, from http://matweb.com/search/DataSheet.aspx?MatGUID=abc4415b0f8b490387e3c922237098da&ckck=1

Montgomery, D. C. (2007). *Engineering Statistics* (Fourth ed.). Hoboken, New Jersey: John Wiley and Sons.

Murthy, D. K. N., Raghupathy, D. V. P., & Sethuram, M. D. (2011). *Friction Welding and Friction Stir Welding*, Bangalore, India.

Paventhan, R., Lakshminarayanan, P. R., & Balasubramanian, V. (2012). Optimization of Friction Welding Process Parameters for Joining Carbon Steel and Stainless Steel. *Journal of iron and steel research, international, 19*(1), 66-71.

Purdue University. Thermophysical Properties Research Center., T., Y. S. (1970). *Thermophysical properties of matter; [the TPRC data series; a comprehensive compilation of data*. New York,: IFI/Plenum.

Raytek. (2010). Miniature Infrared Sensor Operating Instructions. 2013, from http://www.instrumart.com/assets/Raytek-MI3-Manual.pdf

Roger, C. R. (1979). Temperature variation of total hemispherical emissivity of stainless steel AISI 304. *J. Opt. Soc. Am.*, 1384--1390. doi: 10.1364/josa.69.001384

Sahin, M., & Mumin, S. (2005). An investigation into joining of austenitic-stainless steels (AISI 304) with friction welding. *Assembly automation, 25*(2), 140.

Sahin, M., & Sahin, M. (2007). Evaluation of the joint-interface properties, of austenitic-stainless steels (AISI 304) joined by friction welding. *Materials in engineering, 28*(7), 2244-2250.

Sahin, M., & Sahin, M. (2009). Characterization of properties in plastically deformed austenitic-stainless steels joined by friction welding. *Materials in engineering, 30*(1), 135-144.

Satyanarayana, V. V., Reddy, G. M., & Mohandas, T. (2004). Continuous drive friction welding studies on AISI 304 austenitic stainless steel welds. *Materials and manufacturing processes, 19*(3), 487-505.

Shtrikman, M. M. (2010). Linear friction welding. *Welding international, 24*(7), 563-569.

Sluzalec, A. (1990). Thermal effects in friction welding. *International Journal of Mechanical Sciences, 32*(6), 467 - 478. doi: http://dx.doi.org/10.1016/0020-7403(90)90153-A

Taguchi, G. i. (1987). *System of experimental design : engineering methods to optimize quality and minimize costs* (Vol. 1). White Plains, N.Y.
Dearborn, Mich.: UNIPUB/Kraus International Publications ;
American Supplier Institute.

Vill, V. I. (1962). *Friction welding of metals*. New York,: American Welding Society; trade dist. Reinhold Pub. Corp.

Wheeler, A. J., & Ganji, A. R. (2003). *Introduction to Engineering Experimentation* (Second ed.). Upper Saddle River, New Jersey: Pearson Prentice Hall.

APPENDICES

APPENDIX A:

DATA COLLECTION

In the following figure, all the data from this study is presented. There are a few cells empty. This resulted from improper data acquisition. For example, the displacement control was not connected for test A22. The test was still a successful test, so other measurement data was still used for analysis. Cells with a dash in them indicate that the respective measure was not applicable to that test. Different areas are highlighted different colors to represent different testing parameters.

Blue=initial tube-to-tube
Orange=large-upset-tubes
Yellow=bar-to-tube
Green=beveled tube-to-tube (both tubes beveled)
Purple=high speed, constant force tube-to-tube
Grey=low speed, constant force tube-to-tube

The subscripts on each test label correspond to the high and low levels of the various parameters. To fully understand which parameters varied, the Design of Experiments should be looked at. Here, the subscripts represent a singular cell in the 2x2 or 1x2 testing matrices.

	Low	High
Low	1	2
High	3	4

	Control Method	**Forging Force (N)**	**Friction Time (sec)**	**Max Temp (°C)**	**Max Upset (cm)**	**Volumetric Leak Rate (atm*cm^3/s)**	**Ultimate tensile force (N)**	**Yield Force Approx (N)**	**Area Reduction Percentage**
$D14_1$	Time	530	6.1	646	.018	-1.62	409	-	65
$E14_1$	Time	530	5.8	617	.023	-1.19	44	-	72
$F14_1$	Time	530	5.8	604	.01	-4.62	44	-	65.3

					4				
A15 2	Time	530	7.7	857	.05 1	-8.81	1277	-	100
B15 2	Time	530	7.5	795	.04 0	-1.32	1317	-	94
E15$_2$	Time	530	7.5	870	.05 7	-5.64	1347	-	89.9
C16 3	Time	1250	5.9	696	.05 6	-4.78	-	-	47.2
D16 3	Time	1250	5.8	719	.04 1	-.0953	44	-	55.4
E16$_3$	Time	1250	5.5	626	.04 0	-.0911	307	-	60.1
B17 3	Time	1250	5.5	582	.03 4	-1.32	44	-	77.3
C17 4	Time	1250	7.5	956	.12 8	-2.5e-6	2279	-	100
D17 4	Time	1250	7.3	948	.07 1	-19.1	44	-	100
E17$_4$	Time	1250	7.1	928	.07 8	-3.66	941	-	100
F17$_2$	Time	530	7.8	943	.09 5	-1.2e-5	657	-	100
B18 2	Temp	530	7.8	941	.04	-6.5	1089	-	100
B19 2	Temp	530	8.0	962	.06 5	-3.96	1543	-	100
F19$_4$	Temp	1250	7.6	928	.09 2	-3.81	1368	-	98.5
C20 4	Temp	1250	7.7	934	.08 8	-.538	1374	-	100
F20$_4$	Temp	1250	8.1	948	.07 7	-5.20	1855	-	99.6
A21 3	Temp	1250	7.6	726	.05 1	-.146	984	-	76.6
C21 3	Temp	1250	7.8	739	.06 3	-.403	996	-	79.4
E21$_1$	Temp	530	7.1	779	.03 6	-1.95	1317	-	81.2
A22 1	Temp	530	6.9	796	-	-.28	-	-	84.0
B22 1	Temp	530	8.3	775	.03 3	-3.22	314	-	91.9
F22$_1$	Upset	530	8.6	979	.10	-6.78e-6	1065	-	100

					5				
A23 1	Upset	530	9.9	884	.11 5	-7.46e-7	1451	-	100
E23 2	Upset	530	9.5	1057*	.21 6	-1.23e-6	2645	1868	100
F23 2	Upset	530	11.8	957	.18 3	-4.02e-6	1348	-	100
B24 2	Upset	530	11.3	979	.18 9	-7.99e-6	microstructure		100
D24 2	Upset	530	11.8	973	.20 7	-7.52e-6	1294	-	100
F24 3	Upset	1250	9.1	939	.12 1	-6.76e-6	1406	-	100
A25 4	Upset	1250	8.0	1030*	.18 5	-3.59e-6	4233	1913	100
B25 3	Upset	1250	8.3	899	.12 3	-1.66e-5	2001	1112	100
C25 3	Upset	1250	8.2	962	.11 9	-1.16e-6	1313	-	100
A26 4	Upset	1250	9.7	1006*	.20 5	-1.02e-6	1817	1735	100
B26 4	Upset	1250	10.2	1014*	.25 2	-6.46e-6	3645	2180	100
F26 1	Upset	530	12.2	1024*	.13 6	-1.43e-6	3407	2113	-
A27 1	Upset	530	13.7	947	.09 3	-3.03e-6	890	-	-
B27 1	Upset	530	10.3	1006*	.09 6	-1.72e-7	1926	1926	-
C27 1	Upset	530	19.3	976	.09 7	-2.79e-6	-	-	-
D27 1	Upset	530	16.9	1035*	.10 5	-5.44e-6	1108	-	-
E27 2	Upset	530	20.3	993*	.18 5	-1.19e-6	44	-	-
F27 2	Upset	530	25.0	1033*	.20 2	-2.05e-6	1268	-	-
A28 2	Upset	530	27.3	1066*	.19 5	-9.37e-6	1503	-	-
C28 3	Upset	1250	13.1	954	.11 1	-2.30e-6	4288	2224	-
E28 3	Upset	1250	11.7	961	.12 8	-4.74e-6	2077	-	-
A29	Upset	1250	15.3	875	.09	-7.25e-7	1490	-	-

3					7				
B29 3	Upset	1250	13.6	762	.11 2	-1.4e-6	1813	-	-
C29 4	Upset	1250	29.4	941	.24 7	-2.81e-4	1241	-	-
D29 4	Upset	1250	19.0	1125*	.21 7	-6.67e-6	2384	1890	-
E29$_4$	Upset	1250	21.6	960	.20 3	-3.60e-6	2326	1446	-
B30 4	Upset	1250	25.7	1123*	.23 8	-2.09e-7	3406	1779	-
C30 1	Temp	530	4.4	817	.03 9	-4.42	209	-	78.5
D30 1	Temp	530	4.8	777	.04 6	-13.3	423	-	80.3
F30$_1$	Temp	530	4.8	840	.04 1	-14.4	-	-	80.2
C31 1	Temp	530	4.26	763	.03 3	-12.7	489	-	77.8
F31$_1$	Temp	530	3.9	893	.05 8	-25.1	1050	-	94.3
A32 2	Temp	530	6.0	887	.08 4	-4.83	1637	-	100
A33 2	Upset	530	5.1	956	.09 0	-1.22	1744	-	100
C33 2	Upset	530	5.1	923	.06 7	-1.32e-6	431	-	100
D33 2	Upset	530	5.0	776	.06 8	-5.0	1112	-	100
D34 2	Upset	530	24.345	1083*	.18 2	-7.67e-6	Microstructure		-
E34$_2$	Upset	530	24.813	1047*	.19 4	-6.64e-6	437	430	-
F35$_1$	Upset	530	9.89	974	.10 2	-1.45e-5	-	-	100

	RPM	**Constant Force (N)**	**Upset (cm)**	**Leak Proof?**	**Ultimate tensile force (N)**	**Yield Force Approx (N)**
I4	1800	220	.059	Yes	2139	-
G8	1800	220	.029	Yes	-	-
H5	1800	220	.035	Yes	2531	1334.4
I5	1800	220	.018	Yes	560	-

H6	1800	220	.035	No	1548	-
G13	1800	220	.028	Yes	1690	-
H13	1800	220	.045	No	3216	1779.2
I13	1800	220	.025	No	1348	-
G14	1800	220	.03	Yes	2077	1734.72
G9	1200_2	220	.18	-	1868	1668
I9	1200_1	220	.0935	-	1192	-
I10	1200_1	220	.09	-	729	-
I11	1200_1	220	.11	-	1428	1334.4
G12	1200_2	220	.17	-	2206	-
H12	1200_1	220	.128	-	1121	-
I15	1200	220	.07	-	787	-
G16	1200	220	.032	-	1161	-

*Temperatures with * mean they were above the temperature reading of the system. Temps are estimated.

APPENDIX B:

PRESSURE MEASUREMENT CONSIDERATION

- Start with the basic ideal gas law:

$$PV = nRT$$

- In rate form (the entire portion in parenthesis is a function of time):

$$(\dot{PV}) = (n\dot{R}T)$$

- Assume the temperature changes are due to the changes of the room
- Use T as a constant room Temperature.
- The only variable terms become the pressure and the molar leak rate.
- The actual measured temperatures will be used to find an expression for the molar leak rate.
- The next several steps solve for a molar leak rate.

$$PV = nRT$$

$$n = \frac{PV}{RT}$$

$$\dot{n} = \left(\frac{\dot{PV}}{RT}\right)$$

- Substitute this leak rate into the ideal gas equation and apply the equation at room temperature.

$$(\dot{PV})_{new} = \dot{n}RT_{room}$$

- Make a substitution for the molar leak rate:

$$(\dot{PV})_{new} = \left(\frac{\dot{PV}}{RT}\right)RT_{room}$$

- R is assumed constant throughout the process. The final result is below:

$$(\dot{PV})_{new} = \left(\frac{\dot{PV}}{T}\right)_{measured} T_{room}$$

For each time step, the value PV/T is calculated. The rate of change is taken, and this is multiplied by the room temperature. In this way, the leak rate is compensated for temperature changes.

This proved to work with actual data. For example (leaving units off for clarity), a test had a measured PV slope of -4.53e-6 and a measured T slope of -5.49e-5. With the modifications I made above, the resulting PV slope was -2.05e-6.
This indicates that since there is a decreasing temperature (from the room), some of the pressure drop results from this. The modification shows that the leak rate is lower than originally measured.

APPENDIX C:

SAMPLE DRAWING

This drawing was used to place an order for samples.